Distribution Agreement

In presenting this thesis or dissertation as a partial fulfillment of the requirements for an advanced degree from Emory University, I hereby grant to Emory University and its agents the non-exclusive license to archive, make accessible, and display my thesis or dissertation in whole or in part in all forms of media, now or hereafter known, including display on the world wide web. I understand that I may select some access restrictions as part of the online submission of this thesis or dissertation. I retain all ownership rights to the copyright of the thesis or dissertation. I also retain the right to use in future works (such as articles or books) all or part of this thesis or dissertation.

Signature:

_____ _____

David W. White Date

Redox Enzymes for Biocatalysis: From Asymmetric Hydrogenation to CO_2 Reduction

By

David W. White

Doctor of Philosophy

Chemistry

R. Brian Dyer, Ph.D

Advisor

Vincent Conticello, Ph.D

Committee Member

Christine Dunham, Ph.D

Committee Member

Accepted:

Kimberly Jacob Arriola, Ph.D, MPH

Dean of the James T. Laney School of Graduate Studies

Date

Redox Enzymes for Biocatalysis: From Asymmetric Hydrogenation to CO_2 Reduction

By

David W. White

B. S. Troy University, 2017

Advisor: R. Brian Dyer, Ph.D

An abstract of a dissertation submitted to the Faculty of the James T. Laney School of Graduate Studies of Emory University in partial fulfillment of the requirements for the degree of Doctor of Philosophy in Chemistry

2022

Abstract

Redox Enzymes for Biocatalysis: From Asymmetric Hydrogenation to CO_2 Reduction

By David White

Biocatalysis is an integral aspect of society as enzymes are used to catalyze a broad range of industrial reactions with excellent efficiency and selectivity over traditional catalysts. Unfortunately, several drawbacks prevent enzymes from widespread application such as substrate scope and stability. Furthermore, the mechanisms of many enzymes are not fully understood preventing protein engineering or the development of better catalysts. This dissertation focuses on two aspects: the discovery of novel biocatalysts and deciphering the mechanistic details of potential biocatalysts.

Old Yellow Enzymes (OYE) are excellent biocatalysts for asymmetric hydrogenation, a key reaction for the synthesis of numerous industrially relevant products. Unfortunately, the substrate scope of these enzymes is limited with many possessing identical stereoselectivity. By exploring the natural diversity of the OYE family, new, novel enzymes were identified with enhanced catalytic activities and oppositive enantioselectivity. In addition, OYEs capable of desaturation, the reverse reaction, at ambient temperatures were also observed – further expanding the known reactions these enzymes can facilitate.

CO_2 reduction and hydrogen production are important reactions for alternative energy sources and are catalyzed by the metalloenzymes carbon monoxide dehydrogenase (CODH) and hydrogenase. The full catalytic details of both enzymes are currently unknown preventing further application of these proteins as biocatalysts and the development of better, more efficient catalysts. For CODH, direct spectroscopic observation of CO in the active site has yet to be accomplished. To resolve this, the first photosystem incorporating CODH II from *C. hydrogenoformans* was developed with quantum yields 10-fold greater than previous CO_2 to CO photoenzymatic systems. Infrared spectroscopy of the CO inhibited photosystem identified two IR frequencies corresponding to Ni-CO stretches in the active site. Time resolved spectroscopy indicated that both IR bands are involved in the catalytic cycle, indicating that two different bindings of CO to the Ni may be possible. For hydrogenase, the mechanism of reactivation from the oxygen-insensitive inactivated state was observed using photoreduction paired with IR spectroscopy. The [FeFe] hydrogenase from *D. desulfuricans* was observed converting from the H_{tran} state to the resting H_{ox} state, providing evidence for the previously proposed reactivation mechanism for the enzyme.

Combined this work seeks to overcome common obstacles limiting adoption of enzymes as biocatalysts, namely the lack of novel biocatalysts and understanding the mechanistic details underpinning difficult chemical transformations.

Redox Enzymes for Biocatalysis: From Asymmetric Hydrogenation to CO_2 Reduction

By

David W. White

B. S. Troy University, 2017

Advisor: R. Brian Dyer, Ph.D

A dissertation submitted to the Faculty of the James T. Laney School of Graduate Studies of Emory University in partial fulfillment of the requirements for the degree of Doctor of Philosophy in Chemistry

2022

Acknowledgements

I would like to start by thanking the two advisors who have helped me through my grad school career, Dr. Stefan Lutz and Dr. R. Brian Dyer. Both have challenged and encouraged me to become the scientist I am today. I would especially like to thank Dr. Dyer for being patient and providing guidance as I transitioned between labs. I would also like to thank my committee members, Dr. Christine Dunham and Dr. Vincent Conticello, for their helpful suggestions in my research.

I have been blessed with many, many wonderful lab mates, co-workers, and friends during the past 5 years. Starting with the first lab I called home, the former Lutz lab, I would like to thank Ayda Gonzalez, Tamra Blue, Evy Kimbrough, Matthew Jenkins, Sam Iamurri, Kendra Ireland and Elsie Williams for making those first few years of grad school enjoyable. You were my support system and helped build a solid foundation that carried me throughout my years at Emory. To my second home, the Dyer lab, I cannot express how grateful I am for all the help they provided as I switched projects and fields. I would especially like to thank Seth Wiley, Alexia Prokopik, Greg Vansuch, Brooke Andrews, Caterina Netto, Sam Lee, Monica Sanchez and all the other members of the Dyer lab. I would not have been nearly as successful in the second half of grad school without them. Outside of the two labs I have had so much support from fantastic friends. I would like to thank Yasha Duggal, Youngsun Kim, Christella Gordon, Torie Snider and especially Sara Gebre for being an amazing roommate and friend.

I would like to thank my wonderful and incredible girlfriend Parisa Keshavarz-Joud for all her support. She was always by my side whenever I needed it during this long and winding journey. Not only did she provide emotional support, but she also directly contributed to the OYE project

during her time in the Lutz Lab. Needless to say that this dissertation would not have been possible without her, and I am extremely grateful for her support.

Lastly, I'd like to thank my amazing family especially my parents, Ben and Karen White, for their unwavering love they have shown me. All my life they have supported every decision I have made and gone above and beyond to ensure I have everything I need for success. I could not have done this without them, and I appreciate them so very much.

Table of Contents

List of Figures and Tables

Chapter 1

Chapter 2

Chapter 3

Chapter 4

Chapter 1: Introduction

1.1 A Brief Overview of Biocatalysis

Using natural substances to catalyze reactions, termed biocatalysis, is as old as civilization itself with the first documented uses being the fermentation of food and alcoholic beverages.[1-3] Modern biocatalysis began in the 19th century with Anselme Payen and Jean-Françios Persoz discovered that malt could convert starch into sugars, leading to the first identified enzyme dubbed diastase.[2, 4] Today, biocatalysis has emerged as a major industry with a predicted market size of $17.5 billion in 2024.[5] Four main areas exist: food and beverage processing, detergents, biofuel and pharmaceutical (Table 1).[6-8] Other minor areas include using biocatalysis for textile production, paper and pulp processing, and natural gas conversion.

Industry	Applications	Enzymes Used
Food/Beverage	Conversion of starch to sugar	Amylases and glucose isomerases
Pharmaceutical	Synthesis of drugs	Transaminases and ketoreductases
Detergent	Removal of stains and oils	Lipases and proteases
Biofuel	Production of bioethanol and fatty acid esters	Lipases and cellulases

Table 1.1. Sectors of industrial biocatalysis. Adapted from reference Chapman, J.; Ismail, A. E.; Dinu, C. Z. *Catalysts*, 2018, 8(6), 238

Millions of years has allowed nature to design enzymes for highly specific catalysis in life essential reactions. This high specificity causes enzymes to be very attractive for industrial purposes with these catalysts offering excellent regio- and enantioselectivity.[1-3, 5-13] In addition, enzymes are renewable and utilize ambient conditions resulting in a safer and more sustainable synthesis.[12, 14] The environmental aspect of biocatalysis cannot be understated as society is quickly consuming limited resources, notably the precious metals found in organometallic catalysts that are key for numerous industrial transformations.[15, 16] The renewability and high selectivity are double-edged swords as enzymes are designed for specific biological reactions not industrial

purposes. Many enzymes suffer from poor stability and limited substrate scope both factors hindering biocatalysis.[15, 17, 18] Several strategies such as directed evolution to tailor enzymes for industrial processes have been developed to address these issues, but more work is necessary.[10]

1.2 Redox Enzymes and their Cofactors

Redox enzymes, or oxidoreductases, catalyze electron transfers in the form of reduction or oxidation of a substrate.[19] Crucial for life, redox enzymes are involved in various biological processes, but none are more important than those of central metabolism such as cellular respiration and photosynthesis.[20] These redox enzymes build a proton gradient which enables the generation of ATP – the energy 'currency' of biology that allows numerous exergonic reactions vital for life.[21, 22] In the realm of biocatalysis, redox enzymes are widely used with the famous example of ketoreductases to produce chiral alcohols.[23, 24] Ketoreductases catalyze this reaction using a cofactor, namely NADPH, an aspect shared by the majority of redox enzymes.[25]

Cofactors are low molecular weight, non-protein compounds incorporated in enzymes to facilitate a chemical reaction.[26] Typically, these groups interact with the substrate and undergo a chemical transformation but are regenerated at the end of the catalytic cycle. Amino acids are limited to acid-base reactions, but cofactors broaden the chemistry enzymes are capable of. Coenzymes (ex. NADPH) are cofactors that transiently bind to the enzyme while prosthetic groups covalently or non-covalently attach (ex. pyridoxal phosphate).[27] Cofactors range from organic compounds (ex. flavins), metallic clusters (ex. [4Fe-4S]), simple metal ions (ex. Cu, Fe, Zn) or organometallic structures (ex. heme).[25, 28-30] This dissertation will focus on enzymes utilizing flavin and metallic clusters as cofactors.

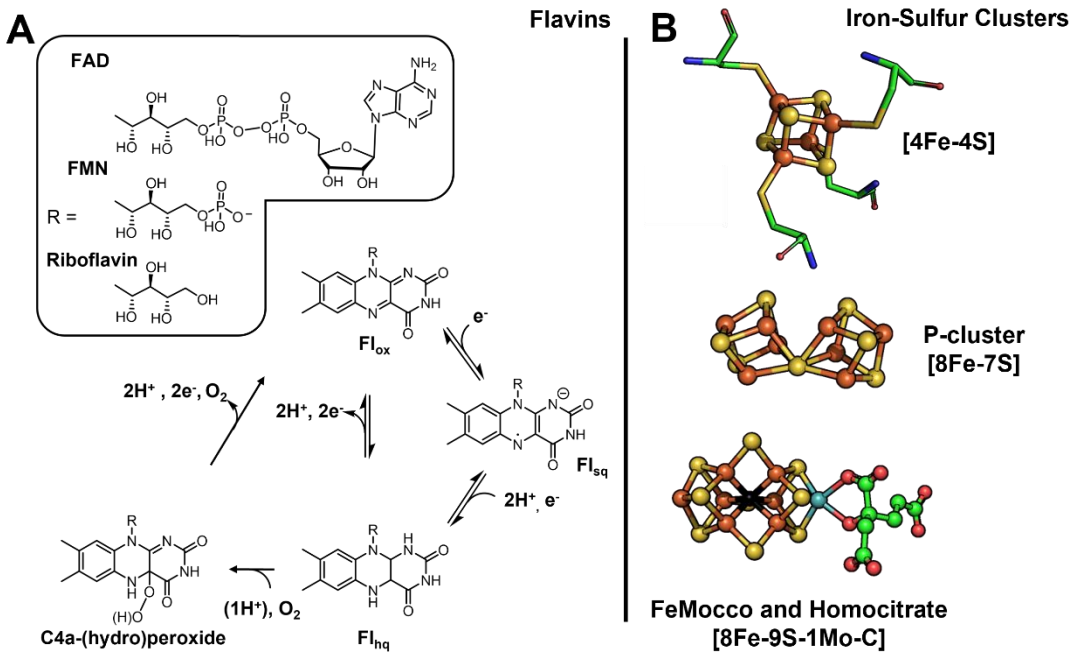

Figure 1.1 Flavin and Iron Sulfur Cluster Cofactors. A) The common catalytic cycle(s) and redox species of flavin cofactors. The box displays the 'tails' of FAD, FMN, and riboflavin. Abbreviations: Fl_{ox} = oxidized flavin, Fl_{sq} = semiquinone, Fl_{hq} = hydroquinone. B) Examples of iron sulfur clusters in enzymes. The common cubane structure of [4Fe-4S] clusters (PDB: 6SG2) and the unique P-cluster and FeMocco cofactors (PDB: 1M1N) of Mo-Nitrogenases.

Riboflavin or vitamin B_2 is an essential nutrient for many organisms (including humans) and consists of a tricyclic isoalloxazine ring and a ribityl tail.[31, 32] While not a cofactor itself, riboflavin is used for the synthesis of the two main flavin cofactors, flavin mononucleotide (FMN) and flavin adenosine dinucleotide (FAD).[31] The isoalloxazine moiety enables exquisite chemical versatility with both flavin cofactors capable of one- and two-electron transfers (Fig. 1A).[33] Flavin-dependent enzymes, or flavoenzymes, exploit this versatility to catalyze a wide range of reactions many of which are useful for biocatalysis.[34] In particular, ene reductases utilize the two electron-reduced hydroquinone state for hydride transfer to activated olefins, producing chiral compounds.[35] Flavin monooxygenases are capable of oxygen insertion in substrates via the

peroxyflavin from the reaction of molecular oxygen and the hydroquinone.[36] Furthermore, flavins are photoactive and recent studies have explored using flavoenzymes for light induced radical catalysis towards novel reactions.[37]

It is estimated that nearly half of all proteins contain metals ranging from singular metal ions to large complex heterometallic clusters.[38] In the case of metallic clusters, one of the most ubiquitous in nature are iron sulfur clusters.[39-41] Formed from iron and inorganic sulfide, these clusters come in a variety of arrangements and are primarily for electron transport due to the intrinsic electron delocalization (Fig. 1B).[40] For enzymes, iron sulfur clusters are often used as wires to move electrons from binding partners to buried active sites but can also form reaction centers especially with the incorporation of other metals.[41, 42] The classic example of this is the Mo-dependent nitrogenase, the catalyst for biological N_2 fixation.[43, 44] Nitrogenase, composed of the Fe protein and MoFe protein, reduces N_2 to 2 NH_3 molecules using 8 electrons/protons and 16 equivalents of ATP.[45] In brief, the Fe protein transfers one electron at a time to the MoFe protein after hydrolysis of two ATP. This exchange occurs from the cubane [4Fe-4S] of the Fe protein to the unique [8Fe-7S] P-cluster which resembles two connected [4Fe-4S] clusters that share a sulfide corner (Fig. 1B). The P-cluster initiates the final electron transfer to the active site FeMoco (containing 7 Fe, 1 Mo, and one carbide ion) where N_2 is finally converted to ammonia (Fig. 1B). It is due to the complexity of the cofactors and the enzyme itself that it is able to catalyze such a challenging reaction.[42, 45] Metallic clusters enable enzymes to catalyze other difficult, small molecule reactions such as CO_2 reduction and hydrogen production, both of which will be discussed in more detail in later sections. Unfortunately, many of these metallic cofactors are oxygen sensitive and rely on accessory proteins for proper enzyme loading.[46, 47] These factors limit the biocatalytic applications, but several are beginning to be utilized specifically for sustainable

fuel production.[48, 49] While not necessarily biocatalysis, general mechanistic understanding of these enzymes and their metallic cluster will enable the development of better sustainable catalysts such as artificial metalloenzymes.[50, 51]

1.3 Asymmetric Hydrogenation via Old Yellow Enzymes

In 2001, William S. Knowles and Ryoji Noyori won half of the Nobel prize for their contributions to asymmetric hydrogenation, enabling chiral products from prochiral starting material.[52] A powerful synthetic tool, asymmetric hydrogenation of alkenes is of particular importance for the pharmaceutical industry with the chirality of a drug directly affecting efficacy.[53, 54] Agrochemical, fragrance, and food industries also utilize asymmetric synthesis to produce chiral compounds. From an atom economy viewpoint, asymmetric hydrogenation is an excellent and 'green' reaction that produces little waste.[55] Unfortunately, the most effective and widely used catalysts are noble metal ions such as Rh, Ru, and Ir which are coordinated by chiral bidentate ligands.[56] The use of these precious metals has raised sustainability issues mostly due to low abundance in the Earth's crust causing increased prices as reserves are becoming depleted.[57] Catalysts using more accessible first row metals are being developed but are not as effective.[57] A more bio-friendly alternative solution is to use ene reductases, particularly those from the Old Yellow Enzyme (OYE) family. [35]

1.3.1 The Old Yellow Enzymes

Originally named "yellow enzyme" when identified in 1932, OYEs were the first flavin-dependent enzyme discovered.[58, 59] Today, the OYE family is the most characterized group of ene reductases and have catalyzed asymmetric hydrogenation reactions for the synthesis of various pharmaceuticals such as pregabalin (anti-epileptic), latanoprost and bitamoprost (glaucoma drugs), and flurbiprofen (anti-inflammatory) with excellent enantioselectivity.[60-63] Catalysis in OYEs is

facilitated using an FMN cofactor, giving the enzymes their signature yellow color.[35] The cofactor is housed within an α8/β8-fold triose-phosphate isomerase (TIM) barrel that forms the 'OYE-like' domain (Fig. 3A). Over a hundred OYEs have been characterized for biocatalytic purposes or understanding their native function.[60, 61] These enzymes are found in a wide range of organisms such as bacteria, fungi, plants, protists, and archaea. Characterized enzymes are organized into 5 classes based on conserved residues with the two largest groups being the OYE1-based Class I and YqjM-based Class II OYEs.[64] Class I OYEs are typically longer and form monomers or homodimers in solution while Class II OYEs are shorter in length and exclusively form functional dimer pairs.[61] Several minor groups exist and the classification system is covered in more detail in Chapter 2.

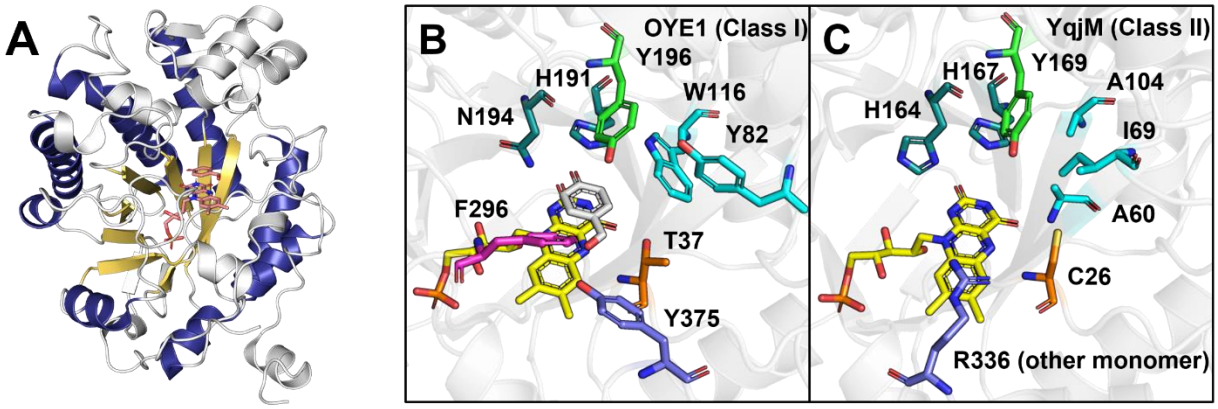

Figure 1.2 The structure and active site residues of OYEs. A) The TIM barrel fold of OYEs with the repeating α-helix (dark blue) and β-sheets (gold) highlighted. The FMN and inhibitor (orange) are also present. (PDB: 1OYB) B) and C) Key active site residues for Class I (OYE1, PDB: 1OYB) and Class II (YqjM, PDB:1Z48). The FMN is yellow, the EWG coordinating residues are dark green, the catalytic tyrosine is light green, the 'right' side residues in cyan, the redox modulator residue in orange, the 'front' side residues in dark blue and the 'left' side in magenta.

The key conserved residues of OYEs are located in the flexible loops between the repeating secondary structures of the TIM barrel (Fig. 2B and 2C). FMN binding is facilitated by electrostatic interactions with the ribityl tail, terminal phosphate, and hydrophilic section of the isoalloxazine ring.[61] The FMN cofactor forms the 'bottom' of the active site with the substrate binding above. The standard OYE substrate is an alkene with an electron withdrawing group (EWG), usually aldehyde, ketone, nitro or ester.[61] Proper substrate binding over FMN is achieved using hydrogen bonding of the EWG to either a double histidine (H164 and H167 in YqjM) or histidine/asparagine pair (H191 and N194 in OYE1) near the 'front' of the active site.[60] Above the substrate is a conserved, catalytic tyrosine (Y196 and Y169 in OYE1 and YqjM) residue at the 'top' of the active site, capable of proton donation.[35] The catalytic cycle for ene reduction follows a ping-pong mechanism starting with reduction of FMN via NAD(P)H. Preference for NADH or NADPH is not well understood in OYEs with recent studies concluding that may be controlled by specific residues or conformations of the β3 loop.[65] Once reduced, the FMN transfers a hydride to the β-position of the activated alkene and the tyrosine residue protonates the α-position, forming a *trans*-hydrogenated product (Fig. 3). Conservation of the key active site residues results in similar substrate binding modes and nearly identical stereoselectivity amongst characterized OYEs.[66] Opposite enantioselectivity can be achieved through substrate design or rational mutagenesis to induce a 'flipped' binding mode.[60]

Directed evolution studies of OYE1 demonstrated W116 (OYE1 numbering) as a key residue which when substituted could enabled the 'flipped' bind mode and production of the

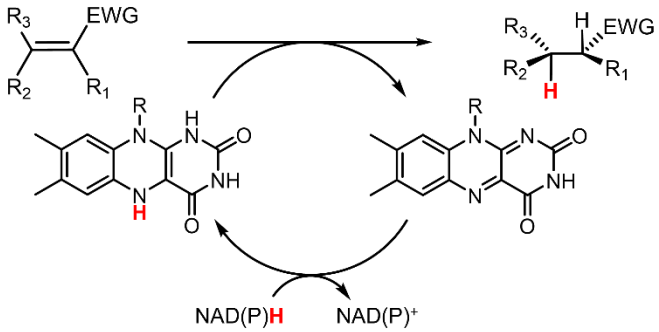

Figure 1.3 The catalytic cycle of OYEs for asymmetric hydrogenation. A hydride (red) is transferred from NAD(P)H to the FMN cofactor. The hydride is transferred to the β of the α,β-unsaturated compound.

opposite enantiomer.[67] The tryptophan is conserved in Class I OYEs and forms a portion of the 'right' side of the active site. Replacement of tryptophan with isoleucine allowed the bulky fragment of carvone to flip to the right side, a different binding orientation to WT and confirmed via crystallography. In addition to W116, mutation of other residues lining the active site pocket including Y82 and F296 ('right' and 'left' side) have resulted in different stereoselectivities for OYE1 and other enzymes.[68, 69] In Class II enzymes, similar opposite selectivity results were observed with 'right' side mutations of A60, I69, and A104 (YqjM numbering) to bulkier residues.[70] Unfortunately, attempts to replicate the mutations in additional OYEs, other than the original enzyme studied, has had mixed results.[60, 68]

Another key residue and hot spot for directed evolution studies is the T37 (OYE1) or C26 (YqjM) that interacts with the N5 of FMN, shown to modulate the redox potential of the enzyme. Mutation of T37 to alanine in OYE1 was shown to decrease the redox potential, but it is unclear to what extent.[71] Catalytically, this mutation increased ene reductase activity 2- to 3-fold which is expected as lowering of the redox potential would cause reduction to be more favorable. For class II enzymes, the same alanine mutation (C25A) did not noticeably lower the redox potential in XenA, but a substantial increase in potential was observed with a serine mutation (C25S).[72] As expected, the C25S variant was less active than WT, but similar to OYE1 the C25A enzyme showed double the activity despite no change in the redox potential. In another study of a class II OYE, the same mutations in OYEo2a showed conflicting results with the C25S and C25G variant

twice as active compared to WT and the C25A.[73] The redox potentials of this variant were not determined. For all OYEs, these mutations also affect NAD(P)H and substrate binding with both factors impacting ene reductase activity.[71-73]

1.3.2 The Other Old Yellow Enzymes

Beyond the OYE-like domain, several related multi-domain subfamilies exist.[74, 75] The oxygen-sensitive 2-enoate reductases contain a separate NAD(P)H binding domain which houses an FAD cofactor.[76] Crystal structures of this subgroup suggest the catalytic cycle begins with reduction of FAD by NAD(P)H, electrons are then transferred to the active site in the OYE-like domain through an intermediate [4Fe-4S] cluster.[77] Other OYEs also utilize NAD(P)H without this secondary domain so it is unclear why the 2-enoate reductases require it and what impact it may have on catalysis. Despite the oxygen sensitivity, 2-enoate reductases are utilized as biocatalysts specifically for the hydrogenation of unsaturated carboxylic acids as a biosynthetic route to nylon production.[78] In contrast to the 2-enoate reductase, the separate domains of 2-aminobenzyoyl-CoA monooxygenase/reductases catalyze two different reactions.[79] At the N-terminus is a flavin-dependent monooxygenase domain resembling *p*-hydroxybenzoate hydroxylase while the C-terminus is the OYE-like domain.[80] The enzyme initially hydroxylates an aromatic substrate and reduces it to dearomatize the compound.[79, 80] Few studies have explored this subgroup, but the enzyme acts as a mini cascade reaction capable of setting the functional group necessary for OYE catalyzed ene reduction.

1.3.3 Native Function and Beyond

A general native function for most OYEs is still elusive.[61] It is speculated that the enzymes may play a role in the degradation of toxic xenobiotic compounds or in oxidative stress responses.[81-83] Several plant and fungal OYEs have been implicated in biosynthetic pathways of

secondary metabolites.[84, 85] OYEs, specifically the 12-oxophytodienoate reductases (OPR) are involved in the biosynthesis of jasmonic acid, used by many plants as a defense and stress response.[86-88] OYEs are also present in the bioproduction of fungal compounds such as aflatoxin, ilicicolin H and ergot alkaloids.[84, 89, 90] Interestingly, OYEs from the parasites *Trypansoma cruzi* (Chagas disease) and *Leishmania donovani* (leishmaniasis) appear to be involved in host-parasite interactions and interact with drugs resulting in increased efficacy of the medicine.[91-93] Nearly all of the native functions mentioned require the enzyme to hydrogenate an activated alkene substrate, but several utilize other reactions such as epimerization.[89]

OYEs are not limited to asymmetric hydrogenation as hydride transfer can catalyze a number of reactions.[94] The degradation of explosives such as TNT have led to several OYEs being utilized for bioremediation processes.[95-97] The enzyme catalyzes the reduction of nitro groups to amines or in the case of TNT, dearomatization as well.[98] The enzymes can also react with molecular oxygen to form hydrogen peroxide to cause spontaneous epoxidation of alkenes and sulfur oxidation.[94] So far one OYE, GkOYE from *Geobacillus kaustophilus*, was observed catalyzing the reverse, desaturase reaction albeit at elevated (70˚C) temperatures.[99] Using the artificial flavin 8-CN-FMN to increase the redox potential allowed OYE1 to catalyze the same reaction, but at the cost of its ene reductase activity.[100] A similar reaction is the redox-neutral disproportionation reaction of cyclic enones to phenols through oxidation aromatization.[101] Merck was able to utilize the reaction to produce naphthols precursors for the synthesis of naproxen and other pharmaceutical drugs.[102] Recent studies have focused on using OYEs for light induced radical catalysis. Exploiting the photocatalytic capabilities of FMN, OYEs were capable of forming C-C bonds including ring formation.[37] Its likely more novel reactions will be discovered expanding the catalytic toolbox of OYEs.

1.4 Carbon Monoxide Dehydrogenase as Catalysts for CO_2 Reduction

Over the past 300 years, fossil fuels have powered the vast technological advancements that moved society from agrarian to industrial.[103] Unfortunately, the price of progress is steep. The reliance on fossil fuels to run society has caused immense harm to the environment.[104-106] Specifically, the combustion of fossil fuels has dramatically increased the amount of carbon dioxide present in the atmosphere, currently over 400 ppm and the highest ever recorded since the last ice age.[107, 108] As a greenhouse gas, the continuous emission of carbon dioxide is directly responsible for the steady rise in global temperatures contributing to unpredictable changes in the climate.[109] The growing world population and ongoing industrial development will only increase the demand of fossil fuels further, exacerbating the issue.[110, 111] Even without the looming threat of ecological disaster, society cannot continue utilizing this resource as it requires millions of years to form, and reserves are rapidly being depleted.[104, 112] New energy solutions must be developed to prevent irreparable harm to the Earth and an energy crisis.[113-115]

1.4.1 Artificial Photosynthesis

Every hour the sun blankets the Earth with more solar energy than what is used by today's society in a year.[114, 116, 117] Photovoltaic cells to harvest this solar energy into electricity have become more efficient and cheaper enabling broader adoption.[117] Unfortunately, sun illumination is diurnal and the highest energy demand is typically after dark, obligating the need to store this energy.[118] Battery technology is currently inefficient in large energy storage with energy densities much lower than that of fossil fuels.[117, 119, 120] Furthermore, several vital energy intensive processes such as long-distance sea or air transportation cannot currently be achieved using solely electricity and will require chemical fuels for the foreseeable future.[117] A promising solution is storing the solar energy in the form of chemical bonds.[48, 51, 121] Essentially this is photosynthesis, the complex

process responsible for most life on Earth, the oxygen in the atmosphere, and technically fossil fuels as they are simply ancient, stored light energy.[122, 123] Photosynthesis converts the abundant resources of light, water and CO_2 to oxygen and chemical energy in the form of sugars.[124] Sunlight is focused by an antenna complex and utilized in Photosystem II to split water into 4 electrons and protons which are transferred to Photosystem I and converted into ATP or NADPH which is utilized by the Calvin cycle to produce carbohydrates using CO_2.[114, 122] Artificial photosynthesis adopts this concept towards utilizing the virtually unlimited quantity of sunlight into synthetic chemical fuels.[114-117]

Light induced CO_2 reduction via artificial photosynthesis could create carbon neutral fuels which would help alleviate the issues of CO_2 emissions and energy storage in a manner acceptable for societal use.[119, 125] The reaction requires an antenna or photosensitizer to harvest light energy and transfer electrons either inter- or intramolecularly to a reaction center to reduce CO_2.[114] Common photosensitizers include semiconductors and metal complexes as organic compounds are not considered due to lower stability despite greater photoefficiencies.[117, 126, 127] For CO_2 reduction, transition metals ranging from metalloporphyrins to Ru complexes in addition to heterogeneous semiconductor catalysts have been developed.[119, 128, 129] The reaction is not trivial, as CO_2 is inert and relatively stable. Comparing the redox half reactions, the one electron reduction of CO_2 requires -1.9 V to form the bent radical anion needed to activate it further.[130, 131] Multi-electron reactions are more thermodynamically favorable, with the two-electron reduction of CO_2 to CO at -0.52 V.[131] Unfortunately, current CO_2 catalysts suffer from low photostability, poor selectivity, and inadequate efficiency necessitating large over-potentials which results in parasitic hydrogen evolution.[131, 132] Nature has already developed excellent efficient and selective CO_2 biocatalysts such as the [NiFe] carbon monoxide dehydrogenases (CODH).[133-135]

1.4.2 The [NiFe] Carbon Monoxide Dehydrogenases

[NiFe] CODHs catalyze a reversible, biological version of the water gas shift reaction converting CO and water into CO_2.[134] Three classes exist for [NiFe] CODHs based on the function of the enzyme with mono-, bi, and multifunctional groups.[135, 136] Monofunctional CODHs do not form an enzyme complex and are catalytically biased toward CO oxidation.[137-139] Natively they are most often associated with energy-conserving hydrogenases for CO metabolism as a sole carbon source.[139] In acetogens, the bifunctional CODHs form a complex with acetyl-CoA synthase (ACS) and are part of the 'Western' branch of the Wood-Ljundahl pathway.[140, 141] Here CODH converts CO_2 into CO which is transferred through a 140 Å hydrophobic tunnel to the A-cluster of ACS where it is transformed into acetyl-CoA for cellular carbon and energy purposes.[131, 142] Lastly the multifunctional CODH, in addition to ACS, is a component of the large acetyl-CoA decarbonyl/synthase complex involved in methanogenesis from acetate.[143]

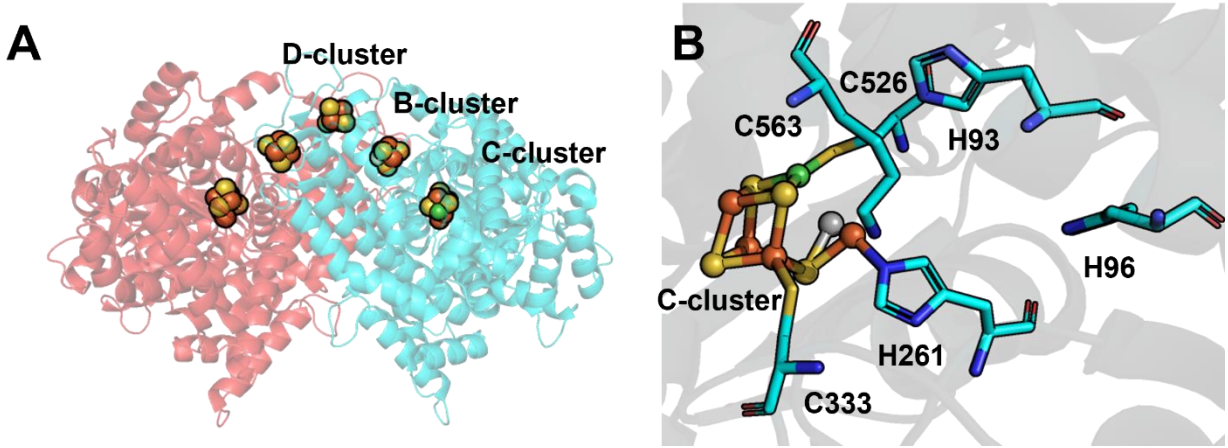

Figure 1.4 The structure and active site of monofunctional CODH. A) The homodimeric structure with the metal clusters highlighted. The two monomers are shown in different colors (red and cyan, PDB: 3B51). B) The C-cluster and key residues in the active site (*Ch*CODH II numbering). The metal cluster is colored with orange representing iron, yellow is sulfur, and nickel is green. The gray is the alternative position of the pendant Fe1. (PDB: 3B51)

The biologically active form of CODHs is a homodimer comprising 5 metal clusters (Fig. 4A).[131, 134-136] Each monomer contains a distorted [$NiFe_3S_4$] cluster termed the C-cluster that resembles a distorted cubane iron sulfur cluster.[135] An additional pendant Fe to the C-cluster is also present. The unusual C-cluster is the active site where CO_2 is reduced to CO.[144] At 11 Å away from each C-cluster is the B-cluster, a [4Fe-4S] which is theorized to facilitate electron transfer to the C-cluster.[131] The B-cluster of one monomer is closer to the C-cluster of the other monomer. Bridging the two subunits is the D-cluster, typically a [4Fe-4S] cluster. Despite being 10 Å from both B-clusters, spectroscopic studies indicate it is not reduced at -530 mV, the redox potential of CO/CO_2 couple, suggesting the D-cluster does not participate in electron transfer.[145] An unusual [2Fe-2S] D-cluster of *Dv*CODH was recently shown to protect the enzyme from oxygen and it is possible that this may be the role of the metal cluster.[146] The multifunctional CODHs contain additional iron sulfur clusters termed E- and F-clusters which are proposed to transfer electrons from ferredoxin to the B-clusters as part of the ACDS complex.[143]

The oxidized state of the C-cluster or C_{ox} is inactive and requires a one electron reduction from the B-cluster to form the resting state of C_{red1}.[131, 135] The proposed mechanism of CO_2 reduction is described in detail in Chapter 3. Briefly, two more electrons are transferred to further reduce the C-cluster to the C_{red2} and CO_2 binds in bent fashion with the carbon atom coordinated to the Ni and an oxygen atom to the pendant Fe.[134, 135, 147] The oxygen coordinated to the Fe is protonated and the C-O bond is cleaved.[135] The remaining CO bound to the Ni disassociates and enters the hydrophobic gas channel while the C-cluster returns to C_{red1}.[134] For CODH/ACS this channel connects to the A-cluster while the monofunctional CODHs contain a unique gas channel to allow diffusion of the product.[142] This channel is blocked off in CODH/ACS presumably to prevent loss of substrate.[131] Apart from the C-cluster, several key residues are necessary for proper

CODH activity. In *Ch*CODH II from *Carboxydothermus hydrogenoformans*, H93, H263 and K563 in the active site all form hydrogen bonds with either CO_2, CO or the water bound to the pendant Fe in the resting state (Fig. 4B).[144, 148, 149] Furthermore, the source of protons for the reaction may come from a histidine tunnel beginning at H93 and stretches to the protein surface.[150] Alanine substitution of residues K563 and H93 were shown to inactivate the enzyme.[150, 151] Despite the extensive studies, the catalytic details are not fully resolved yet.

As a catalyst, CODH has been integrated into a variety of electro- and photocatalytic systems. Incorporation of CODH into an electrode also enables exploitation of the reversibility of the enzymes. In this case, *Rr*CODH from *Rhodospirillum rubrum* was immobilized onto multiwalled carbon nanotubes and used as a catalyst for CO_2 reduction and CO oxidation with turnover frequencies up to 420 s^{-1} and 150 s^{-1}.[152] CO oxidation produces CO_2 which is not ideal, but could be generates electrons and could be coupled with endergonic reactions. *Ch*CODH I from *C. hydrogenoformans* was combined with a hydrogenase in a graphite electrode for the water gas shift reaction, producing H_2 from CO oxidation.[153] Using a cobaltocene derived redox polymer as a mediator, *Ch*CODH II also from *C. hydrogenoformans*, was able to reach turnover frequencies of 2.7 s^{-1}.[154] For photobiocatalysis, no other CO_2 reducing enzyme is utilized more than *Ch*CODH I.[155] Recently, a photosystem composed of silver nanoclusters and CODH I attached to TiO_2 exhibited excellent stability with 250000 turnovers and a max turnover frequency of 20 s^{-1} though the quantum efficiency or photons into product was low at 1.5%.[156] Further use of CODH for biocatalyst are limited, mainly due to issues such as oxygen sensitivity and complicated heterologous expression although recent studies have attempted to address this.[157, 158] Beyond biocatalysis, understanding the mechanistic factors that enable CODH to facilitate this difficult

reaction with low, almost nonexistent overpotentials and Earth abundant metals will enable the development of better, more efficient catalysts.[159-162]

1.5 Hydrogen Production using Hydrogenase

Hydrogen is one of the key alternative energy resources for transitioning away fossil fuels due to its high energy density and lack of CO_2 emissions upon combustion.[163-165] These factors render hydrogen an ideal energy carrier and storage medium for intermittent renewable energy sources such as solar and wind or artificial photosynthesis.[50, 116, 166] Beyond energy, ammonia is almost entirely produced via the hydrogen-fueled Haber-Bosch process.[167] Ammonia is used to manufacture fertilizer which improves crop productivity and has enabled the explosion in global population.[168] Due to these uses and others such as oil refining and metallurgy, hydrogen demand is expected to increase to 120 million tons by 2024.[169, 170] Current hydrogen production is not sustainable as the vast majority is produced using fossil fuel process such as steam methane reforming or coal gasification which emit CO_2.[169] Carbon capture technologies have been utilized but are costly and not completely effective.[171] The ideal route for green hydrogen production is water electrolysis. Currently, the process only accounts for 4% of all hydrogen produced as water electrolysis requires precious metal catalysts operating at large overpotentials resulting in a costly and inefficient method.[172, 173] An alternative to these catalysts are metalloenzymes such as hydrogenases which are capable of efficient hydrogen evolution using earth abundant metals.[174]

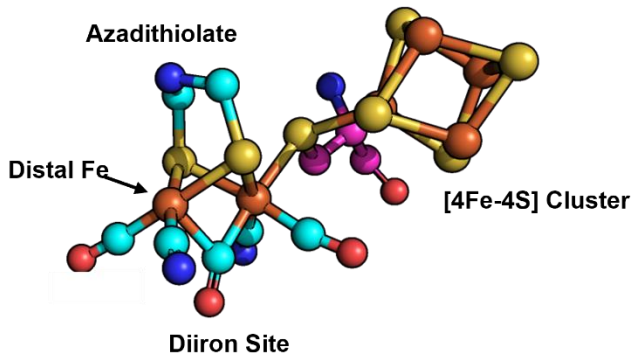

Figure 1.5 The H-cluster of [FeFe] hydrogenases. On the left is the diiron site with the azadithiolate ligand and the distal Fe. On the right is the [4Fe-4S] cluster. In between is a cysteine (magenta, PDB: 6YF4)

Three classes of hydrogenase exist based on the cofactor structure: [FeFe], [NiFe], and [Fe] only.[175-177] Of the three, the [FeFe] hydrogenase are catalytically biased towards proton reduction with rates in excess of 10,000 H_2/s but are highly oxygen sensitive in contrast to the [NiFe].[174, 178, 179] All [FeFe] hydrogenases contain a unique H-cluster cofactor composed of a diiron metallic reaction site connected to a [4Fe-4S] cluster via a cysteine residue (Fig. 5). The [4Fe-4S] cluster helps store and transfer electrons for proton reduction at diiron site.[174] An azadithiolate ligand bridges the two metals of the diiron site with the nitrogen functioning as a base in addition to the acidic distal Fe forming a 'frustrated Lewis pair' for catalysis.[174] Also, the iron ions are coordinated by strong-field ligands of carbon monoxide and cyanide which are vital for determining the catalytic cycle as the infrared stretches shift based on the electronics of the H-cluster.[180] Beyond the catalytic cofactor, additional iron sulfur clusters are present for electron transfer from binding partners to the H-cluster.[176] Likewise, conserved ionizable residues relay the necessary protons to the active site.[181]

The catalytic bias of [FeFe] hydrogenases has led to the enzymes being incorporated into a variety of photobiocatalytic systems. Using a molecular wire, the [FeFe] hydrogenases have been tethered to Photosystem I for hydrogen production with rates of >560 s^{-1}.[182] Semiconductor photosensitizers have also been utilized, such as CdS nanorods enabling quantum efficiencies of

~20% possible.[183] Despite these progresses, oxygen sensitivity remains the major obstacle for further catalytic uses of this enzyme.[184] Several [FeFe] hydrogenases are capable of forming an inactive O_2 tolerant state, preventing degradation and this will be discussed in more detail in Chapter 4.[185, 186] Similar to CODH, the active site and interacting residues have been a template for numerous mimetics attempting to reproduce the excellent catalytic performance of hydrogenase.[187-191] Further studies into these enzymes will provide insights to catalyst development.

1.6 Aims and Scope of the Dissertation

Enzymes perform the necessary reactions for all of life. Millions of years of selection has designed enzymes to be efficient and specific both useful characteristics for industrial catalysts. For biocatalysis, enzymes have been used since ancient times, but several limitations exist for enzyme-based catalysis. This dissertation investigated three separate enzymes capable of key catalytic transformation for society.

Chapter 2 focuses on the exploring the genetic diversity of the Old Yellow Enzyme family specifically to evaluate the family's biocatalytic potential for asymmetric hydrogenation and beyond. Bioinformatic techniques were employed revealing a wealth of new sequence and phylogenetic information. Representative sequences from these unexplored regions were selected and evaluated as possible new biocatalysts. This work represents the first comprehensive exploration of the enzyme and provides several key findings into understanding and application of OYEs.

Chapter 3 examines the mechanism of CO_2 reduction in carbon monoxide dehydrogenases using spectroscopic techniques. To facilitate this, an efficient biohybrid photosystem was developed to activate the enzyme. The photosystem aided in light initiated steady-state and pre-

steady state infrared investigations of CODH-catalyzed CO_2 reduction. This reaction is particularly difficult, and it is not well understood how the enzyme is able to function efficiently. The development of the photosystem and spectroscopic studies will be used to unravel this mechanism.

Lastly, the mechanism of reactivation for the oxygen tolerant state of [FeFe] hydrogenases is explored in Chapter 4. Using light titrations to reduce the enzyme allows for the observations of the catalytic cycle using spectroscopy.

1.7 References

1. Pyser, J. B.; Chakrabarty, S.; Romero, E. O.; Narayan, A. R., State-of-the-art biocatalysis. *ACS Cent. Sci.* **2021,** *7* (7), 1105-1116.

2. Bornscheuer, U.; Buchholz, K., Highlights in biocatalysis–historical landmarks and current trends. *Engineering in Life Sciences* **2005,** *5* (4), 309-323.

3. Turner, M. K., Biocatalysis in organic chemistry (Part I): past and present. *Trends Biotechnol.* **1995,** *13* (5), 173-177.

4. Buchholz, K.; Kasche, V.; Bornscheuer, U. T., *Biocatalysts and enzyme technology*. John Wiley & Sons: 2012.

5. Pellis, A.; Cantone, S.; Ebert, C.; Gardossi, L., Evolving biocatalysis to meet bioeconomy challenges and opportunities. *New biotechnology* **2018,** *40*, 154-169.

6. Zaks, A., Industrial biocatalysis. *Curr. Opin. Chem. Biol.* **2001,** *5* (2), 130-136.

7. Basso, A.; Serban, S., Industrial applications of immobilized enzymes—A review. *Molecular Catalysis* **2019,** *479*, 110607.

8. Chapman, J.; Ismail, A. E.; Dinu, C. Z. Industrial Applications of Enzymes: Recent Advances, Techniques, and Outlooks *Catalysts* [Online], 2018.

9. Bell, E. L.; Finnigan, W.; France, S. P.; Green, A. P.; Hayes, M. A.; Hepworth, L. J.; Lovelock, S. L.; Niikura, H.; Osuna, S.; Romero, E., Biocatalysis. *Nature Reviews Methods Primers* **2021,** *1* (1), 1-21.

10. Bornscheuer, U. T.; Huisman, G. W.; Kazlauskas, R. J.; Lutz, S.; Moore, J. C.; Robins, K., Engineering the third wave of biocatalysis. *Nature* **2012,** *485* (7397), 185-194.

11. Rodríguez Benítez, A.; Narayan, A. R., Frontiers in biocatalysis: profiling function across sequence space. ACS Publications: 2019.

12. Woodley, J. M., New frontiers in biocatalysis for sustainable synthesis. *Current Opinion in Green and Sustainable Chemistry* **2020,** *21*, 22-26.

13. Wu, S.; Snajdrova, R.; Moore, J. C.; Baldenius, K.; Bornscheuer, U. T., Biocatalysis: enzymatic synthesis for industrial applications. *Angew. Chem. Int. Ed.* **2021,** *60* (1), 88-119.

14. Woodley, J. M., Accelerating the implementation of biocatalysis in industry. *Appl. Microbiol. Biotechnol.* **2019,** *103* (12), 4733-4739.

15. Sheldon, R. A.; Brady, D., Broadening the scope of biocatalysis in sustainable organic synthesis. *ChemSusChem* **2019,** *12* (13), 2859-2881.

16. Sheldon, R. A.; Brady, D.; Bode, M. L., The Hitchhiker's guide to biocatalysis: recent advances in the use of enzymes in organic synthesis. *Chemical science* **2020,** *11* (10), 2587-2605.

17. Woodley, J. M., Ensuring the Sustainability of Biocatalysis. *ChemSusChem* **2022**, e202102683.

18. Adams, J. P.; Brown, M. J. B.; Diaz-Rodriguez, A.; Lloyd, R. C.; Roiban, G. D., Biocatalysis: a pharma perspective. *Adv. Synth. Catal.* **2019,** *361* (11), 2421-2432.

19. Prier, C. K.; Kosjek, B., Recent preparative applications of redox enzymes. *Curr. Opin. Chem. Biol.* **2019,** *49*, 105-112.

20. Léger, C.; Bertrand, P., Direct electrochemistry of redox enzymes as a tool for mechanistic studies. *Chem. Rev.* **2008,** *108* (7), 2379-2438.

21. Mountfort, D. O., Evidence for ATP synthesis driven by a proton gradient in Methanosarcinabarkeri. *Biochem. Biophys. Res. Commun.* **1978,** *85* (4), 1346-1351.

22. Kramer, D. M.; Cruz, J. A.; Kanazawa, A., Balancing the central roles of the thylakoid proton gradient. *Trends in plant science* **2003,** *8* (1), 27-32.

23. Clouthier, C. M.; Pelletier, J. N., Expanding the organic toolbox: a guide to integrating biocatalysis in synthesis. *Chem. Soc. Rev.* **2012,** *41* (4), 1585-1605.

24. Pollard, D. J.; Woodley, J. M., Biocatalysis for pharmaceutical intermediates: the future is now. *Trends Biotechnol.* **2007,** *25* (2), 66-73.

25. Liu, W.; Wang, P., Cofactor regeneration for sustainable enzymatic biosynthesis. *Biotechnol. Adv.* **2007,** *25* (4), 369-384.

26. Kara, S.; Schrittwieser, J. H.; Hollmann, F.; Ansorge-Schumacher, M. B., Recent trends and novel concepts in cofactor-dependent biotransformations. *Appl. Microbiol. Biotechnol.* **2014,** *98* (4), 1517-1529.

27. Mordhorst, S.; Andexer, J. N., Round, round we go–strategies for enzymatic cofactor regeneration. *Natural Product Reports* **2020,** *37* (10), 1316-1333.

28. Richter, M., Functional diversity of organic molecule enzyme cofactors. *Natural product reports* **2013,** *30* (10), 1324-1345.

29. Hausinger, R. P., New metal cofactors and recent metallocofactor insights. *Current opinion in structural biology* **2019,** *59*, 1-8.

30. Andreini, C.; Bertini, I.; Cavallaro, G.; Holliday, G. L.; Thornton, J. M., Metal ions in biological catalysis: from enzyme databases to general principles. *JBIC Journal of Biological Inorganic Chemistry* **2008,** *13* (8), 1205-1218.

31. Pinto, J. T.; Zempleni, J., Riboflavin. *Advances in Nutrition* **2016,** *7* (5), 973-975.

32. Schwechheimer, S. K.; Park, E. Y.; Revuelta, J. L.; Becker, J.; Wittmann, C., Biotechnology of riboflavin. *Appl. Microbiol. Biotechnol.* **2016,** *100* (5), 2107-2119.

33. Dockrey, S. A. B.; Narayan, A. R. H., Flavin-dependent biocatalysts in synthesis. *Tetrahedron* **2019,** *75* (9), 1115-1121.

34. de Gonzalo, G.; Fraaije, M. W., Recent developments in flavin-based catalysis. *ChemCatChem* **2013,** *5* (2), 403-415.

35. Toogood, H. S.; Scrutton, N. S., New developments in 'ene'-reductase catalysed biological hydrogenations. *Curr. Opin. Chem. Biol.* **2014,** *19*, 107-115.

36. Huijbers, M. M. E.; Montersino, S.; Westphal, A. H.; Tischler, D.; van Berkel, W. J. H., Flavin dependent monooxygenases. *Arch. Biochem. Biophys.* **2014,** *544*, 2-17.

37. Black, M. J.; Biegasiewicz, K. F.; Meichan, A. J.; Oblinsky, D. G.; Kudisch, B.; Scholes, G. D.; Hyster, T. K., Asymmetric redox-neutral radical cyclization catalysed by flavin-dependent 'ene'-reductases. *Nature chemistry* **2020,** *12* (1), 71-75.

38. Finkelstein, J., Metalloproteins. *Nature* **2009,** *460* (7257), 813-813.

39. Brzóska, K.; Meczyńska, S.; Kruszewski, M., Iron-sulfur cluster proteins: electron transfer and beyond. *Acta Biochim. Pol.* **2006,** *53* (4), 685-691.

40. Johnson, D. C.; Dean, D. R.; Smith, A. D.; Johnson, M. K., Structure, function, and formation of biological iron-sulfur clusters. *Annu. Rev. Biochem* **2005,** *74*, 247.

41. Beinert, H.; Holm, R. H.; Münck, E., Iron-Sulfur Clusters: Nature's Modular, Multipurpose Structures. *Science* **1997,** *277* (5326), 653-659.

42. Fontecilla-Camps, J. C.; Amara, P.; Cavazza, C.; Nicolet, Y.; Volbeda, A., Structure–function relationships of anaerobic gas-processing metalloenzymes. *Nature* **2009,** *460* (7257), 814-822.

43. Rutledge, H. L.; Tezcan, F. A., Electron Transfer in Nitrogenase. *Chem. Rev.* **2020,** *120* (12), 5158-5193.

44. Seefeldt, L. C.; Yang, Z.-Y.; Lukoyanov, D. A.; Harris, D. F.; Dean, D. R.; Raugei, S.; Hoffman, B. M., Reduction of Substrates by Nitrogenases. *Chem. Rev.* **2020,** *120* (12), 5082-5106.

45. Seefeldt, L. C.; Hoffman, B. M.; Dean, D. R., Mechanism of Mo-Dependent Nitrogenase. *Annu. Rev. Biochem* **2009,** *78* (1), 701-722.

46. Leach, M. R.; Zamble, D. B., Metallocenter assembly of the hydrogenase enzymes. *Curr. Opin. Chem. Biol.* **2007,** *11* (2), 159-165.

47. Boer, J. L.; Mulrooney, S. B.; Hausinger, R. P., Nickel-dependent metalloenzymes. *Arch. Biochem. Biophys.* **2014,** *544*, 142-152.

48. Evans, R. M.; Siritanaratkul, B.; Megarity, C. F.; Pandey, K.; Esterle, T. F.; Badiani, S.; Armstrong, F. A., The value of enzymes in solar fuels research – efficient electrocatalysts through evolution. *Chem. Soc. Rev.* **2019,** *48* (7), 2039-2052.

49. Fang, X.; Kalathil, S.; Reisner, E., Semi-biological approaches to solar-to-chemical conversion. *Chem. Soc. Rev.* **2020,** *49* (14), 4926-4952.

50. Esmieu, C.; Raleiras, P.; Berggren, G., From protein engineering to artificial enzymes – biological and biomimetic approaches towards sustainable hydrogen production. *Sustainable Energy & Fuels* **2018,** *2* (4), 724-750.

51. del Barrio, M.; Sensi, M.; Orain, C.; Baffert, C.; Dementin, S.; Fourmond, V.; Léger, C., Electrochemical Investigations of Hydrogenases and Other Enzymes That Produce and Use Solar Fuels. *Acc. Chem. Res.* **2018,** *51* (3), 769-777.

52. Knowles, W. S., Asymmetric Hydrogenations (Nobel Lecture) Copyright© The Nobel Foundation 2002. We thank the Nobel Foundation, Stockholm, for permission to print this lecture. *Angew. Chem. Int. Ed.* **2002,** *41* (12), 1998.

53. Ager, D. J.; de Vries, A. H. M.; de Vries, J. G., Asymmetric homogeneous hydrogenations at scale. *Chem. Soc. Rev.* **2012,** *41* (8), 3340.

54. Jagan Mohan, S.; Chandra Mohan, E.; Yamsani, M. R., Chirality and its Importance in Pharmaceutical Field- An Overview. *International Journal of Pharmaceutical Sciences and Nanotechnology* **1970,** *1* (4), 309-316.

55. Johnson, N. B.; Lennon, I. C.; Moran, P. H.; Ramsden, J. A., Industrial-Scale Synthesis and Applications of Asymmetric Hydrogenation Catalysts. *Acc. Chem. Res.* **2007,** *40* (12), 1291-1299.

56. Wang, H.; Wen, J.; Zhang, X., Chiral Tridentate Ligands in Transition Metal-Catalyzed Asymmetric Hydrogenation. *Chem. Rev.* **2021,** *121* (13), 7530-7567.

57. Wen, J.; Wang, F.; Zhang, X., Asymmetric hydrogenation catalyzed by first-row transition metal complexes. *Chem. Soc. Rev.* **2021,** *50* (5), 3211-3237.

58. Parmeggiani, F.; Brenna, E.; Colombo, D.; Gatti, F. G.; Tentori, F.; Tessaro, D., "A Study in Yellow": Investigations in the Stereoselectivity of Ene-Reductases. *ChemBioChem* **2021,** *23* (1).

59. Heller, A.; Ulstrup, J., Detlev Müller's Discovery of Glucose Oxidase in 1925. *Anal. Chem.* **2021,** *93* (18), 7148-7149.

60. Shi, Q.; Wang, H.; Liu, J.; Li, S.; Guo, J.; Li, H.; Jia, X.; Huo, H.; Zheng, Z.; You, S.; Qin, B., Old yellow enzymes: structures and structure-guided engineering for stereocomplementary bioreduction. *Appl. Microbiol. Biotechnol.* **2020,** *104* (19), 8155-8170.

61. Scholtissek, A.; Tischler, D.; Westphal, A.; van Berkel, W.; Paul, C., Old Yellow Enzyme-Catalysed Asymmetric Hydrogenation: Linking Family Roots with Improved Catalysis. *Catalysts* **2017,** *7* (12), 130.

62. Winkler, C. K.; Faber, K.; Hall, M., Biocatalytic reduction of activated C C-bonds and beyond: emerging trends. *Curr. Opin. Chem. Biol.* **2018,** *43*, 97-105.

63. Winkler, C. K.; Clay, D.; Davies, S.; O'Neill, P.; McDaid, P.; Debarge, S.; Steflik, J.; Karmilowicz, M.; Wong, J. W.; Faber, K., Chemoenzymatic asymmetric synthesis of pregabalin precursors via asymmetric bioreduction of β-cyanoacrylate esters using ene-reductases. *The Journal of organic chemistry* **2013,** *78* (4), 1525-1533.

64. Peters, C.; Frasson, D.; Sievers, M.; Buller, R., Novel Old Yellow Enzyme Subclasses. *ChemBioChem* **2019,** *20* (12), 1569-1577.

65. Iorgu, A. I.; Hedison, T. M.; Hay, S.; Scrutton, N. S., Selectivity through discriminatory induced fit enables switching of<scp>NAD</scp>(P)H coenzyme specificity in Old Yellow Enzyme ene-reductases. *The FEBS Journal* **2019,** *286* (16), 3117-3128.

66. Amato, E. D.; Stewart, J. D., Applications of protein engineering to members of the old yellow enzyme family. *Biotechnol. Adv.* **2015,** *33* (5), 624-631.

67. Padhi, S. K.; Bougioukou, D. J.; Stewart, J. D., Site-saturation mutagenesis of tryptophan 116 of Saccharomyces pastorianus old yellow enzyme uncovers stereocomplementary variants. *Journal of the American Chemical Society* **2009,** *131* (9), 3271-3280.

68. Walton, A. Z.; Sullivan, B.; Patterson-Orazem, A. n. C.; Stewart, J. D., Residues controlling facial selectivity in an alkene reductase and semirational alterations to create stereocomplementary variants. *ACS catalysis* **2014,** *4* (7), 2307-2318.

69. Powell Iii, R. W.; Buteler, M. P.; Lenka, S.; Crotti, M.; Santangelo, S.; Burg, M. J.; Bruner, S.; Brenna, E.; Roitberg, A. E.; Stewart, J. D., Investigating Saccharomyces cerevisiae alkene reductase OYE 3 by substrate profiling, X-ray crystallography and computational methods. *Catalysis Science & Technology* **2018,** *8* (19), 5003-5016.

70. Bougioukou, D. J.; Kille, S.; Taglieber, A.; Reetz, M. T., Directed evolution of an enantioselective enoate-reductase: testing the utility of iterative saturation mutagenesis. *Adv. Synth. Catal.* **2009,** *351* (18), 3287-3305.

71. Xu, D.; Kohli, R. M.; Massey, V., The role of threonine 37 in flavin reactivity of the old yellow enzyme. *Proceedings of the National Academy of Sciences* **1999,** *96* (7), 3556-3561.

72. Spiegelhauer, O.; Mende, S.; Dickert, F.; Knauer, S. H.; Ullmann, G. M.; Dobbek, H., Cysteine as a modulator residue in the active site of xenobiotic reductase A: a structural, thermodynamic and kinetic study. *J. Mol. Biol.* **2010,** *398* (1), 66-82.

73. Scholtissek, A.; Gädke, E.; Paul, C. E.; Westphal, A. H.; Van Berkel, W. J. H.; Tischler, D., Catalytic performance of a class III old yellow enzyme and its cysteine variants. *Frontiers in microbiology* **2018,** *9*, 2410.

74. Williams, R. E.; Bruce, N. C., 'New uses for an old enzyme'–the old yellow enzyme family of flavoenzymes. *Microbiology* **2002,** *148* (6), 1607-1614.

75. Stuermer, R.; Hauer, B.; Hall, M.; Faber, K., Asymmetric bioreduction of activated C= C bonds using enoate reductases from the old yellow enzyme family. *Curr. Opin. Chem. Biol.* **2007,** *11* (2), 203-213.

76. Sun, J.; Lin, Y.; Shen, X.; Jain, R.; Sun, X.; Yuan, Q.; Yan, Y., Aerobic biosynthesis of hydrocinnamic acids in Escherichia coli with a strictly oxygen-sensitive enoate reductase. *Metab. Eng.* **2016,** *35*, 75-82.

77. Hubbard, P. A.; Liang, X.; Schulz, H.; Kim, J.-J. P., The crystal structure and reaction mechanism of Escherichia coli 2, 4-dienoyl-CoA reductase. *J. Biol. Chem.* **2003,** *278* (39), 37553-37560.

78. Joo, J. C.; Khusnutdinova, A. N.; Flick, R.; Kim, T.; Bornscheuer, U. T.; Yakunin, A. F.; Mahadevan, R., Alkene hydrogenation activity of enoate reductases for an environmentally benign biosynthesis of adipic acid. *Chemical science* **2017,** *8* (2), 1406-1413.

79. Buder, R.; Fuchs, G., 2-Aminobenzoyl-CoA monooxygenase/reductase, a novel type of flavoenzyme. Purification and some properties of the enzyme. *Eur. J. Biochem.* **1989,** *185* (3), 629-35.

80. Langkau, B.; Vock, P.; Massey, V.; Fuchs, G.; Ghisla, S., 2-Aminobenzoyl-CoA monooxygenase/reductase. Evidence for two distinct loci catalyzing substrate monooxygenation and hydrogenation. *Eur. J. Biochem.* **1995,** *230* (2), 676-85.

81. Haarer, B. K.; Amberg, D. C., Old yellow enzyme protects the actin cytoskeleton from oxidative stress. *Molecular biology of the cell* **2004,** *15* (10), 4522-4531.

82. Odat, O.; Matta, S.; Khalil, H.; Kampranis, S. C.; Pfau, R.; Tsichlis, P. N.; Makris, A. M., Old yellow enzymes, highly homologous FMN oxidoreductases with modulating roles in oxidative stress and programmed cell death in yeast. *J. Biol. Chem.* **2007,** *282* (49), 36010-36023.

83. Fitzpatrick, T. B.; Amrhein, N.; Macheroux, P., Characterization of YqjM, an Old Yellow Enzyme homolog from Bacillus subtilis involved in the oxidative stress response. *J. Biol. Chem.* **2003,** *278* (22), 19891-19897.

84. Cheng, J. Z.; Coyle, C. M.; Panaccione, D. G.; O'Connor, S. E., A role for old yellow enzyme in ergot alkaloid biosynthesis. *Journal of the American Chemical Society* **2010,** *132* (6), 1776-1777.

85. Schaller, F.; Weiler, E. W., Molecular Cloning and Characterization of 12-Oxophytodienoate Reductase, an Enzyme of the Octadecanoid Signaling Pathway

fromArabidopsis thaliana: structural and functional relationship to yeast old yellow enzyme. *J. Biol. Chem.* **1997,** *272* (44), 28066-28072.

86. Müssig, C.; Biesgen, C.; Lisso, J.; Uwer, U.; Weiler, E. W.; Altmann, T., A novel stress-inducible 12-oxophytodienoate reductase from Arabidopsis thaliana provides a potential link between brassinosteroid-action and jasmonic-acid synthesis. *Journal of plant physiology* **2000,** *157* (2), 143-152.

87. Schaller, A.; Stintzi, A., Enzymes in jasmonate biosynthesis–structure, function, regulation. *Phytochemistry* **2009,** *70* (13-14), 1532-1538.

88. Sobajima, H.; Takeda, M.; Sugimori, M.; Kobashi, N.; Kiribuchi, K.; Cho, E.-M.; Akimoto, C.; Yamaguchi, T.; Minami, E.; Shibuya, N., Cloning and characterization of a jasmonic acid-responsive gene encoding 12-oxophytodienoic acid reductase in suspension-cultured rice cells. *Planta* **2003,** *216* (4), 692-698.

89. Zhang, Z.; Jamieson, C. S.; Zhao, Y.-L.; Li, D.; Ohashi, M.; Houk, K. N.; Tang, Y., Enzyme-Catalyzed Inverse-Electron Demand Diels–Alder Reaction in the Biosynthesis of Antifungal Ilicicolin H. *Journal of the American Chemical Society* **2019,** *141* (14), 5659-5663.

90. Roze, L. V.; Hong, S.-Y.; Linz, J. E., Aflatoxin biosynthesis: current frontiers. *Annu. Rev. Food Sci. Technol* **2013,** *4*, 293-311.

91. Murta, S. M. F.; Krieger, M. A.; Montenegro, L. R.; Campos, F. F. M.; Probst, C. M.; Avila, A. R.; Muto, N. H.; de Oliveira, R. C.; Nunes, L. R.; Nirdé, P., Deletion of copies of the gene encoding old yellow enzyme (TcOYE), a NAD (P) H flavin oxidoreductase, associates with in vitro-induced benznidazole resistance in Trypanosoma cruzi. *Molecular and biochemical parasitology* **2006,** *146* (2), 151-162.

92. Kubata, B. K.; Kabututu, Z.; Nozaki, T.; Munday, C. J.; Fukuzumi, S.; Ohkubo, K.; Lazarus, M.; Maruyama, T.; Martin, S. K.; Duszenko, M., A key role for old yellow enzyme in the metabolism of drugs by Trypanosoma cruzi. *The Journal of experimental medicine* **2002,** *196* (9), 1241-1252.

93. Wyllie, S.; Roberts, A. J.; Norval, S.; Patterson, S.; Foth, B. J.; Berriman, M.; Read, K. D.; Fairlamb, A. H., Activation of Bicyclic Nitro-drugs by a Novel Nitroreductase (NTR2) in Leishmania. *PLOS Pathogens* **2016,** *12* (11), e1005971.

94. Durchschein, K.; Hall, M.; Faber, K., Unusual reactions mediated by FMN-dependent ene- and nitro-reductases. *Green chemistry* **2013,** *15* (7), 1764-1772.

95. Nyanhongo, G. S.; Schroeder, M.; Steiner, W.; Gübitz, G. M., Biodegradation of 2, 4, 6-trinitrotoluene (TNT): An enzymatic perspective. *Biocatal. Biotransform.* **2005,** *23* (2), 53-69.

96. Zhu, B.; Peng, R.-H.; Fu, X.-Y.; Jin, X.-F.; Zhao, W.; Xu, J.; Han, H.-J.; Gao, J.-J.; Xu, Z.-S.; Bian, L., Enhanced transformation of TNT by Arabidopsis plants expressing an old yellow enzyme. *PloS one* **2012,** *7* (7), e39861.

97. Wittich, R.-M.; Haïdour, A.; Van Dillewijn, P.; Ramos, J.-L., OYE flavoprotein reductases initiate the condensation of TNT-derived intermediates to secondary diarylamines and nitrite. *Environmental science & technology* **2008,** *42* (3), 734-739.

98. Williams, R. E.; Rathbone, D. A.; Scrutton, N. S.; Bruce, N. C., Biotransformation of explosives by the old yellow enzyme family of flavoproteins. *Applied and environmental microbiology* **2004,** *70* (6), 3566-3574.

99. Schittmayer, M.; Glieder, A.; Uhl, M. K.; Winkler, A.; Zach, S.; Schrittwieser, J. H.; Kroutil, W.; Macheroux, P.; Gruber, K.; Kambourakis, S., Old yellow enzyme-catalyzed dehydrogenation of saturated ketones. *Adv. Synth. Catal.* **2011,** *353* (2-3), 268-274.

100. Murthy, Y. V. S. N.; Meah, Y.; Massey, V., Conversion of a flavoprotein reductase to a desaturase by manipulation of the flavin redox potential. *Journal of the American Chemical Society* **1999,** *121* (22), 5344-5345.

101. Vaz, A. D. N.; Chakraborty, S.; Massey, V., Old yellow enzyme: aromatization of cyclic enones and the mechanism of a novel dismutation reaction. *Biochemistry* **1995,** *34* (13), 4246-4256.

102. Kelly, P. P.; Lipscomb, D.; Quinn, D. J.; Lemon, K.; Caswell, J.; Spratt, J.; Kosjek, B.; Truppo, M.; Moody, T. S., Ene Reductase enzymes for the aromatisation of tetralones and cyclohexenones to naphthols and phenols. *Adv. Synth. Catal.* **2016,** *358* (5), 731-736.

103. McDonough, W.; Braungart, M., The next industrial revolution. In *Sustainable solutions*, Routledge: 2017; pp 139-150.

104. Höök, M.; Tang, X., Depletion of fossil fuels and anthropogenic climate change—A review. *Energy policy* **2013,** *52*, 797-809.

105. Wuebbles, D. J.; Jain, A. K., Concerns about climate change and the role of fossil fuel use. *Fuel Process. Technol.* **2001,** *71* (1-3), 99-119.

106. Johnsson, F.; Kjärstad, J.; Rootzén, J., The threat to climate change mitigation posed by the abundance of fossil fuels. *Climate Policy* **2019,** *19* (2), 258-274.

107. Bala, G., Digesting 400 ppm for global mean CO2 concentration. *Curr Sci* **2013,** *104* (11), 1471-1472.

108. Maginn, E. J., What to Do with CO2. ACS Publications: 2010; Vol. 1, pp 3478-3479.

109. Montzka, S. A.; Dlugokencky, E. J.; Butler, J. H., Non-CO2 greenhouse gases and climate change. *Nature* **2011,** *476* (7358), 43-50.

110. Farhidi, F., Impact of fossil fuel transition and population expansion on economic growth. *Environment, Development and Sustainability* **2022**, 1-39.

111. De Cian, E.; Sferra, F.; Tavoni, M., The influence of economic growth, population, and fossil fuel scarcity on energy investments. *Climatic Change* **2016,** *136* (1), 39-55.

112. Capellán-Pérez, I.; Mediavilla, M.; de Castro, C.; Carpintero, Ó.; Miguel, L. J., Fossil fuel depletion and socio-economic scenarios: An integrated approach. *Energy* **2014,** *77*, 641-666.

113. York, R., Do alternative energy sources displace fossil fuels? *Nature climate change* **2012,** *2* (6), 441-443.

114. Barber, J.; Tran, P. D., From natural to artificial photosynthesis. *Journal of The Royal Society Interface* **2013,** *10* (81), 20120984.

115. Berardi, S.; Drouet, S.; Francàs, L.; Gimbert-Suriñach, C.; Guttentag, M.; Richmond, C.; Stoll, T.; Llobet, A., Molecular artificial photosynthesis. *Chem. Soc. Rev.* **2014,** *43* (22), 7501-7519.

116. Benniston, A. C.; Harriman, A., Artificial photosynthesis. *Mater. Today* **2008,** *11* (12), 26-34.

117. Zhang, B.; Sun, L., Artificial photosynthesis: opportunities and challenges of molecular catalysts. *Chem. Soc. Rev.* **2019,** *48* (7), 2216-2264.

118. Hou, Y.; Vidu, R.; Stroeve, P., Solar energy storage methods. *Industrial & engineering chemistry research* **2011,** *50* (15), 8954-8964.

119. Li, X.; Yu, J.; Jaroniec, M.; Chen, X., Cocatalysts for selective photoreduction of CO2 into solar fuels. *Chem. Rev.* **2019,** *119* (6), 3962-4179.

120. Poullikkas, A., A comparative overview of large-scale battery systems for electricity storage. *Renewable and Sustainable energy reviews* **2013,** *27*, 778-788.

121. Nocera, D. G., Solar fuels and solar chemicals industry. *Acc. Chem. Res.* **2017,** *50* (3), 616-619.

122. Hohmann-Marriott, M. F.; Blankenship, R. E., Evolution of photosynthesis. *Annual review of plant biology* **2011,** *62* (1), 515-548.

123. Stirbet, A.; Lazár, D.; Guo, Y.; Govindjee, G., Photosynthesis: basics, history and modelling. *Annals of Botany* **2020,** *126* (4), 511-537.

124. Evans, J. R., Improving photosynthesis. *Plant physiology* **2013,** *162* (4), 1780-1793.

125. Wu, J.; Huang, Y.; Ye, W.; Li, Y., CO2 reduction: from the electrochemical to photochemical approach. *Advanced Science* **2017,** *4* (11), 1700194.

126. Wang, L., Recent Advances in Metal-Based Molecular Photosensitizers for Artificial Photosynthesis. *Catalysts* **2022,** *12* (8), 919.

127. Puntoriero, F.; La Ganga, G.; Cancelliere, A. M.; Campagna, S., Recent progresses in molecular-based artificial photosynthesis. *Current Opinion in Green and Sustainable Chemistry* **2022**, 100636.

128. Neaţu, Ş.; Maciá-Agulló, J. A.; Garcia, H., Solar light photocatalytic CO2 reduction: general considerations and selected bench-mark photocatalysts. *International journal of molecular sciences* **2014,** *15* (4), 5246-5262.

129. Steinlechner, C.; Roesel, A. F.; Oberem, E.; Päpcke, A.; Rockstroh, N.; Gloaguen, F.; Lochbrunner, S.; Ludwig, R.; Spannenberg, A.; Junge, H., Selective earth-abundant system for CO2 reduction: comparing photo-and electrocatalytic processes. *ACS Catalysis* **2019,** *9* (3), 2091-2100.

130. Qiao, J.; Liu, Y.; Hong, F.; Zhang, J., A review of catalysts for the electroreduction of carbon dioxide to produce low-carbon fuels. *Chem. Soc. Rev.* **2014,** *43* (2), 631-675.

131. Can, M.; Armstrong, F. A.; Ragsdale, S. W., Structure, function, and mechanism of the nickel metalloenzymes, CO dehydrogenase, and acetyl-CoA synthase. *Chem. Rev.* **2014,** *114* (8), 4149-4174.

132. Takeda, H.; Cometto, C.; Ishitani, O.; Robert, M., Electrons, Photons, Protons and Earth-Abundant Metal Complexes for Molecular Catalysis of CO2 Reduction. *ACS Catalysis* **2017,** *7* (1), 70-88.

133. Evans, D. J., Chemistry relating to the nickel enzymes CODH and ACS. *Coord. Chem. Rev.* **2005,** *249* (15-16), 1582-1595.

134. Alfano, M.; Cavazza, C., The biologically mediated water–gas shift reaction: structure, function and biosynthesis of monofunctional [NiFe]-carbon monoxide dehydrogenases. *Sustainable Energy & Fuels* **2018,** *2* (8), 1653-1670.

135. Dobbek, H., Mechanism of Ni, Fe-Containing carbon monoxide dehydrogenases. *Metallocofactors that Activate Small Molecules* **2018**, 153-166.

136. Jeoung, J.-H.; Martins, B. M.; Dobbek, H., Carbon monoxide dehydrogenases. *Metalloproteins* **2019**, 37-54.

137. Jain, S.; Katsyv, A.; Basen, M.; Müller, V., The monofunctional CO dehydrogenase CooS is essential for growth of Thermoanaerobacter kivui on carbon monoxide. *Extremophiles* **2022,** *26* (1), 1-12.

138. Svetlitchnyi, V.; Peschel, C.; Acker, G.; Meyer, O., Two membrane-associated NiFeS-carbon monoxide dehydrogenases from the anaerobic carbon-monoxide-utilizing eubacterium Carboxydothermus hydrogenoformans. *J. Bacteriol.* **2001,** *183* (17), 5134-5144.

139. Techtmann, S. M.; Colman, A. S.; Robb, F. T., 'That which does not kill us only makes us stronger': the role of carbon monoxide in thermophilic microbial consortia. *Environ. Microbiol.* **2009,** *11* (5), 1027-1037.

140. Ragsdale, S. W., Enzymology of the Wood–Ljungdahl pathway of acetogenesis. *Ann. N.Y. Acad. Sci.* **2008,** *1125* (1), 129-136.

141. Ragsdale, S. W.; Pierce, E., Acetogenesis and the Wood–Ljungdahl pathway of CO2 fixation. *Biochimica et Biophysica Acta (BBA)-Proteins and Proteomics* **2008,** *1784* (12), 1873-1898.

142. Biester, A.; Dementin, S.; Drennan, C. L., Visualizing the gas channel of a monofunctional carbon monoxide dehydrogenase. *J. Inorg. Biochem.* **2022,** *230*, 111774.

143. Gong, W.; Hao, B.; Wei, Z.; Ferguson Jr, D. J.; Tallant, T.; Krzycki, J. A.; Chan, M. K., Structure of the α2ε2 Ni-dependent CO dehydrogenase component of the Methanosarcina barkeri acetyl-CoA decarbonylase/synthase complex. *Proceedings of the National Academy of Sciences* **2008,** *105* (28), 9558-9563.

144. Heo, J.; Staples, C. R.; Ludden, P. W., Redox-dependent CO2 reduction activity of CO dehydrogenase from Rhodospirillum rubrum. *Biochemistry* **2001,** *40* (25), 7604-7611.

145. Craft, J. L.; Ludden, P. W.; Brunold, T. C., Spectroscopic Studies of Nickel-Deficient Carbon Monoxide Dehydrogenase from Rhodospirillum rubrum: Nature of the Iron− Sulfur Clusters. *Biochemistry* **2002,** *41* (5), 1681-1688.

146. Wittenborn, E. C.; Guendon, C.; Merrouch, M.; Benvenuti, M.; Fourmond, V.; Léger, C.; Drennan, C. L.; Dementin, S., The solvent-exposed Fe–S D-cluster contributes to oxygen-resistance in Desulfovibrio vulgaris Ni–Fe carbon monoxide dehydrogenase. *ACS catalysis* **2020,** *10* (13), 7328-7335.

147. Fesseler, J.; Jeoung, J. H.; Dobbek, H., How the [NiFe4S4] cluster of CO dehydrogenase activates CO2 and NCO−. *Angew. Chem. Int. Ed.* **2015,** *54* (29), 8560-8564.

148. Dobbek, H.; Svetlitchnyi, V.; Gremer, L.; Huber, R.; Meyer, O., Crystal structure of a carbon monoxide dehydrogenase reveals a [Ni-4Fe-5S] cluster. *Science* **2001,** *293* (5533), 1281-1285.

149. Drennan, C. L.; Heo, J.; Sintchak, M. D.; Schreiter, E.; Ludden, P. W., Life on carbon monoxide: X-ray structure of Rhodospirillum rubrum Ni-Fe-S carbon monoxide dehydrogenase. *Proceedings of the National Academy of Sciences* **2001,** *98* (21), 11973-11978.

150. Kim, E. J.; Feng, J.; Bramlett, M. R.; Lindahl, P. A., Evidence for a proton transfer network and a required persulfide-bond-forming cysteine residue in Ni-containing carbon monoxide dehydrogenases. *Biochemistry* **2004,** *43* (19), 5728-5734.

151. Seravalli, J.; Ragsdale, S. W., 13C NMR characterization of an exchange reaction between CO and CO2 catalyzed by carbon monoxide dehydrogenase. *Biochemistry* **2008,** *47* (26), 6770-6781.

152. Contaldo, U.; Guigliarelli, B.; Pérard, J.; Rinaldi, C.; Le Goff, A.; Cavazza, C., Efficient Electrochemical CO2/CO Interconversion by an Engineered Carbon Monoxide Dehydrogenase on a Gas-Diffusion Carbon Nanotube-Based Bioelectrode. *ACS Catalysis* **2021,** *11* (9), 5808-5817.

153. Lazarus, O.; Woolerton, T. W.; Parkin, A.; Lukey, M. J.; Reisner, E.; Seravalli, J.; Pierce, E.; Ragsdale, S. W.; Sargent, F.; Armstrong, F. A., Water− Gas Shift Reaction Catalyzed by Redox Enzymes on Conducting Graphite Platelets. *Journal of the American Chemical Society* **2009,** *131* (40), 14154-14155.

154. Becker, J. M.; Lielpetere, A.; Szczesny, J.; Junqueira, J. R. C.; Rodríguez-Maciá, P.; Birrell, J. A.; Conzuelo, F.; Schuhmann, W., Bioelectrocatalytic CO2 Reduction by Redox

Polymer-Wired Carbon Monoxide Dehydrogenase Gas Diffusion Electrodes. *ACS Applied Materials & Interfaces* **2022**.

155. Wang, Y.; He, D.; Chen, H.; Wang, D., Catalysts in electro-, photo-and photoelectrocatalytic CO2 reduction reactions. *Journal of Photochemistry and Photobiology C: Photochemistry Reviews* **2019,** *40*, 117-149.

156. Zhang, L.; Can, M.; Ragsdale, S. W.; Armstrong, F. A., Fast and selective photoreduction of CO2 to CO catalyzed by a complex of carbon monoxide dehydrogenase, TiO2, and Ag nanoclusters. *ACS catalysis* **2018,** *8* (4), 2789-2795.

157. Kim, S. M.; Lee, J.; Kang, S. H.; Heo, Y.; Yoon, H.-J.; Hahn, J.-S.; Lee, H. H.; Kim, Y. H., O2-tolerant CO dehydrogenase via tunnel redesign for the removal of CO from industrial flue gas. *Nature Catalysis* **2022,** *5* (9), 807-817.

158. Inoue, T.; Yoshida, T.; Wada, K.; Daifuku, T.; Fukuyama, K.; Sako, Y., A simple, large-scale overexpression method of deriving carbon monoxide dehydrogenase II from thermophilic bacterium Carboxydothermus hydrogenoformans. *Bioscience, biotechnology, and biochemistry* **2011,** *75* (7), 1392-1394.

159. Edwards, E. H.; Bren, K. L., Light-driven catalysis with engineered enzymes and biomimetic systems. *Biotechnol. Appl. Biochem.* **2020,** *67* (4), 463-483.

160. Majumdar, A., Bioinorganic modeling chemistry of carbon monoxide dehydrogenases: description of model complexes, current status and possible future scopes. *Dalton Transactions* **2014,** *43* (32), 12135-12145.

161. Li, Y.; Gomez-Mingot, M.; Fogeron, T.; Fontecave, M., Carbon dioxide Reduction: A Bioinspired Catalysis Approach. *Acc. Chem. Res.* **2021,** *54* (23), 4250-4261.

162. Mankad, N. P., Learning from Nature: Bio-inspired Heterobinuclear Electrocatalysts for Selective CO2 Reduction. *Trends in Chemistry* **2021,** *3* (3), 159-160.

163. Johnston, B.; Mayo, M. C.; Khare, A., Hydrogen: the energy source for the 21st century. *Technovation* **2005,** *25* (6), 569-585.

164. Mazloomi, K.; Gomes, C., Hydrogen as an energy carrier: Prospects and challenges. *Renewable and Sustainable Energy Reviews* **2012,** *16* (5), 3024-3033.

165. Ahmed, A.; Al-Amin, A. Q.; Ambrose, A. F.; Saidur, R., Hydrogen fuel and transport system: A sustainable and environmental future. *Int. J. Hydrogen Energy* **2016,** *41* (3), 1369-1380.

166. Kim, D.; Sakimoto, K. K.; Hong, D.; Yang, P., Artificial photosynthesis for sustainable fuel and chemical production. *Angew. Chem. Int. Ed.* **2015,** *54* (11), 3259-3266.

167. Ramachandran, R.; Menon, R. K., An overview of industrial uses of hydrogen. *Int. J. Hydrogen Energy* **1998,** *23* (7), 593-598.

168. Yüzbaşıoğlu, A. E.; Avşar, C.; Gezerman, A. O., The current situation in the use of ammonia as a sustainable energy source and its industrial potential. *Current Research in Green and Sustainable Chemistry* **2022**, 100307.

169. Ball, M.; Wietschel, M., The future of hydrogen–opportunities and challenges. *Int. J. Hydrogen Energy* **2009,** *34* (2), 615-627.

170. Osman, A. I.; Mehta, N.; Elgarahy, A. M.; Hefny, M.; Al-Hinai, A.; Al-Muhtaseb, A. a. H.; Rooney, D. W., Hydrogen production, storage, utilisation and environmental impacts: a review. *Environmental Chemistry Letters* **2021**, 1-36.

171. Yu, M.; Wang, K.; Vredenburg, H., Insights into low-carbon hydrogen production methods: Green, blue and aqua hydrogen. *Int. J. Hydrogen Energy* **2021,** *46* (41), 21261-21273.

172. Dincer, I.; Acar, C., Review and evaluation of hydrogen production methods for better sustainability. *Int. J. Hydrogen Energy* **2015,** *40* (34), 11094-11111.

173. Matheu, R.; Garrido-Barros, P.; Gil-Sepulcre, M.; Ertem, M. Z.; Sala, X.; Gimbert-Suriñach, C.; Llobet, A., The development of molecular water oxidation catalysts. *Nature Reviews Chemistry* **2019,** *3* (5), 331-341.

174. Birrell, J. A.; Rodriguez-Macia, P.; Reijerse, E. J.; Martini, M. A.; Lubitz, W., The catalytic cycle of [FeFe] hydrogenase: A tale of two sites. *Coord. Chem. Rev.* **2021,** *449*, 214191.

175. Heinekey, D. M., Hydrogenase enzymes: recent structural studies and active site models. *J. Organomet. Chem.* **2009,** *694* (17), 2671-2680.

176. Mulder, D. W.; Shepard, E. M.; Meuser, J. E.; Joshi, N.; King, P. W.; Posewitz, M. C.; Broderick, J. B.; Peters, J. W., Insights into [FeFe]-hydrogenase structure, mechanism, and maturation. *Structure* **2011,** *19* (8), 1038-1052.

177. Shima, S.; Thauer, R. K., A third type of hydrogenase catalyzing H2 activation. *The chemical record* **2007,** *7* (1), 37-46.

178. Land, H.; Senger, M.; Berggren, G.; Stripp, S. T., Current state of [FeFe]-hydrogenase research: biodiversity and spectroscopic investigations. *ACS catalysis* **2020,** *10* (13), 7069-7086.

179. Madden, C.; Vaughn, M. D.; Díez-Pérez, I.; Brown, K. A.; King, P. W.; Gust, D.; Moore, A. L.; Moore, T. A., Catalytic turnover of [FeFe]-hydrogenase based on single-molecule imaging. *Journal of the American Chemical Society* **2012,** *134* (3), 1577-1582.

180. Mirmohades, M.; Adamska-Venkatesh, A.; Sommer, C.; Reijerse, E.; Lomoth, R.; Lubitz, W.; Hammarstrom, L., Following [FeFe] hydrogenase active site intermediates by time-resolved mid-IR spectroscopy. *The Journal of Physical Chemistry Letters* **2016,** *7* (16), 3290-3293.

181. Ginovska-Pangovska, B.; Ho, M.-H.; Linehan, J. C.; Cheng, Y.; Dupuis, M.; Raugei, S.; Shaw, W. J., Molecular dynamics study of the proposed proton transport pathways in [FeFe]-hydrogenase. *Biochimica et Biophysica Acta (BBA)-Bioenergetics* **2014,** *1837* (1), 131-138.

182. Lubner, C. E.; Knörzer, P.; Silva, P. J. N.; Vincent, K. A.; Happe, T.; Bryant, D. A.; Golbeck, J. H., Wiring an [FeFe]-hydrogenase with photosystem I for light-induced hydrogen production. *Biochemistry* **2010,** *49* (48), 10264-10266.

183. Brown, K. A.; Wilker, M. B.; Boehm, M.; Dukovic, G.; King, P. W., Characterization of photochemical processes for H2 production by CdS nanorod–[FeFe] hydrogenase complexes. *Journal of the American Chemical Society* **2012,** *134* (12), 5627-5636.

184. Swanson, K. D.; Ratzloff, M. W.; Mulder, D. W.; Artz, J. H.; Ghose, S.; Hoffman, A.; White, S.; Zadvornyy, O. A.; Broderick, J. B.; Bothner, B., [FeFe]-hydrogenase oxygen inactivation is initiated at the H cluster 2Fe subcluster. *Journal of the American Chemical Society* **2015,** *137* (5), 1809-1816.

185. Winkler, M.; Duan, J.; Rutz, A.; Felbek, C.; Scholtysek, L.; Lampret, O.; Jaenecke, J.; Apfel, U.-P.; Gilardi, G.; Valetti, F., A safety cap protects hydrogenase from oxygen attack. *Nature communications* **2021,** *12* (1), 1-10.

186. Rodríguez-Maciá, P.; Galle, L. M.; Bjornsson, R.; Lorent, C.; Zebger, I.; Yoda, Y.; Cramer, S. P.; DeBeer, S.; Span, I.; Birrell, J. A., Caught in the Hinact: Crystal Structure and Spectroscopy Reveal a Sulfur Bound to the Active Site of an O2-stable State of [FeFe] Hydrogenase. *Angew. Chem. Int. Ed.* **2020,** *59* (38), 16786-16794.

187. Xu, T.; Chen, D.; Hu, X., Hydrogen-activating models of hydrogenases. *Coord. Chem. Rev.* **2015,** *303*, 32-41.

188. Gao, S.; Fan, W.; Liu, Y.; Jiang, D.; Duan, Q., Artificial water-soluble systems inspired by [FeFe]-hydrogenases for electro-and photocatalytic hydrogen production. *Int. J. Hydrogen Energy* **2020,** *45* (7), 4305-4327.

189. Gao, S.; Liu, Y.; Shao, Y.; Jiang, D.; Duan, Q., Iron carbonyl compounds with aromatic dithiolate bridges as organometallic mimics of [FeFe] hydrogenases. *Coord. Chem. Rev.* **2020,** *402*, 213081.

190. Wang, C.; Lai, Z.; Huang, G.; Pan, H. J., Current State of [Fe]-Hydrogenase and Its Biomimetic Models. *Chemistry–A European Journal* **2022,** *28* (57), e202201499.

191. Brezinski, W. P.; Karayilan, M.; Clary, K. E.; Pavlopoulos, N. G.; Li, S.; Fu, L.; Matyjaszewski, K.; Evans, D. H.; Glass, R. S.; Lichtenberger, D. L., [FeFe]-Hydrogenase Mimetic Metallopolymers with Enhanced Catalytic Activity for Hydrogen Production in Water. *Angew. Chem. Int. Ed.* **2018,** *57* (37), 11898-11902.

Chapter 2: Exploration of the Biocatalytic Potential of the Old Yellow Enzyme Family

Work done in collaboration with Dr. Janine Copp from the University of British Columbia, and Dr. Samantha Iamurri, Parisa Keshavarz-Joud, and Tamra Blue

2.1 Introduction

Old Yellow Enzymes (OYE) are a family of flavoenzymes capable of asymmetric trans-hydrogenation of activated alkenes with high regio- and stereoselectivity.[1-4] Since the discovery of the first OYE from brewer's bottom yeast 90 years ago, 126 such enzymes have been isolated and characterized (Fig. 1).[1, 2] For the majority of these enzymes the native substrate or physiological roles have yet to be deciphered.[5] The standard OYE reaction is a hydride transfer from the reduced FMN cofactor to an unsaturated compound with an electron-withdrawing group (EWG) coordinated via hydrogen bonding. The chemical identity of the EWG is essential for OYE activity as aldehydes, ketones, esters, and nitro groups are preferred with limited activity for carboxylic acids and nitrile compounds.[3] The catalytic versatility of the FMN cofactor allows OYEs to perform a variety of reactions including nitro reduction.[6]

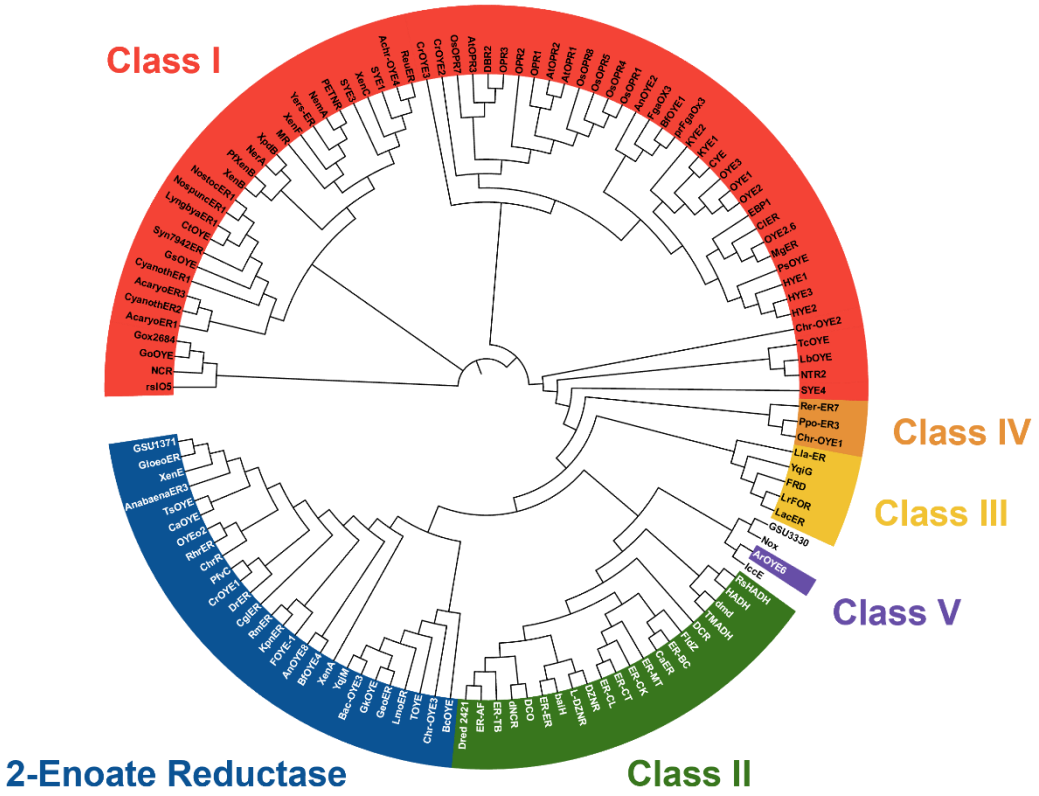

Figure 2.1 Phylogenetic tree of previously characterized OYEs. The five classes are represented by colors with red for Class I, green for Class II, yellow for Class III, orange for Class IV, and purple for the one Class V enzyme. Orphan OYEs that have yet to be included are not colored. Blue is for the 2-Enoate Reductases not currently classified. Visualized using iTOL.

Traditionally, the OYE family was split into two subgroups: 'classical' represented by OYE (*Saccharomyces pastorianus*), and 'thermophilic' represented by YqjM (*Bacillus subtilis*).[3] This separation is defined by conserved catalytic residues and structural features between the two groups such as the C-termini 'arginine finger' which protrudes into the adjacent active site for 'thermophilic' enzyme complexes but not observed in 'classical' OYEs.[2] Recent identification of several 'orphan' OYEs belonging to neither group has led to a confusing amount of new classification systems.[2, 7, 8] Computational studies by Nizam et al. suggested the existence of a potential third all-fungal class of OYEs represented by ArOYE6, but it is the only characterized

enzyme from this group.[7, 9, 10] The current and most comprehensive system was proposed by Peters et al. grouping the known OYEs into 5 classes based on phylogenetics (Fig. 1).[8] Classes I and II correspond to the 'classical' and 'thermophilic' designations of previous classifications. Two new classes, Classes III and IV, were proposed each with only three characterized enzymes and Class V consists of the all-fungal group of ArOYE6.[9] It is unclear what aspects separate or defines these classes as all three conserve similar residues to Class I and II enzymes.[8] The lack of a native function has also hampered classification systems as characterized OYEs typically display a similar substrate profile.[11] Several OYEs such as IccE and Nox, do not fit within the current system and it is likely they represent new classes/subgroups. Rarely included in the discussion is the multi-domain group 2-enoate reductases which contain an OYE-like domain.[12, 13] These enzymes also contain a separate NAD(P)H binding domain with an iron sulfur cluster and are studied for their slightly different substrate profile which includes unsaturated carboxylic acids, unlike other OYEs.[13]

The ability of OYEs to set two stereocenters with high enantioselectivity under ambient conditions has garnered nearly 3 decades of extensive study towards turning these enzymes into biocatalysts.[1, 3-5, 11, 14-16] OYEs have been applied towards the synthesis of industrial synthons for macrocyclic antibiotics and anticonvulsants in addition to flavor chemicals such as menthol.[17-20] Unfortunately, several key shortcomings prevent widespread adaptation of OYEs for industrial processes, namely the limited substrate scope and nearly identical stereoselectivity.[11] Reduction of the substrate is dependent on the adjacent EWG with nitriles and carboxylic acids particularly challenging for most characterized enzymes.[2] The size of the compound is also restricted in characterized OYEs due to the relatively small size of the active site.[11] In addition, OYEs typically produce the same enantiomer due to identical binding modes of substrates in the active site.[1, 4]

Access to either enantiomer would be ideal for synthetic applications. Other factors including enzyme stability, productivity, and expensive cofactor requirements (NAD(P)H) also hamper large-scale application. Current efforts to engineer known OYEs to solve these issues have been productive but are time consuming, costly and cannot meet industrial needs - thus new, novel OYE biocatalysts must be discovered to meet this demand.[1, 21]

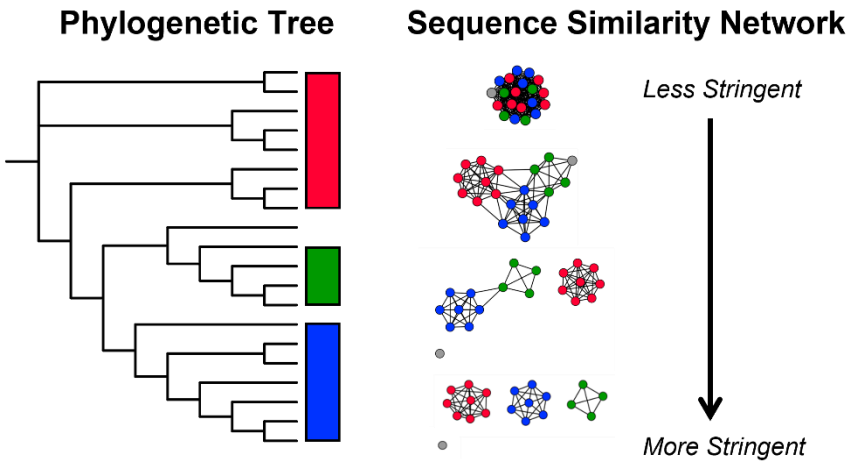

Figure 2.2 An example of sequence similarity networks (SSN). Sequences are represented by nodes and grouped all together in clusters at lower thresholds like the root of a phylogenetic tree. As the threshold is increased and edges are removed, similar sequences begin to form clusters like the branches of the tree. Note SSNs do not show phylogeny. Visualized in Cytoscape. Adapted from reference: Atkinson, H. J.; Morris, J. H.; Ferrin, T. E.; Babbitt, P. C., *PloS one* **2009,** *4* (2), e4345.

The rapid development of sequencing technology has revealed millions of uncharacterized protein sequences that await in databases, representing a near-limitless reservoir of potential biocatalysts.[22-24] Exploration of this vast sequence space through enzyme family profiling has become a promising approach for novel biocatalyst identification with studies investigating halogenases, phosphatases, methyltransferases, dehalogenases and imine reductases.[21, 25-28] Evaluating the natural diversity of enzymes has been fueled by inexpensive gene synthesis and the

development of bioinformatic-based in silco screening tools.[25, 29-31] Notably, protein sequence similarity networks (SSN) simplify the visualization of large enzyme families and acts as a framework for the selection of robust libraries of diverse representative sequences.[28] In SSNs, sequences are denoted by nodes and connected via edges correspond to the all versus all BLAST E-values between the two sequences (Fig 2).[32, 33] This E-value is analogous to sequence similarity with closely related sequences having a shorter edge between the nodes than a less related pair. Adjustment of the edge threshold reveals clusters of related sequences which should be isofunctional and share common characteristics. Beyond biocatalysts, bioinformatics and substrate profiling are vital for enzymology and evolutionary biology as it attempts to bridge the ever-growing gap between characterized enzymes and unknown sequences.[34-36] The OYE family is no exception to this gap as the family remains relatively underexplored with only 0.1% of identified enzymes having any experimental characterization.[37] Furthermore, the lack of a native substrate for most enzymes combined with the newly identified classes of OYEs hint at genetic and catalytic diversity of the family.[2, 8] With over 120,000 uncharacterized sequences, it is likely that the full biocatalytic potential of OYEs has yet to be unlocked.

2. 2 - Results and Discussion

2.2.1 – Mapping the OYE Family using SSN

A comprehensive overview of the OYE family was constructed using a SSN of 70,366 OYE sequences at the edge threshold of 10^{-85} (Fig. 3A). This threshold was selected as it organized the known OYE classes and the 2-Enoate reductases into distinct clusters. At this threshold, sequences with greater than ~35% sequence identity group together with many clusters containing enzymes with specific conserved residues or motifs. Overall, the majority (~85%) of OYE sequences are bacterial in origin and range between 300-450 amino acids in length though enzymes

were found in all kingdoms of life and in various sizes. The SSN analysis resulted in 20 major clusters, each containing >100 unique sequences and combined represent 99.8% of the sequences present in the SSN. Of the major clusters, 10 contained at least one of the 126 previously reported OYEs (Fig. 3A), though only 5 of these clusters were represented by more than one characterized enzyme. The other 10 clusters have no known biological roles or documented activities.

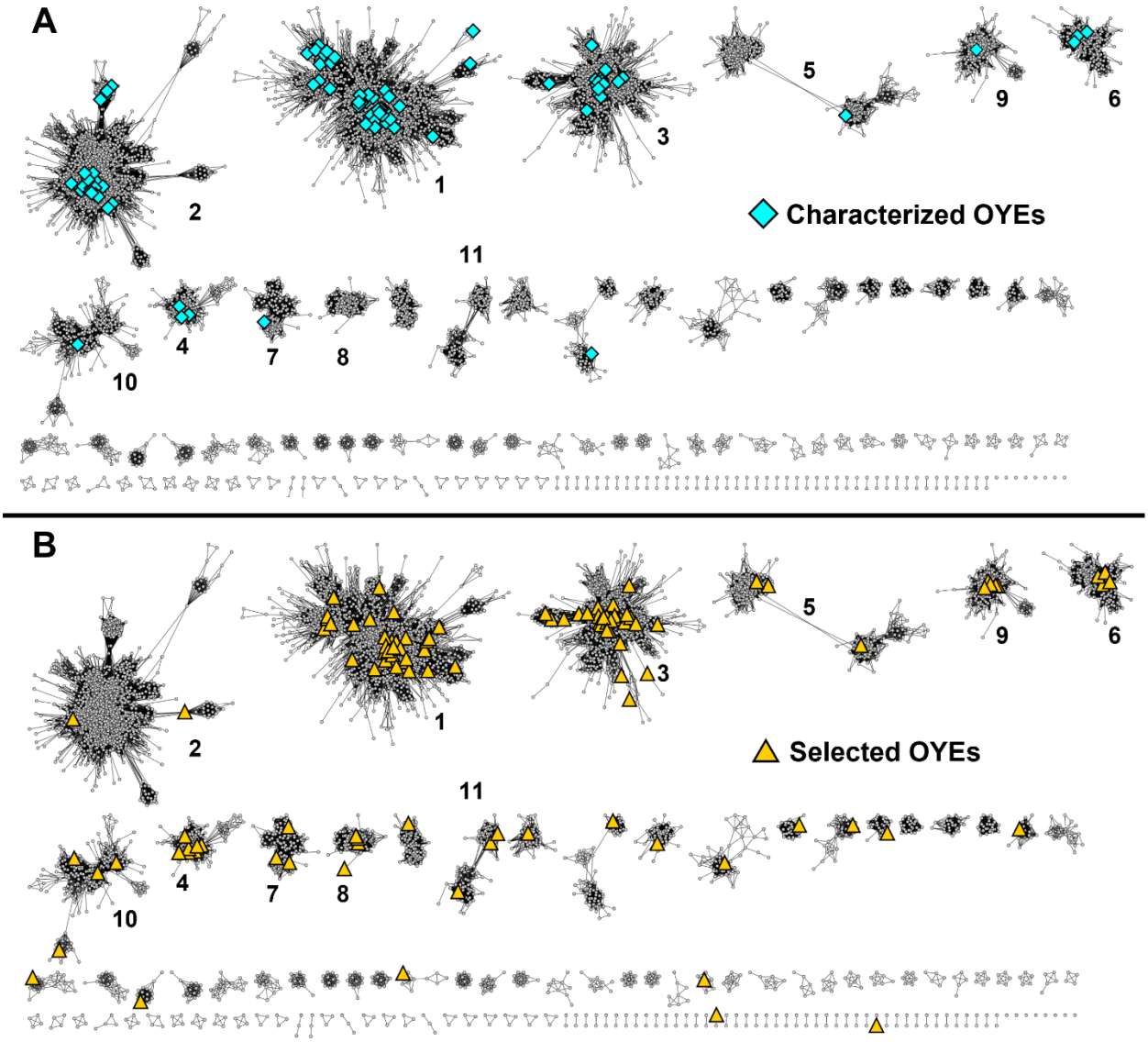

Figure 2.3 Two views of the SSN of the OYE family. Numbering is based on the size or number of sequences in the cluster with cluster 1 being the largest. A) The previously characterized OYEs (blue diamonds) are highlighted in the SSN map showing the explored clusters. B) The same view of the OYE family, but displaying the selected sequences (orange triangles) for biochemical evaluation. 50% ID for nodes and E-value threshold of 10^{-85}. Created in Cytoscape

2.2.2 - Individual Cluster Analysis

Clusters 1 through 3 represent the three largest groups, each containing ~25% of OYE family members. The largest group, cluster 1, comprises the previous classification of Class I or 'classical' OYEs including the fungal OYE1-like, the plant OPR-like, and the bacterial PETNR-like enzymes.[2] Half of all characterized OYEs are located within this group including the majority of those with solved crystal structures.[1, 2] Cluster 2 consists of the 2-enoate reductases with the majority of these sequences containing the second FAD binding domain. The third largest group, cluster 3, encompasses the Class II or 'thermophilic OYEs'.[3] Two defining features of this class and observed in the cluster is the conserved cysteine residue (other OYEs contain a threonine) known to interact with the flavin cofactor as a redox modulator and the C-terminal 'arginine finger' that interacts with another monomer's active site.[38] Surprisingly, a significant portion (15%) of cluster 3 are the multidomain 2-aminobenzyoyl-CoA monooxygenase/reductases – a related OYE subgroup that is rarely associated with the family.[39]

The remaining clusters comprise roughly the last 25% of the OYE family. Unlike the three large clusters, the remaining groups are only lightly sampled or completely unexplored. Cluster 4 contains the characterized Class IV OYEs: Chr-OYE1, Rer-ER7, and Ppo-ER3. Enzymes from this cluster contain a ~20 amino acid insertion in between β-sheet 7 and α-helix 7, in agreeance from previous analysis of Class IV enzymes.[8] At the chosen SSN threshold, cluster 5 is composed of two loosely connected smaller subclusters contained entirely of either bacterial or fungal sequences. Within the fungal subcluster is the sole characterized cluster 5 OYE, IccE from *Penicillium variabile* and one of the orphan OYEs, that has confirmed epimerization activity – vital for the natural synthesis of the fungicide ilicicolin H.[40] Cluster 6 consists of most of Class III OYEs such as YqiG, LacER, and LrFOR, while cluster 13 contains the remaining Class III OYE:

Lla-ER.[8] Clusters 6, 13 and the unexplored 8 conserve the histidine and asparagine residue pair that is shown to coordinate the carbonyl moiety of the substrate. In nearly every other cluster this is a conserved double histidine pair, except for specific subclusters of cluster 1. Interestingly, nearly ~20% of cluster 6 are >900 amino acid in sequence length with domains related to fumarate reductase/flavocytochrome C. One such enzyme has been characterized, FRD from *Klebsiella pneumoniae*, with NADH oxidation and fumarate reductase activity, though it is uncertain the specific role of the OYE-like domain within this enzyme.[41]

The sole representative of cluster 7 is Nox from *Rhodococcus erythropolis* MI2, an 'orphan' OYE that has yet to be organized within a class.[42] Cluster 7 enzymes, including Nox, contain a conserved $CxxCxxCx_nC$ motif of a 4Fe-4S cluster near the C-terminus and aligns with the iron sulfur cluster coordinating residues of 2-enoate reductases crystal structures. It is unclear what the function of the possible iron sulfur cluster is for cluster 7 enzymes - whether structural or for electron transfer to/from an auxiliary binding partner. Previous characterization demonstrated that Nox could oxidize NADH, but it is unclear if a fully formed metal cluster was present in the enzyme during the assay.[42] Regardless, this iron sulfur cluster motif is also conserved in clusters 10, 14, 18, and 20.

The sole representative of Class V OYEs, ArOYE6 from *Ascochyta rabiei*, is in cluster 9. Recently, ArOYE6 was crystallized, revealing a novel C terminus region of ~75 amino acids that was confirmed to be vital for FMN binding.[10] Other sequences from this cluster also contain a similar C-terminus region that is typically 50-100 amino acids longer than canonical OYEs such as OYE1 and YqjM. Cluster 9 is also unique in that it is comprised solely of eukaryotic OYEs of which >20% are originate from nematodes. Clusters 8, 11, 12, and 14-20 have yet to be

characterized. Clusters beyond 13 begin to narrow in taxonomy and sequence similarity, likely indicating that these clusters may be small offshoots of larger clusters.

2.2.3 - Phylogenetic Analysis and Reorganization of the OYE Family

To investigate the relationships between the identified clusters, the phylogeny of the OYE family was explored using ~500 representative sequences (Fig. 4). Unsurprisingly, enzymes from clusters 1-3 formed distinct groups separate from each other. From the remaining clusters, three distinct groups of clusters emerge: clusters 4 and 8, then clusters 6, 11, and 13, and lastly clusters 5, 7, 9, and 10. Interestingly, the last group appears to be related to the 2-enoate reductases of cluster 2. Cluster 12 does not group with other clusters and is currently an 'orphan' cluster until other similar clusters are identified.

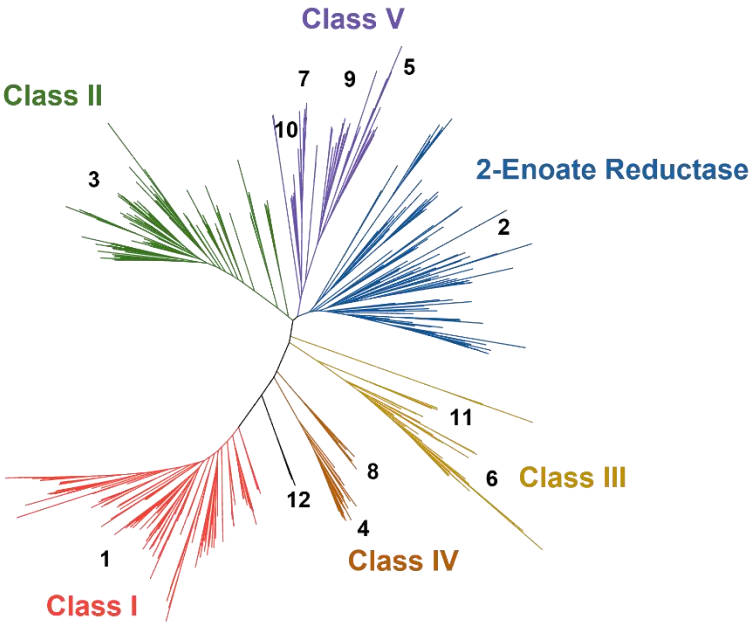

Figure 2.4 Unrooted phylogenetic tree of the OYE family. The approximate location of each cluster is noted in black. The updated classes are labeled using the previous colors of red for Class I, green for Class II, yellow for Class III, orange for Class IV, purple for class V, and blue for 2-Enoated reductases. Phylogenetic tree was formed using multiple sequence alignments using PROMALS3D and the tree calculated using IQ-Tree. Visualized using iTOL.

With the continuous discovery of new OYE sequences, it is inevitable that these clusters will change over time. A reorganization method is proposed to incorporate these bioinformatic results and rectify the numerous attempts at classifying the OYE family. Based on the phylogenetic analysis, the clusters organize into 5 groups similar to the previously described 5 classes of the most recent classification (Fig. 4).[8] To simplify, these 5 classes are kept with the additions of subclasses to designate the unique clusters identified in this study. The revised classes are as follows: Class I: Cluster 1, Class II: Cluster 3, Class III: Clusters 6, 11, and 13, Class IV: Cluster 4 and 8, and Class V: Clusters 5, 7, 9, and 10. The 2-enoate reductases of cluster 2 are excluded from this classification as these enzymes are historically considered a separate group, but if need be would be placed in Class V.[43] Clusters 14-20 are likely offshoots of larger clusters and will be included in the 5 classes but not individual subclasses. For the remainder of this chapter, the cluster designation will be used to avoid confusion.

2.2.4 - Selection of Novel OYE Sequences for In Vitro Screening

The bioinformatic analysis identified vast sections of uninvestigated sequence space in the OYE family which likely contain novel biocatalysts. To explore this, 125 sequences were selected to systematically sample the OYE family (Fig. 1c; Table S3). This selection included 119 novel protein sequences and 6 known OYEs to serve as internal controls. Enzyme selection was guided by complementarity to known OYEs, proportional representation of cluster size, and variation in conserved active site regions (ex: T37, Y82, W116, and N194 in OYE1 numbering). Representatives from uncharacterized (sub)clusters and taxonomy were prioritized, whilst avoiding candidates from organisms that may be problematic for protein expression in *E. coli*. Sequences of atypical length, < 240 aa and >555 aa, were avoided to eliminate protein fragments and multi-domain proteins that may be insoluble due to complex folding and unmet cofactor

requirements. By these criteria, the majority of enzymes from cluster 2 were eliminated from experimental consideration as they are typically >600 amino acids in length and contain multiple domains.

2.2.5 - Selection of Substrate Mixes, Reaction Conditions, and Characterized OYE Activity

For rapid, semi-quantitative functional screening, the selected sequences were synthesized using an in vitro transcription/translation system (IVTT).[44] These reactions were supplemented with purified GroEL/GroES chaperones, FMN and FAD for proper folding and cofactor loading. As a validation, IVTT screening results were confirmed with traditionally purified enzymes for novel OYEs. Likewise, solubility data for all library members were obtained in parallel by small-scale heterologous expression in *E. coli*. These studies suggest that 118 OYEs (95%) could be overexpressed; 87 (70%) produced a soluble fraction. Interestingly, protein insolubility did not correlate with kingdom, affecting ~30% of representatives from bacteria and fungi and ~50% from archaea, plantae, metazoan and metagenomic DNA, respectively. Sequences from most clusters had at least one soluble representative except for clusters 5, 7, and 10. Notably selected sequences from clusters 7 and 10 contain the [4Fe-4S] motif which our expression system would struggle to properly load, possibly explaining the insolubility of these enzymes.

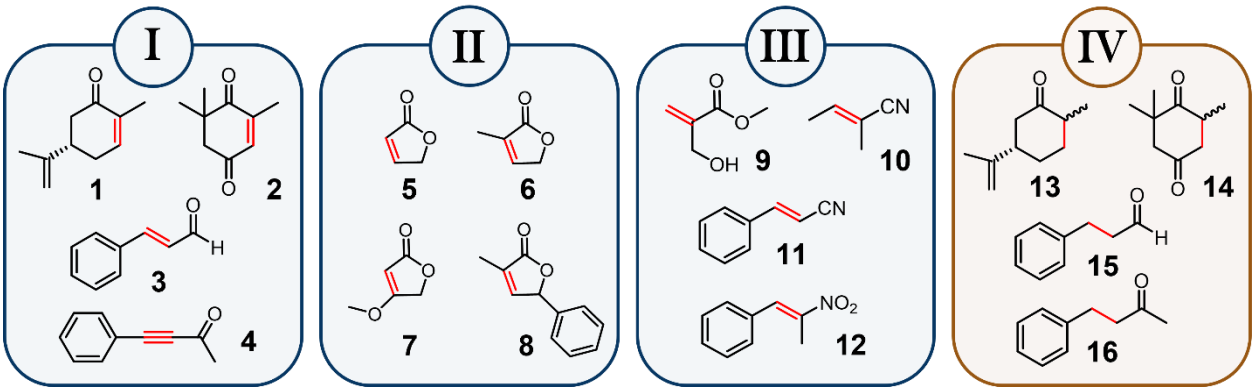

Figure 2.5 The substrate mixes. The 16 substrates used in this study are shown organized into 4 mixes. The color of the mix is the type of chemistry expected with blue for ene reduction and gold for desaturation. Highlighted in red is the bond which will be reduced (I-III) or desaturated (IV).

The selected OYEs were screened against 16 different substrates organized into 4 mixes (Fig. 6). Mix I contained (*S*)-carvone (**1**), ketoisophorone (**2**), cinnamaldehyde (**3**), and 4-phenylbut-3-yn-2-one (**4**). These compounds are standard OYE substrates, serving as controls for typical ene reductase activity while probing enantioselectivity with **1** and **2**.[45-47] The phenyl alkyne, **4**, also was included to observe if selected sequences could perform sequential reductions to the alkane. Mix II consisted of various furanones (**5-8**) as precursors for high-value chiral synthons.[17] These substrates contained substitutions at the α and β position which can be difficult for characterized OYEs.[11] The bulky substrate **8** was used to probe the active site volume of the selected sequences. Mix III represented challenging substrates that known OYEs have little to no activity for. The precursor to the Roche ester (**9**) is involved in various industrial synthesis and selective reduction of unsaturated nitriles (**10-11**) would be beneficial for 'click' chemistry.[19, 48] Lastly the nitro alkene (**12**) was incorporated to probe for nitro versus alkene reduction.[6] In addition to alkene reduction, growing interest in the desaturase activity of OYEs prompted the testing of reverse, oxidative chemistry for the selected sequences.[49] Accordingly, mix IV used alkanes (**13-16**), the products of our four reference compounds, as substrates. Reactions with mix

IV were conducted without nicotinamide cofactors and in the presence of atmospheric oxygen. Although reports have previously described OYE desaturase activity, it has required either artificial flavin cofactors or non-physiological temperatures.[50, 51] All reactions were quenched after 24 hours of reaction time then subjected to GC/MS analysis.

The screening protocol was validated with six known OYEs (OYE1, NemA, YqiG, PETNR, $FgaOx_3$, and TcOYE) to confirm the previously reported substrate conversion profiles.[11, 52-54] Of note, the closely related NemA and PETNR both exhibited desaturase activity with mix IV in addition to the expected conversion of substrates in mixes I and III. Separately, this study significantly expanded the substrate scope of $FgaOx_3$ from *Aspergillus fumigatus* and TcOYE from *Trypanosoma cruzi* – two enzymes previously studied only for native function.[53, 54] $FgaOx_3$ converted substrates in mixes I and III, while TcOYE displayed broad activity across all four reaction mixes and was the most promiscuous enzyme converting 9 of the 16 substrates. In the next sections, novel OYEs identified as potential biocatalysts will be compared to the activity profile of OYE1 from the screen as this characterized enzyme displays typical ene reductase activity and reduces half of the substrates.

2.2.6 - Overall OYE Activity and Cluster Specific Trends

After screening the novel 119 OYEs, 75 (60%) enzymes displayed activity in at least 1 mix, representing 14 different clusters. Sequences from clusters 5, 7, 10 and 16 were insoluble, but several enzymes were active in the screen. Vice versa, the representatives from clusters 15, 17, and 21 were soluble but inactive. Differences between solubility and activity between traditional and cell free expression are likely due to the inherent differences of each system. In the case of the soluble/inactive sequences, it could be that the right substrate was not identified.

Overall, activity was detected for 13 substrates; only **7**, **10**, and **11** were not reduced by one of the 75 active enzymes. Substrate **7** contains an ether moiety at the β position, which is particularly difficult for OYEs to activate.[17] Unsurprisingly, the nitriles (**10** and **11**) were not reduced as the functional group is hard for the enzymes to properly coordinate. Alkene reduction of **12** was observed, but no nitro reduction was detected by any of the enzymes. Clear activity trends were recognized from specific clusters (Fig. 6). For instance, cluster 1 enzymes have a variety of substrate profiles but preferred **12**. Likewise, cluster 3 showed preference for **1**, but could not readily convert **4** or **12**. This opposite preference could be due to the geometry of the active site. Characterized cluster 1 sequences conserve hydrophobic residues at the binding position of the phenyl group of **12** in the active site. In contrast, cluster 3 enzymes conserve the 'arginine finger' near this position in this active site, replacing this hydrophobic region with that of a charged residue.[1] In other clusters, sequences from cluster 4 convert all of mix I while being inactive in mix II and cluster 6 OYEs preferred to convert substrate **3** and **12** over other substrates – similar to cluster 1 enzymes. From the sequence info, it is unknown why clusters 4 and 6 display specific activity profiles.

Intriguingly, significant desaturase activity was observed across the family. Of the 125 enzymes screened, 33 enzymes from 8 distinct clusters converted at least one substrate in mix IV, indicating widespread desaturase activity within the OYE family (Fig. 6). Activity was commonly detected for substrates **13** and **14**, with enzymes and clusters typically showing a preference. For example, OYEs with desaturase activity in cluster 3 only convert **13** while enzymes from cluster 4 show a strong preference for **14**. (Fig 2b) This is similar to trends observed in the same clusters for the forward reaction. Notably, conversion for **15** was only detected by BmOYE1 from *Bacillus marmarensis*, an OYE from cluster 6, while no activity was observed for **16**.

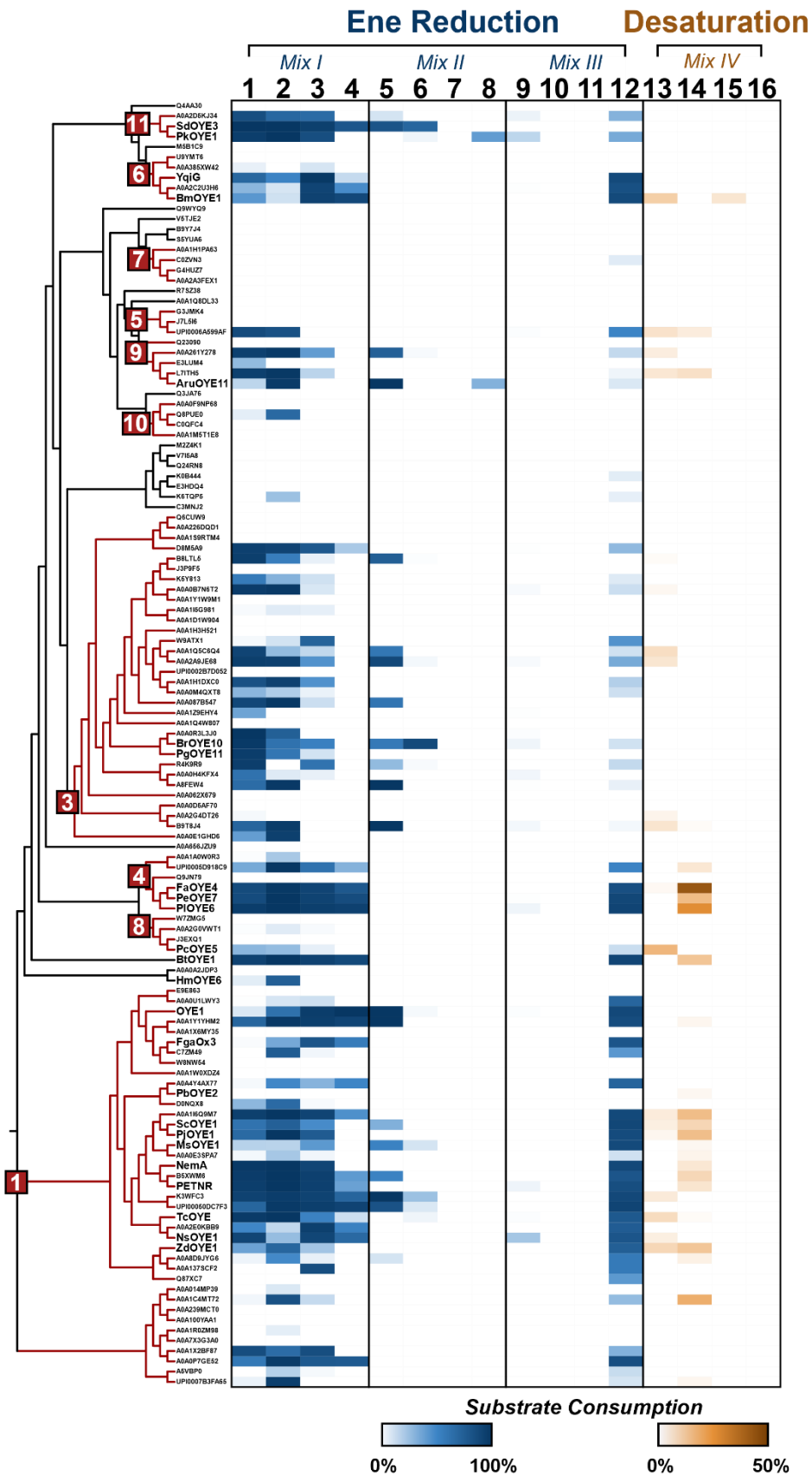
Ene Reduction
Desaturation
Mix I
Mix II
Mix III
Mix IV
1 2 3 4 5 6 7 8 9 10 11 12 13 14 15 16
SdOYE3
PkOYE1
YqiG
BmOYE1
AruOYE11
BrOYE10
PgOYE11
FaOYE4
PeOYE7
PlOYE6
PcOYE5
BtOYE1
HmOYE6
OYE1
FgaOx3
PbOYE2
ScOYE1
PiOYE1
MsOYE1
NemA
PETNR
TcOYE
NsOYE1
ZdOYE1
Substrate Consumption
0%
100%
0%
50%

Figure 2.6 Heatmap of substrate consumption by the selected OYEs. The heatmap displays the percentage of substrate the selected sequences consumed in 24 hours. The darker the color, the more substrate consumed (blue for ene reduction, gold for desaturation). Desaturase activity is to 50% to provide help visualize the widespread activity. The substrates are labeled up with boxes around the mixes. On the left side is a phylogenetic tree purely for organizing the sequences into clusters (red boxes and lines). Mentioned OYEs are named and uniprot codes are used for the remainder. Created in iTOL.

2.2.7 - Interesting Biocatalytic Candidates of Mixes I-III

Several selected sequences displayed significantly improved or novel catalytic activity when compared to characterized enzymes such as OYE1 (Fig. 7A-G). In mix I, 3 enzymes reduced all substrates >85% within 24 hours (Fig. 7A). OYE1 in comparison reduces all mix I substrates but only converts <10% of **1** and ~60% of **2**. Two enzymes are from cluster 4: PlOYE6 and PeOYE7 from *Pseudomonas lutea* and *Priestia endophytica* respectively, while the other OYE, BtOYE1 from *Bacillus thuringiensis*, is from the uncharacterized cluster 12. Mix 1 also probed enantioselectivity of the selected sequences with **1** and **2** as characterized OYEs display a strong preference for (R) enantiomer in both reactions. A cluster 3 enzyme, PgOYE11 from *Pseudomonas sp.* GM48, and a cluster 16 enzyme, HmOYE6 from *Hypsizygus marmoreus*, both converted a racemic mix of **2p** suggesting these OYEs are capable of the 'flipped' (rotated vs the axis of the carbonyls) or 'reverse' (opposite coordinated carbonyl) binding orientations when compared to other OYEs (Fig. 7B).[55] Improved conversion of (S)-**2p** could provide a starting point for future mutational studies.

Substrates **5** and **6** in mix II only differ by a methyl group, however**,** OYE1 heavily prefers **5** over **6** converting 100% vs <10%. Improved conversion of **6** was detected from two enzymes, SdOYE3 and BrOYE10 from *Sphingomonas dokdonensis* and *Bradyrhizobium sp*. R5

respectively, though there are slight differences between their substrate profiles (Fig. 7C). SdOYE3, from the uncharacterized cluster 11, converts both substrates >70% but shows a slight preference towards **5**, while BrOYE10, from cluster 3, prefers **6** - converting 9-fold more than OYE1. (Fig 2e) For substrates **8**, no conversion was detected for characterized enzymes. An OYE from cluster 11, PkOYE1 from an unidentified proteobacterium, and AruOYE11 from *Aspergillus ruber* and cluster 9, were the only enzymes to display activity for **8** (Fig. 7D). This bulky substrate likely indicates that their respective active sites may be slightly larger than other known OYEs. (Fig 2f) Interestingly, PkOYE1 does not reduce **5** but does convert the methylated **6,** showing a similar preference as the other cluster 11 enzyme, SdOYE3.

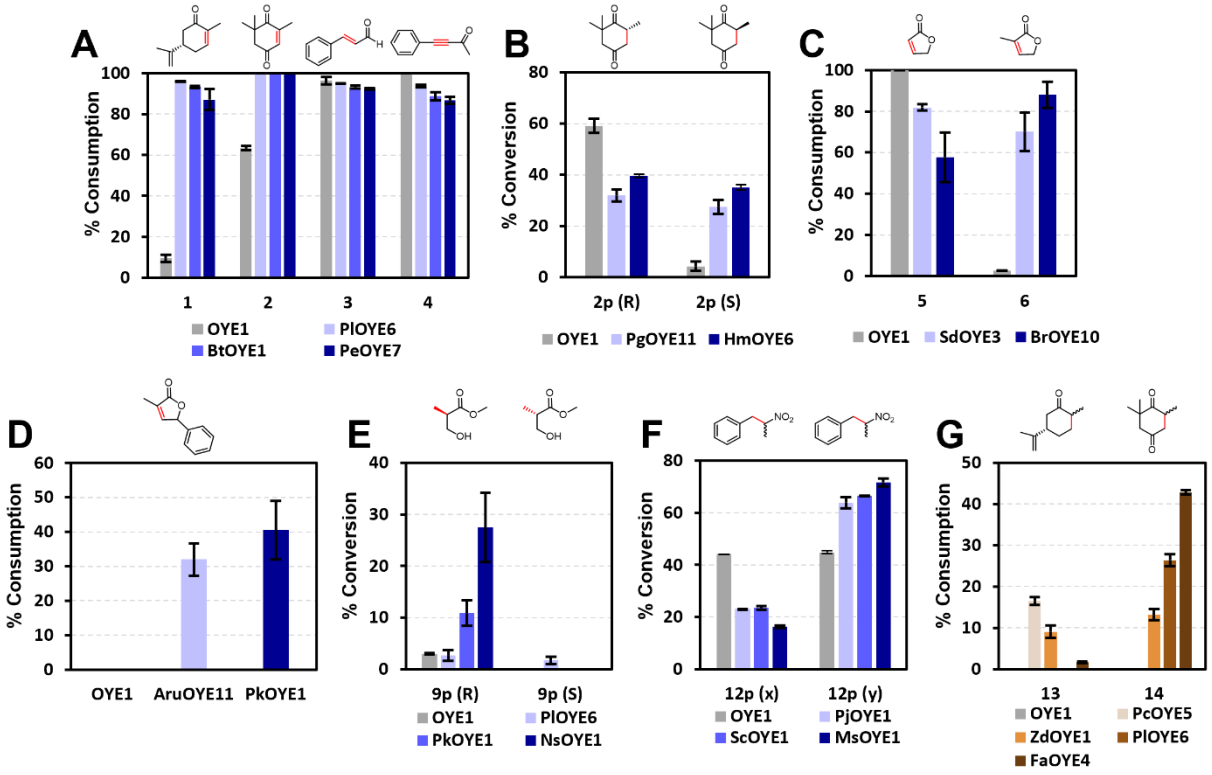

Figure 2.7 Activity of potential biocatalysts. The unique catalytic activity of potential biocatalysts is shown above. Colors represent the type of activity with blue for ene reduction and gold for desaturation. The substrate or product is shown above the graph.

In mix III, improved catalytic activity and enhanced enantioselectivity was also detected. For characterized OYEs, **9** remains a challenging substrate. PkOYE1 and the cluster 1 enzyme NsOYE1, from *Neptuniibacter sp.,* convert 6- and 9-fold more of **9** when compared to OYE1 and other characterized enzymes (Fig. 7E). It is intriguing that PkOYE1 converts the bulkiest substrate (**8**) and one of the smallest substrates (**9**) at relative high levels of conversion. Hailing from an uncharacterized cluster with no solved structures, it is unclear what the active site geometry of this enzyme is. SdOYE3 shows no conversion for either substrate, hinting that this unusual activity may be specific to PkOYE1 and not the cluster. PkOYE1 is not easily expressible despite several mutational efforts, preventing further experiments. Beyond improved conversion, PlOYE6 produced a racemic mix whereas OYE1 and other enzymes heavily prefer the (R)-enantiomer. This could also prove to be the starting point for future mutational studies to produce the (S)-enantiomer. Lastly, alkene reduction of **12** results in a racemic mixture for the majority of enzymes except for cluster 1 enzymes: ScOYE1, MsOYE1, and PjOYE1 from *Stenotrophomonas chelatiphaga*, *Methylophaga sp*., and an unidentified proteobacterium, respectively (Fig. 7F). These enzymes all preferred the same enantiomer over the other, but the identity of the favored enantiomer could not be resolved. The methyl group at the α position of **12** creates the possibility of a stereocenter after reduction. Therefore, these 3 enzymes must have a preferred binding orientation for the substrate, likely a steric interaction with the methyl group.

While most of the desaturase activity for **13** and **14** was detected at low conversion levels, several enzymes displayed considerable oxidative capabilities (>10%). In particular, the two cluster 4 OYEs, PlOYE6 mentioned earlier and FaOYE4 from *Flavobacterium sp.* ABG, converted >25% of **14** within 24 hours with the latter enzyme reducing >40%. (Fig. 7G) For substrate **13,** the highest activity was detected for PcOYE5, a cluster 8 enzyme from *Pseudomonas*

chloritidismutans, which has >15% conversion but could not convert **14** (Fig 7G). Several OYEs displayed substrate promiscuity for the desaturase reaction, such as ZdOYE1, a cluster 1 enzyme from an unclassified marine bacterium, that converted both **13** and **14** >10% (Fig 7G). Another cluster 1 enzyme, PbOYE2 from *Pseudomonas batumici*, was only active in mix IV with zero conversion detected in the other mixes. It is unclear whether this enzyme is only capable of desaturase activity as it could reduce other substrates not screened.

2.2.8 - Redox Potential and Other Explanations for Desaturase Activity

Few studies have explored the reverse, oxidative chemistry of OYEs.[49] Massey et al. demonstrated that OYE1, an enzyme with no native desaturase activity, could be converted into a desaturase enzyme by increasing its redox potential via incorporation of artificial flavins.[50] This suggests that the redox potential of an OYE may be critical to desaturase activity. Using the xanthine/xanthine oxidase method to determine flavoprotein redox potentials, 4 OYEs were examined with distinct and varied desaturase activity: PlOYE6, FaOYE4, PcOYE5, and ZdOYE1.[56] OYE1 was included as a negative control and exhibited a redox potential midpoint of -227 mV, in agreeance with previous studies.[57, 58] Interestingly a correlation between redox potential and desaturase activity was not observed: two OYEs, PcOYE5, and ZdOYE1, exhibited a more positive (+~25 mV) redox potential than OYE1, but PlOYE6 was more negative (-20 mV) (Fig 3a). Unfortunately, FaOYE4 was too unstable to properly measure the redox potential of the enzyme, but as the enzyme is from the same cluster and has a similar substrate profile to PlOYE6 then it likely has a similar redox potential. Regardless, the differences in redox potential between the enzymes with activity vs OYE1 are only slight when compared to the artificial flavins of the previous study.[50] Furthermore, the trend appears to be that enzymes with the highest desaturase activity coincidentally have the highest ene reductase activity (PlOYE6 and FaOYE4) for select

substrates. In the previous study, the conversion of OYE1 into a desaturase enzyme via redox potential resulted in the removal of ene reductase activity.[50] If an increased redox potential was the main factor in desaturase activity, then an opposite trend should be observed as the enzymes should be less capable of ene reduction. Therefore, redox potential may influence the desaturase activity of certain OYEs, but other factors must also contribute especially for the selected OYEs.

Enzyme	Redox Potential	1 (%)	2 (%)	13 (%)	14 (%)
ZdOYE1	**-202 mV**	**38.2**	**70.3**	**9.1**	**13.2**
PcOYE5	**-204 mV**	**30.4**	**27.8**	**16.5**	**n.d.**
OYE1	**-227 mV**	**9.5**	**63.4**	**n.d.**	**n.d.**
PlOYE6	**-241 mV**	**96.1**	**100**	**n.d.**	**26.4**

Table 2.1 Redox potentials vs substrate consumption for selected OYEs. The desaturase OYEs are organized in decreasing value of redox potential. The percent consumption of mix 1 and mix 4 substrates are included to show ene reductase and desaturase of the enzymes.

Another possibility concerns the pK_a of the conserved tyrosine residue located above the substrate in the active site. In the forward (ene reductase) reaction, this residue either donates the proton after the initial hydride transfer or it coordinates a catalytic water molecule.[2] It is highly likely that this tyrosine participates in the reverse reaction as well. It is possible that the local environment of the desaturase enzymes lowers the pK_a of the Tyr, deprotonating the side chain at physiological conditions and potentially helping to facilitate hydride transfer to the flavin. Though this shift would have to be significant as the typical pK_a of tyrosine is 10. The reaction pH for mix IV was higher (8.5) than the other mixes (7.5) and early preliminary results also indicate that the

reaction displays a pH dependence, though more experimentation is needed to confirm. Mutation of the tyrosine residue in the desaturase enzyme should also affect the activity confirming the role of the residue

Another factor could be the choice of substrates as enzymes with high desaturase activity also displayed a strong preference in the forward reaction towards the product of mix IV substrates. Thus, it is possible many OYEs are capable of native desaturase activity, but it is a matter of proper substrate binding. Nearly all desaturase activity was observed for **13** and **14,** the two substrates with less degrees of freedom than **15** and **16** – especially at the α and β positions. OYE1 prefers **3** and **4** in mix I (products of **15** and **16**) with poor activity for **1** and **2** (products of **13** and **14**). It is possible OYE1 may have native desaturase activity if more substrates are explored.

2.3 - Conclusions

In this chapter, the OYE family was systematically organized and explored through a platform of bioinformatic and biochemical techniques to broaden the current understanding of OYEs. While this family is extensively studied, SSN and phylogenetic analysis allowed for reorganization of the OYE family while highlighting unknown regions that are ideal for further biocatalytic investigation. The bioinformatic results revealed several unusual groups within the family such as entirely eukaryotic cluster 9 with the first animal OYEs and the presence of a conserved iron sulfur cluster motif found within single domain sequences of clusters 7, 10, 14, 18 and 20. Furthermore, SSN analysis also revealed the relation of multi-domain OYE subgroups to traditional enzymes with the 2-aminobenzyoyl-CoA monooxygenase/reductases and fumarate reductase/flavocytochrome C belonging to clusters 3 and 6. Groups were identified for former ‘orphan’ OYEs such as IccE and Nox. Phylogenetic analysis resulted in the 20 major clusters forming 5 distinct groups which are roughly similar to previous organization attempts.[8] These 5

groups and the clusters within form the basis of the newly proposed class/subclass system for the OYE family. It is likely though that continuous reevaluation of the family is necessary as 50,000+ new OYE sequences have been identified since this study began.

The bioinformatic analysis identified 125 (119 novel and 6 characterized) diverse representative sequences which were screened using cell free expression and GC/MS based assays. Of the selected sequences, 48% (60) were soluble and 62% (77) were active towards at least one substrate - representing a >50% increase in the number of characterized OYEs. Surprisingly, desaturase activity was observed throughout the enzyme family. Previously concluded to only occur at elevated temperatures or through artificial flavins, this significantly expands the enzymatic versatility of OYEs.[50, 51] In addition to desaturase activity, several trends were observed for cluster specific solubility and activity data. Sequences from the iron sulfur motif clusters were insoluble, likely due to improper metal cluster loading, but a few of the cell free expressed enzymes were active. Cluster 1 enzymes preferred **12** while cluster 3 enzymes struggled with the substrate, likely due to differences in conserved residues near the back of the active site.[1] Enzymes from cluster 4 displayed the highest ene reductase and desaturase activity. Further exploration of this cluster could identify more excellent biocatalysts.

In total 14 novel enzymes were identified as potential biocatalysts. Of note, PlOYE6 is an excellent ene reductases converting all substrates of mix I, exhibiting significant desaturase activity specifically for **14** and the highest activity for **9p (S)**. Two enzymes, PkOYE1 and NsOYE1, showed greatly (6- and 9-fold) enhanced conversion for the challenging substrate **9**. Additionally, PkOYE1 and AruOYE11 convert the large bulky **8** which OYE1 and the other characterized enzymes did not. Enzymes with unusual enantioselectivity and improved catalysis

were identified in every mix and all of these enzymes are promising starting points for further directed evolution studies as possible industrial biocatalysts or to understand their unique activity.

Despite previous indications, the observed desaturase activity does not appear to be heavily influenced by an enzyme's redox potential and must be dependent on other factors. Two desaturase enzymes displayed slightly higher redox potential compared to the desaturase inactive OYE1 while the redox potential was lower for one of the most active enzymes. Other factors which may impact desaturase capability include the pK_a of the catalytic tyrosine residue or substrate binding of the saturated compounds. Regardless, these results shift the consensus understanding of the mechanism for the reverse reaction in OYEs.

This combined approach of bioinformatics and synthetic biology has revealed a wealth of knowledge concerning OYEs yet highlights the vast unknown that remains for the enzyme family. These results act as the basis for several different avenues of further exploration into the OYE family. The immediate goal is to fully decipher the observed desaturase activity, namely exploring the protonation steps via mutational studies of the tyrosine residue and determining the pH rate dependence of the reaction. Further substrate screening is also needed to fully interrogate role of substrate binding on desaturase activity of the selected enzymes. Beyond desaturase activity, it is likely these enzymes are capable of other novel chemistry and additional substrates screens are being developed. The bioinformatic analysis revealed the presence of unusual OYE subgroups, chiefly the putative iron sulfur containing enzymes. Investigation into the functionality of this metal cluster would be a worthwhile endeavor from an enzyme evolutionary standpoint or as a biocatalyst capable of reduction through direct electrochemistry.[59] Lastly this platform for enzyme family screening could be enhanced by incorporating machine learning algorithms.[60] By combining the bioinformatic and screening analysis with homology modeling, a robust dataset of

sequence-structure-function information would enable machine learning to identify factors controlling the observed unique activity and guiding future rounds of selection. This new approach could then be utilized to explore other large, diverse enzyme families.

2.4 - Materials and Methods:

2.4.1 - Generation of SSNs

Sequence similarity networks were generated by collaborator Dr. Janine Copp at the University of British Columbia using 70,366 protein sequences associated with the PFAM designation PF00724 'OYE-Like'.[61] An edge-threshold of 10^{-85} was selected as it separated characterized enzymes from known enzyme classes (Classes I, II, and 2-enoate reductases) into distinct clusters.

2.4.2 - Generation of Phylogenetic Trees

A comprehensive phylogenetic tree for the OYE family was constructed using a proportional representative selection of all characterized (including this study) sequences in addition to a further supplement of enzymes resulting in 470 sequences from the 20 major clusters. The enzymes were aligned using PROMALS3D which considers secondary structure prediction and crystallographic data in conjunction with sequence info.[62] Only the OYE-like domain of each sequence was used. The resulting clustal alignment was used to generate a phylogenetic tree with IQTree using the WAG substitution model and freerate heterogeneity.[63] The tree was visualized using iTOL.[64]

2.4.3 - Determination of the Solubility of Selected OYEs

OYE sequences were expressed in BL21 cells in 5 mL 2xYT media with kanamycin. Initial growth was incubated at 37˚C until an OD600 of 0.6 was observed. Then the cells were induced using Isopropyl β-D-1-thiogalactopyranoside (IPTG) to a final concentration of 0.3 mM. The cells

expressed at 20˚C overnight and the next day were spun down at 4000 g at 3 min to pellets which were chemically lysed with BugBuster (EMD). The solutions were rocked for 20 min to fully lyse the cells. Then the samples were centrifuged for 10 min at 8000 g. The supernatant (soluble) was removed, and the resulting pellet (insoluble) was resuspended with DI water. Both fractions were loaded onto an SDS-PAGE gel for solubility analysis.

2.4.4 - Expression of OYE Sequences using Modified PURExpress

Selected novel OYE sequences were codon optimized for *E. coli* expression then synthesized/placed into pET28a plasmids by the DOE Joint Genome Institute. For in vitro expression of selected sequences, the PURExpress kit from New England Biolabs was used for rapid production of the enzymes. Here in vitro expression reactions were performed in duplicates with the following components: PURExpress Solution A, Solution B, 200 ng of Template DNA, 100 μM FMN and FAD, 5 μM of GroEL, 10 μM GroES, 20 U Murine RNAse Inhibitor, and RNAse Free Water. FMN and FAD were added to fulfill the potential cofactor requirements of the novel OYE sequences. GroES and GroEL were added to improve proper protein folding of the target enzyme. Purification and quantification of both GroES and GroEL were based on literature.[65] In addition to the novel OYE sequences, a positive control of OYE1 in pET14b and negative control of dihydrofolate were expressed with each batch of in vitro expression. Reactions were incubated at 37 C for 2.5 hours then quenched on ice before aliquots were added into an activity assay.

2.4.5 - Activity Assay Conditions for Novel OYE Sequences

To determine the ene reductase and desaturase activity of selected OYE sequences, in vitro expressed protein was aliquoted into reaction mixtures and allowed to react for 24 hours. Substrates were purchased from Sigma Aldrich except for **8** which was a gift from Melanie Hall

at the University of Graz. For mixes I-III (ene reductase), reaction mixtures contained 2 U of glucose dehydrogenase, 100 mM glucose, 200 μM of NADH and NADPH and 250 μM (1 mM for mix III) of each substrate in a buffer of 50 mM Tris HCL pH 7.5. Glucose dehydrogenase and glucose were added to recycle NAD(P)H to ensure sufficient reducing equivalents. Purification of this enzyme was performed using methods from literature.[66] Reactions also occurred under anaerobic conditions to prevent competition with oxygen. For mix IV (desaturase), reaction mixtures only contained 20 mM pyrophosphate buffer ph 8.5 with 250 μM of each substrate under aerobic conditions. Reaction conditions for desaturase activity were adapted from literature.[50] Each reaction was performed in duplicate and after 24 hours were quenched using ethyl acetate. In addition, substrates and products were extracted twice using ethyl acetate containing 500 μM cyclohexane (internal standard) then placed onto GC/MS for analysis.

2.4.6 - GC/MS Parameters

GC/MS quantification was performed using Shimadzu QP2010 SE instrument using an FID detector with helium as a carrier gas. A chiral CycloSil-B column was used to separate the compounds. Mixture GC/MS protocols were developed and are as follows: *Mix I/IV*: Injection temperature 250 ˚C, oven 110 ˚C with ramp to 150 ˚C at 2 ˚C/min, hold for 5 min. *Mix II*: Injection temperature 220 ˚C, oven 80 ˚C hold for 1 min then ramp to 100 ˚C at 1 ˚C/min hold for 1 min then ramp to 185 ˚C at 2.5 ˚C/min. *Mix III*: Injection temperature 210 ˚C, oven 75 ˚C hold for 5 min then ramp to 100 ˚C at 2 ˚C/min, ramp to 200 ˚C at 10 ˚C/min hold for 5 min.

2.4.7 - Expression and Purification of Selected OYE Sequences

Plasmids were transformed into chemically competent E. coli BL21 (DE3) cells and spread onto kanamycin (30 mg/mL) agar plates and allowed to grow overnight at 37˚C. Colonies were picked and 5 mL LB with kanamycin were inoculated overnight. The next day, 1 mL of the

overnight culture was used to inoculate 250 mL of 2xYT medium (with kanamycin) for expression. The culture was allowed to grow until an OD600 of 0.55-0.7 was reached. At the desired OD, the expression cultures were induced with 0.3 mM IPTG and expressed for 18-22 hours for 20˚C. After expression cells were poured into tubes and spun at 4000 g for 20 minutes. The supernatant was decanted, and tubes were placed into freezer (-20˚C) to aid with lysing.

Frozen cell pellets were thawed on ice until liquid then resuspended in buffer 1 (40 mM Tris-HCl pH 8.0, 10 mM NaCl) with 2.5 μL/g of DNase I and 50 μL/g of protease inhibitor cocktail. The solution was chilled on ice for 20 minutes and then sonicated for 3 minutes (10-sec pulse/20-sec off). The mixture was centrifuged for 30 minutes at 4000 g and 4˚C. The supernatant was loaded onto a 5 mL HiTrap Q FastFlow anion-exchange column. The column was washed with buffer 1 for 2 column volumes (CV). Over the course of 15-20 CVs, a linear gradient from buffer 1 to 100% buffer 2 (40 mM Tris-HCl pH 8.0, 1 M NaCl) was used to elute the protein, identifying via the UV-vis absorption of the protein (280 nm) and flavin (450 nm). The protein was collected and concentrated using Millipore filter unit with 10 kDa MWCO. A size exclusion column (Superdex 200, 10/300 GL column) was used to finish purification. Fractions for both columns were analyzed via SDS-PAGE to ensure purity.

2.4.8 - Xanthine-Xanthine Oxidase Assay for OYE Redox Determination

In this assay, xanthine oxidase was used to slowly provide electrons for reduction of the enzyme and a reference dye while monitoring using a Cary UV-vis spectrometer. As OYE1 has a literature redox value of -227 mV, anthraquinone-2-sulfonate, -225 mV, was selected as the reference dye.[56, 58] Other dyes were considered and utilized such as cresyl violet (-166 mV) and phenosafranine (-252) but were too far in redox potential for most OYEs to be properly measured. In an airtight vial, 20 μM of the target OYE, 20 μM methyl viologen, 400 μM xanthine, and 40

μM anthraquinone-2-sulfonate were added to 50 mM $NaPO_4$ buffer at pH 7. In a glass bulb in the side of the cuvette, 100 nM xanthine oxidase was added. The cuvette was subjected to 10 rounds of vacuum and Ar to fully deoxygenate the solution. An initial scan was taken before the reaction, then the solution was tipped to add the xanthine oxidase and UV-vis spectra were collected. Concentration of reduced and oxidized species were determined using absorbance with 331 nm for anthraquinone-2-sulfonate and 460 nm for selected OYEs. Redox potential was calculated using a derived Nernst Equation (1) and explained in further detail in the literature.[56]

$$E_m(protein) = E_m(dye) - y\ intercept * \left(\frac{2.3RT}{nF}\right) \quad (1)$$

F is the faradaic constant and n the number of electrons transferred which is 2. The y-intercept is from the plot of log oxidized/reduced protein vs dye.

References

1. Shi, Q.; Wang, H.; Liu, J.; Li, S.; Guo, J.; Li, H.; Jia, X.; Huo, H.; Zheng, Z.; You, S.; Qin, B., Old yellow enzymes: structures and structure-guided engineering for stereocomplementary bioreduction. *Appl. Microbiol. Biotechnol.* **2020,** *104* (19), 8155-8170.

2. Scholtissek, A.; Tischler, D.; Westphal, A.; van Berkel, W.; Paul, C., Old Yellow Enzyme-Catalysed Asymmetric Hydrogenation: Linking Family Roots with Improved Catalysis. *Catalysts* **2017,** *7* (12), 130.

3. Toogood, H. S.; Scrutton, N. S., New developments in 'ene'-reductase catalysed biological hydrogenations. *Curr. Opin. Chem. Biol.* **2014,** *19*, 107-115.

4. Parmeggiani, F.; Brenna, E.; Colombo, D.; Gatti, F. G.; Tentori, F.; Tessaro, D., "A Study in Yellow": Investigations in the Stereoselectivity of Ene-Reductases. *ChemBioChem* **2021,** *23* (1).

5. Williams, R. E.; Bruce, N. C., 'New uses for an old enzyme'–the old yellow enzyme family of flavoenzymes. *Microbiology* **2002,** *148* (6), 1607-1614.

6. Durchschein, K.; Hall, M.; Faber, K., Unusual reactions mediated by FMN-dependent ene- and nitro-reductases. *Green chemistry* **2013,** *15* (7), 1764-1772.

7. Nizam, S.; Verma, S.; Borah, N. N.; Gazara, R. K.; Verma, P. K., Comprehensive genome-wide analysis reveals different classes of enigmatic old yellow enzyme in fungi. *Scientific reports* **2014,** *4* (1), 1-11.

8. Peters, C.; Frasson, D.; Sievers, M.; Buller, R., Novel Old Yellow Enzyme Subclasses. *ChemBioChem* **2019,** *20* (12), 1569-1577.

9. Nizam, S.; Gazara, R. K.; Verma, S.; Singh, K.; Verma, P. K., Comparative structural modeling of six old yellow enzymes (OYEs) from the necrotrophic fungus Ascochyta rabiei:

insight into novel OYE classes with differences in cofactor binding, organization of active site residues and stereopreferences. *PloS one* **2014,** *9* (4), e95989.

10. Singh, Y.; Sharma, R.; Mishra, M.; Verma, P. K.; Saxena, A. K., Crystal structure of ArOYE6 reveals a novel C-terminal helical extension and mechanistic insights into the distinct class III OYEs from pathogenic fungi. *The FEBS Journal* **2022**.

11. Amato, E. D.; Stewart, J. D., Applications of protein engineering to members of the old yellow enzyme family. *Biotechnol. Adv.* **2015,** *33* (5), 624-631.

12. Joo, J. C.; Khusnutdinova, A. N.; Flick, R.; Kim, T.; Bornscheuer, U. T.; Yakunin, A. F.; Mahadevan, R., Alkene hydrogenation activity of enoate reductases for an environmentally benign biosynthesis of adipic acid. *Chemical science* **2017,** *8* (2), 1406-1413.

13. Sun, J.; Lin, Y.; Shen, X.; Jain, R.; Sun, X.; Yuan, Q.; Yan, Y., Aerobic biosynthesis of hydrocinnamic acids in Escherichia coli with a strictly oxygen-sensitive enoate reductase. *Metab. Eng.* **2016,** *35*, 75-82.

14. Vaz, A. D. N.; Chakraborty, S.; Massey, V., Old yellow enzyme: aromatization of cyclic enones and the mechanism of a novel dismutation reaction. *Biochemistry* **1995,** *34* (13), 4246-4256.

15. Black, M. J.; Biegasiewicz, K. F.; Meichan, A. J.; Oblinsky, D. G.; Kudisch, B.; Scholes, G. D.; Hyster, T. K., Asymmetric redox-neutral radical cyclization catalysed by flavin-dependent 'ene'-reductases. *Nature chemistry* **2020,** *12* (1), 71-75.

16. Stuermer, R.; Hauer, B.; Hall, M.; Faber, K., Asymmetric bioreduction of activated C= C bonds using enoate reductases from the old yellow enzyme family. *Curr. Opin. Chem. Biol.* **2007,** *11* (2), 203-213.

17. Turrini, N. G.; Hall, M.; Faber, K., Enzymatic Synthesis of Optically Active Lactones via Asymmetric Bioreduction using Ene-Reductases from the Old Yellow Enzyme Family. *Adv. Synth. Catal.* **2015,** *357* (8), 1861-1871.

18. Winkler, C. K.; Clay, D.; Davies, S.; O'Neill, P.; McDaid, P.; Debarge, S.; Steflik, J.; Karmilowicz, M.; Wong, J. W.; Faber, K., Chemoenzymatic asymmetric synthesis of pregabalin precursors via asymmetric bioreduction of β-cyanoacrylate esters using ene-reductases. *The Journal of organic chemistry* **2013,** *78* (4), 1525-1533.

19. Kosjek, B.; Fleitz, F. J.; Dormer, P. G.; Kuethe, J. T.; Devine, P. N., Asymmetric bioreduction of α, β-unsaturated nitriles and ketones. *Tetrahedron: Asymmetry* **2008,** *19* (12), 1403-1406.

20. Ying, X.; Yu, S.; Huang, M.; Wei, R.; Meng, S.; Cheng, F.; Yu, M.; Ying, M.; Zhao, M.; Wang, Z., Engineering the enantioselectivity of yeast old yellow enzyme OYE2y in asymmetric reduction of (E/Z)-citral to (R)-citronellal. *Molecules* **2019,** *24* (6), 1057.

21. Marshall, J. R.; Yao, P.; Montgomery, S. L.; Finnigan, J. D.; Thorpe, T. W.; Palmer, R. B.; Mangas-Sanchez, J.; Duncan, R. A. M.; Heath, R. S.; Graham, K. M., Screening and characterization of a diverse panel of metagenomic imine reductases for biocatalytic reductive amination. *Nature chemistry* **2021,** *13* (2), 140-148.

22. Chen, C.; Huang, H.; Wu, C. H., Protein bioinformatics databases and resources. *Protein Bioinformatics* **2017**, 3-39.

23. Furnham, N.; Garavelli, J. S.; Apweiler, R.; Thornton, J. M., Missing in action: enzyme functional annotations in biological databases. *Nature chemical biology* **2009,** *5* (8), 521-525.

24. Schnoes, A. M.; Brown, S. D.; Dodevski, I.; Babbitt, P. C., Annotation error in public databases: misannotation of molecular function in enzyme superfamilies. *PLoS computational biology* **2009,** *5* (12), e1000605.

25. Fisher, B. F.; Snodgrass, H. M.; Jones, K. A.; Andorfer, M. C.; Lewis, J. C., Site-selective C–H halogenation using flavin-dependent halogenases identified via family-wide activity profiling. *ACS central science* **2019,** *5* (11), 1844-1856.

26. Huang, H.; Pandya, C.; Liu, C.; Al-Obaidi, N. F.; Wang, M.; Zheng, L.; Toews Keating, S.; Aono, M.; Love, J. D.; Evans, B., Panoramic view of a superfamily of phosphatases through substrate profiling. *Proceedings of the National Academy of Sciences* **2015,** *112* (16), E1974-E1983.

27. Schülke, K. H.; Ospina, F.; Hörnschemeyer, K.; Gergel, S.; Hammer, S. C., Substrate Profiling of Anion Methyltransferases for Promiscuous Synthesis of S-Adenosylmethionine Analogs from Haloalkanes. *ChemBioChem* **2022,** *23* (4), e202100632.

28. Vanacek, P.; Sebestova, E.; Babkova, P.; Bidmanova, S.; Daniel, L.; Dvorak, P.; Stepankova, V.; Chaloupkova, R.; Brezovsky, J.; Prokop, Z., Exploration of enzyme diversity by integrating bioinformatics with expression analysis and biochemical characterization. *Acs Catalysis* **2018,** *8* (3), 2402-2412.

29. Hughes, R. A.; Ellington, A. D., Synthetic DNA synthesis and assembly: putting the synthetic in synthetic biology. *Cold Spring Harbor perspectives in biology* **2017,** *9* (1), a023812.

30. Bell, E. L.; Finnigan, W.; France, S. P.; Green, A. P.; Hayes, M. A.; Hepworth, L. J.; Lovelock, S. L.; Niikura, H.; Osuna, S.; Romero, E., Biocatalysis. *Nature Reviews Methods Primers* **2021,** *1* (1), 1-21.

31. Jacques, P.; Béchet, M.; Bigan, M.; Caly, D.; Chataigné, G.; Coutte, F.; Flahaut, C.; Heuson, E.; Leclère, V.; Lecouturier, D., High-throughput strategies for the discovery and engineering of enzymes for biocatalysis. *Bioprocess and biosystems engineering* **2017,** *40* (2), 161-180.

32. Atkinson, H. J.; Morris, J. H.; Ferrin, T. E.; Babbitt, P. C., Using sequence similarity networks for visualization of relationships across diverse protein superfamilies. *PloS one* **2009,** *4* (2), e4345.

33. Gerlt, J. A.; Bouvier, J. T.; Davidson, D. B.; Imker, H. J.; Sadkhin, B.; Slater, D. R.; Whalen, K. L., Enzyme function initiative-enzyme similarity tool (EFI-EST): a web tool for generating protein sequence similarity networks. *Biochimica Et Biophysica Acta (BBA)-Proteins and Proteomics* **2015,** *1854* (8), 1019-1037.

34. Copp, J. N.; Akiva, E.; Babbitt, P. C.; Tokuriki, N., Revealing unexplored sequence-function space using sequence similarity networks. *Biochemistry* **2018,** *57* (31), 4651-4662.

35. Cheng, S.; Karkar, S.; Bapteste, E.; Yee, N.; Falkowski, P.; Bhattacharya, D., Sequence similarity network reveals the imprints of major diversification events in the evolution of microbial life. *Frontiers in Ecology and Evolution* **2014,** *2*, 72.

36. Lundin, D.; Poole, A. M.; Sjöberg, B.-M.; Högbom, M., Use of structural phylogenetic networks for classification of the ferritin-like superfamily. *J. Biol. Chem.* **2012,** *287* (24), 20565-20575.

37. The UniProt, C., UniProt: the universal protein knowledgebase in 2021. *Nucleic Acids Res.* **2021,** *49* (D1), D480-D489.

38. Spiegelhauer, O.; Mende, S.; Dickert, F.; Knauer, S. H.; Ullmann, G. M.; Dobbek, H., Cysteine as a modulator residue in the active site of xenobiotic reductase A: a structural, thermodynamic and kinetic study. *J. Mol. Biol.* **2010,** *398* (1), 66-82.

39. Buder, R.; Fuchs, G., 2-Aminobenzoyl-CoA monooxygenase/reductase, a novel type of flavoenzyme. Purification and some properties of the enzyme. *Eur. J. Biochem.* **1989,** *185* (3), 629-35.

40. Zhang, Z.; Jamieson, C. S.; Zhao, Y.-L.; Li, D.; Ohashi, M.; Houk, K. N.; Tang, Y., Enzyme-Catalyzed Inverse-Electron Demand Diels–Alder Reaction in the Biosynthesis of Antifungal Ilicicolin H. *Journal of the American Chemical Society* **2019,** *141* (14), 5659-5663.

41. Bertsova, Y. V.; Oleynikov, I. P.; Bogachev, A. V., A new water-soluble bacterial NADH: fumarate oxidoreductase. *FEMS Microbiol. Lett.* **2020,** *367* (20), fnaa175.

42. Khairy, H.; Wübbeler, J. H.; Steinbüchel, A., The NADH: flavin oxidoreductase Nox from Rhodococcus erythropolis MI2 is the key enzyme of 4, 4′-dithiodibutyric acid degradation. *Lett. Appl. Microbiol.* **2016,** *63* (6), 434-441.

43. Toogood, H. S.; Scrutton, N. S., Discovery, characterization, engineering, and applications of ene-reductases for industrial biocatalysis. *ACS catalysis* **2018,** *8* (4), 3532-3549.

44. Cui, Y.; Chen, X.; Wang, Z.; Lu, Y., Cell-Free PURE System: Evolution and Achievements. *BioDesign Research* **2022,** *2022*.

45. Wu, S.; Wang, B.; Yan, H., Semi-rational protein engineering of a novel ene-reductase from Galdieria sulphuraria for asymmetric reduction of (R)-carvone and ketoisophorone. *Biotechnol. Appl. Biochem.* **2022**.

46. Kumar Roy, T.; Sreedharan, R.; Ghosh, P.; Gandhi, T.; Maiti, D., Ene-Reductase: A Multifaceted Biocatalyst in Organic Synthesis. *Chemistry–A European Journal* **2022,** *28* (21), e202103949.

47. Colombo, D.; Brenna, E.; Gatti, F. G.; Ghezzi, M. C.; Monti, D.; Parmeggiani, F.; Tentori, F., Chemoselective Biohydrogenation of Alkenes in the Presence of Alkynes for the Homologation of 2-Alkynals/3-Alkyn-2-ones into 4-Alkynals/Alkynols. *Adv. Synth. Catal.* **2019,** *361* (11), 2638-2648.

48. Stueckler, C.; Winkler, C. K.; Bonnekessel, M.; Faber, K., Asymmetric synthesis of (R)-3-hydroxy-2-methylpropanoate ('Roche ester') and derivatives via biocatalytic C□ C-bond reduction. *Adv. Synth. Catal.* **2010,** *352* (14-15), 2663-2666.

49. Nestl, B. M.; Hammer, S. C.; Nebel, B. A.; Hauer, B., New generation of biocatalysts for organic synthesis. *Angew. Chem. Int. Ed.* **2014,** *53* (12), 3070-3095.

50. Murthy, Y. V. S. N.; Meah, Y.; Massey, V., Conversion of a flavoprotein reductase to a desaturase by manipulation of the flavin redox potential. *Journal of the American Chemical Society* **1999,** *121* (22), 5344-5345.

51. Schittmayer, M.; Glieder, A.; Uhl, M. K.; Winkler, A.; Zach, S.; Schrittwieser, J. H.; Kroutil, W.; Macheroux, P.; Gruber, K.; Kambourakis, S., Old yellow enzyme-catalyzed dehydrogenation of saturated ketones. *Adv. Synth. Catal.* **2011,** *353* (2-3), 268-274.

52. Sheng, X.; Yan, M.; Xu, L.; Wei, M., Identification and characterization of a novel old yellow enzyme from Bacillus subtilis str. 168. *J. Mol. Catal. B: Enzym.* **2016,** *130*, 18-24.

53. Gerhards, N.; Li, S.-M., A bifunctional old yellow enzyme from Penicillium roqueforti is involved in ergot alkaloid biosynthesis. *Organic & Biomolecular Chemistry* **2017,** *15* (38), 8059-8071.

54. Murakami, M. T.; Rodrigues, N. C.; Gava, L. M.; Honorato, R. V.; Canduri, F.; Barbosa, L. R. S.; Oliva, G.; Borges, J. C., Structural studies of the Trypanosoma cruzi Old Yellow Enzyme: insights into enzyme dynamics and specificity. *Biophys. Chem.* **2013,** *184*, 44-53.

55. Padhi, S. K.; Bougioukou, D. J.; Stewart, J. D., Site-saturation mutagenesis of tryptophan 116 of Saccharomyces pastorianus old yellow enzyme uncovers stereocomplementary variants. *Journal of the American Chemical Society* **2009,** *131* (9), 3271-3280.

56. Christgen, S. L.; Becker, S. M.; Becker, D. F., Methods for determining the reduction potentials of flavin enzymes. In *Methods Enzymol.*, Elsevier: 2019; Vol. 620, pp 1-25.

57. Xu, D.; Kohli, R. M.; Massey, V., The role of threonine 37 in flavin reactivity of the old yellow enzyme. *Proceedings of the National Academy of Sciences* **1999,** *96* (7), 3556-3561.

58. Messiha, H. L.; Bruce, N. C.; Sattelle, B. M.; Sutcliffe, M. J.; Munro, A. W.; Scrutton, N. S., Role of active site residues and solvent in proton transfer and the modulation of flavin reduction potential in bacterial morphinone reductase. *J. Biol. Chem.* **2005,** *280* (29), 27103-27110.

59. Léger, C.; Bertrand, P., Direct electrochemistry of redox enzymes as a tool for mechanistic studies. *Chem. Rev.* **2008,** *108* (7), 2379-2438.

60. Yang, K. K.; Wu, Z.; Arnold, F. H., Machine-learning-guided directed evolution for protein engineering. *Nature methods* **2019,** *16* (8), 687-694.

61. Mistry, J.; Chuguransky, S.; Williams, L.; Qureshi, M.; Salazar, G. A.; Sonnhammer, E. L. L.; Tosatto, S. C. E.; Paladin, L.; Raj, S.; Richardson, L. J., Pfam: The protein families database in 2021. *Nucleic Acids Res.* **2021,** *49* (D1), D412-D419.

62. Pei, J.; Kim, B.-H.; Grishin, N. V., PROMALS3D: a tool for multiple protein sequence and structure alignments. *Nucleic Acids Res.* **2008,** *36* (7), 2295-2300.

63. Nguyen, L.-T.; Schmidt, H. A.; Von Haeseler, A.; Minh, B. Q., IQ-TREE: a fast and effective stochastic algorithm for estimating maximum-likelihood phylogenies. *Molecular biology and evolution* **2015,** *32* (1), 268-274.

64. Letunic, I.; Bork, P., Interactive Tree Of Life (iTOL) v5: an online tool for phylogenetic tree display and annotation. *Nucleic Acids Res.* **2021,** *49* (W1), W293-W296.

65. Kamireddi, M.; Eisenstein, E.; Reddy, P., Stable Expression and Rapid Purification ofEscherichia coliGroEL and GroES Chaperonins. *Protein expression and purification* **1997,** *11* (1), 47-52.

66. Smith, L. D.; Budgen, N.; Bungard, S. J.; Danson, M. J.; Hough, D. W., Purification and characterization of glucose dehydrogenase from the thermoacidophilic archaebacterium Thermoplasma acidophilum. *Biochem. J* **1989,** *261* (3), 973-977.

Chapter 3: Light-Triggered Investigations into the Mechanism of Carbon Monoxide Dehydrogenase

3.1 – Introduction

[NiFe] carbon monoxide dehydrogenases (CODH) catalyze the reversible two electron reduction of CO_2 to CO at high rates with excellent selectivity - both desirable traits for sustainable energy production.[1-3] The reaction is catalyzed by the C-cluster, a unique [$NiFe_3S_4$] cluster attached to a pendant Fe (termed Fe1) coordinated by a water/hydroxide ligand.[2, 4] The C-cluster is known to adopt 4 different oxidation states: the oxidized and inactive C_{ox}, one-electron reduced and catalytic resting state C_{red1}, a two-electron reduced C_{int} state, and the three-electron reduced C_{red2} which binds to CO_2.[1] CODHs adopt a homodimeric structure containing 2 C-cluster, 2 [4Fe-4S] B-clusters and 1 D-cluster which is either another [4Fe-4S] or [2Fe-2S] depending on the enzyme.[2, 5] Spectroscopic and electrochemical evidence suggest the B-cluster participates in electron transfer to the C-cluster while the D-cluster may not.[6, 7]

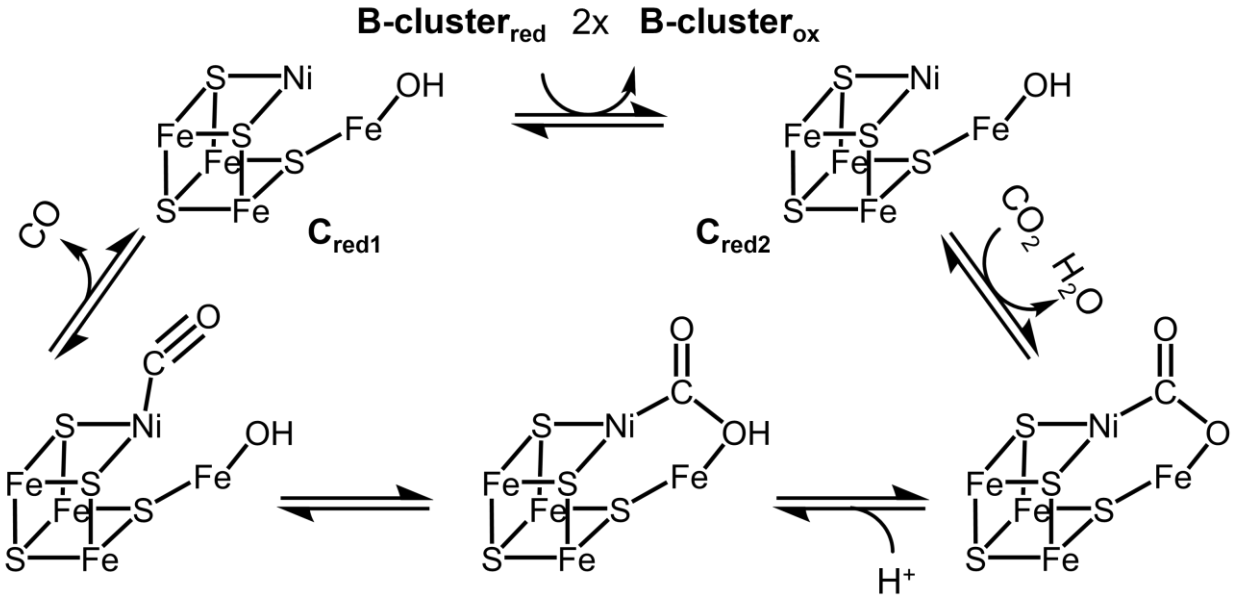

Figure 3.1 The proposed mechanism of [NiFe] CODH. The B-cluster is the adjacent [4Fe-4S] cluster and 2x refers to the number of electrons transferred to the C-cluster.

Extensive studies in the past two decades have resulted in a basic model for the mechanism of CODH (Fig. 1). For CO_2 reduction, the reaction begins with the transfer of electrons from an external electron donor, likely a reduced ferredoxin, to the B-cluster.[1-3] Electrons then move to the active site reducing the C-cluster from the C_{red1} to the C_{red2} state. The reduction potential for this redox couple is -530 mV, close to the potential of two electron CO_2/CO couple.[3] CO_2 binding is proposed to occur once the active site is reduced to the C_{red2} state. One structure of a CO_2-bound CODH has been resolved and it required a reduction potential of -600 mV to obtain, likely reducing the C-cluster to the C_{red2} state.[8] Electrochemical and EPR studies with the inhibitor cyanate, isoelectronic to CO_2, suggests it only binds in the C_{red2} state with increasing the redox potential, to favor the C_{red1} state, removes the inhibitor.[9] The binding of CO_2 displaces the water/hydroxide ligand of Fe1 and forms a bridging carboxylate, μ_2-η^2 coordination, between the Ni and Fe1. In the CO_2-bound crystal structure, the bound carboxylate forms a bent orientation with an angle of 117˚, suggesting a two electron reduced state for the ligand.[8] Next, a protonation event likely occurs on the oxygen atom bound to Fe1 which helps facilitate C-O bond cleavage, forming CO coordinated to the Ni.[1, 3] Orientation of the bound CO is controversial as crystal structures have shown both a bent and a linear Ni-C-O arrangement. The only CO-bound structure is of CODH from *M. barkeri* of the CODH/ACDS complex and showed the bent arrangement (Fig. 2A).[10] It was proposed that a conserved isoleucine residue sterically promotes this binding orientation and it may destabilize the ground state.[11] An independent study of the electron density from this structure could not verify that CO was present in the active site and bound to the Ni.[12] Further crystal structures using the inhibitor cyanide, isoelectronic to CO, showed both bent and linear arrangements.[13, 14] The hydroxyl ligand is not present in the crystal structures showing the linear arrangement, but is for the bent orientation (Fig. 2B).[1] After formation, CO disassociates from the

Ni, leaves the active site for the gas channels, and the C-cluster is at the resting state of C_{red1}. While numerous studies have coalesced into this proposed mechanism, the full catalytic details are not resolved with specific questions concerning CO formation and binding.

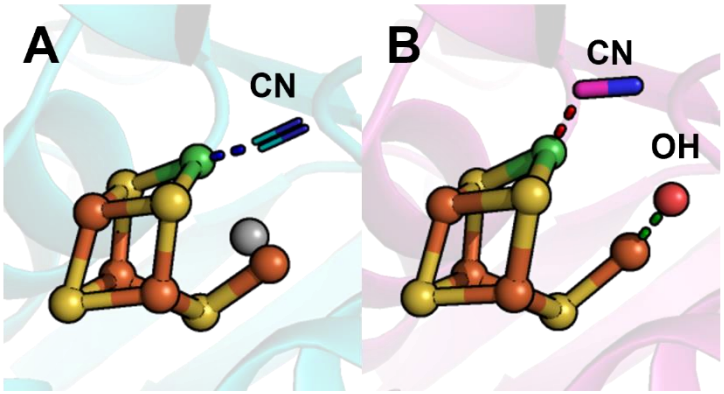

Figure 3.2 The linear vs bent orientation of CN bound to the C-cluster. A) The linear arrangement of the Ni-C-N. Grey is the alternative position for the pendant Fe1. (PDB: 3I39) B) The bent orientation with the hydroxyl ligand (red) bound to Fe1. (PDB: 3I04)

Unlike other metalloenzymes such as hydrogenases, no easily identifiable spectroscopic handles exist for CODH. Thus, studies have focused on using inhibitors analogous to CO_2 and CO for further investigation of the catalytic mechanism.[15] Cyanide has been used to determine the binding orientation of CO in the active site with both the bent and linear arrangements for Ni-CN being observed.[10, 13] Recently, Ciaccafava et. al resolved a single IR band for this Ni-CN stretch in CODH, suggesting only one binding orientation – though computational experiments were unable to resolve whether bent or linear.[15] In a follow-up study, the authors were able to observe the two-electron reduction of cyanate to cyanide through IR spectroscopy.[16] It's unclear though how accurate the two inhibitors are for mimicking CO_2 reduction. Direct observation of CO binding using IR should be possible as M-CO stretches are IR active and have been observed in other metalloenzymes such as hydrogenase, but the relatively quick turnover frequency of the

enzymes has prevented this.[1] One study using CODH/ACS from *Moorella thermoacetica* was able to identify several distinct IR peaks once the enzyme complex was flushed with CO.[17] The IR bands were at 2078, 2044, 1996, 1970, 1960, and 1901 cm^{-1} with the 1996 cm^{-1} peak later confirmed to correspond to the A-cluster of ACS.[18] The remaining IR features were attributed to bound CO to the C-cluster. This is in sharp contrast to the single Ni-CN stretch of later studies. Currently, no study has narrowed down the specific Ni-CO IR band of CO bound to the active site of CODH.

A promising new strategy for mechanistic enzymology of oxidoreductases involves the combination of photobiocatalysis and time resolved spectroscopy.[19, 20] Photobiocatalysis entails using a photosensitizer to generate electrons which can trigger a rapid drop in the potential of the solution, termed a potential jump.[20-22] Electrons are then either directly transferred to the enzyme or indirectly with a redox mediator. Unparalleled control over the mechanism can be achieved using light to initiate the reaction – revealing previously obscured kinetic steps.[19] The combination of light induced potential jump and spectroscopic techniques has previously been employed to decipher mechanistic details of hydrogenases and ribonucleotide reductases.[23-25] In the case of [FeFe] hydrogenase, this method confirmed the catalytic relevance of observed infrared states while also identifying a new intermediate state.[24] A similar such strategy could be utilized to unravel the kinetic details of CODH catalyzed CO_2 reduction. Before this is possible, first CODH must be able to be photoactivated.

In the past decade, significant effort has focused on utilizing CODH I from *Carboxydothermus hydrogenoformans* as a photocatalyst, not for mechanistic studies, but as method for artificial photosynthesis, i.e., storage of solar energy in chemical bonds.[26-29] Several strategies include using photosensitizers such as semiconductor nanorods or silver nanoclusters

tethered to TiO_2 nanoparticles with the latter achieving the highest quantum efficiency (photons converted to product) of 1.5%.[28] This is significantly lower than photoenzymatic hydrogen production which has observed quantum efficiencies upwards of 80%.[30] While CODH I has been extensively employed for photoreduction of CO_2, CODH II, also from *C. hydrogenoformans*, is the typical model CO_2 reducing enzyme.[3] The majority of the previously mentioned structurally and inhibitor studies of CODHs were investigating CODH II. The enzyme receives much attention towards mechanistic studies due to its crystal structure being solved.[7, 14, 31] The two *C. hydrogenoformans* enzymes are related but are distinct in sequence (~50% identity), native function, and catalytic capabilities.[32] Notably, CODH II is nearly 10-fold more susceptible to CO-induced product inhibition when compared to CODH I.[33] Despite the numerous mechanistic studies, a photosystem has yet to be established for CODH II. Photoactivating CODH II would allow for time-resolved spectroscopic studies into its mechanism.

3.2 - Results and Discussion

3.2.1 – Development of an Efficient CODH II-based Photosystem for CO_2 Reduction

Using the well-established hydrogenase-based photosystems as a template, the general setup for photoreduction of CO_2 via CODH II was composed of 3 main components: a photosensitizer to generate electrons/initiate the reaction, a redox mediator to efficiently shuttle electrons, and CODH II to catalyze the reaction (Fig. 3).[30, 34] Nanocrystalline semiconductors were selected as the photosensitizer with mercaptopropionic acid (MPA) capped CdSe/CdS ‘dot-in-rods’ (DIR) utilized. The core/shell characteristic of DIRs allows for excellent photo efficiency due to longer-lived electron-hole separation between the two layers of nanomaterials.[35] Furthermore, DIRs have also been previously used in other photobiocatalytic systems with great success.[24, 30]

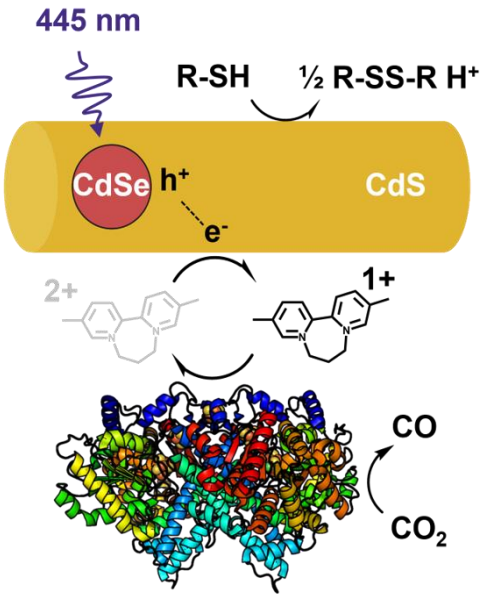

Figure 3.3 Schematic of the CODH II-based photosystem. Illumination of CdSe/CdS dot-in-rod (DIR) generates an exciton that reduces mediator DQ53; electron transfer to CODH II initiates enzyme turnover (PDB: 1SUF).

The redox mediator was incorporated to facilitate efficient electron transfer between the photosensitizer and the enzyme. Previous studies on other CODH-based photosystems, including those using similar semiconductor nanocrystalline photosensitizers, concluded that low electron availability hampered the overall efficiency.[28, 29] Likewise in comparable hydrogenase-based photosystems, the incorporation of a redox mediator such as propyl-diquat (PDQ) improved the quantum yield of hydrogen production to ~80%.[30] Thus for CO_2 reduction, a similar redox mediator to PDQ, DQ53, was selected for its relatively low redox midpoint potential at -635 mV.[36] CODH II switches from CO oxidation to CO_2 reduction at -520 mV, so its essential the redox mediator can reach that potential (or below) to provide the necessary driving force for the enzyme.[33]

All 3 components were anoxically added to a cuvette in a phosphate buffer. For the substrate, the headspace was thoroughly purged with CO_2 to ensure maximum turnover efficiency of the enzyme. CODH II reduces CO_2, but does not bind it tightly with a K_m value of 8 mM.[33] The reaction was monitored in real time using UV vis spectroscopy as the radical species of DQ53 increases in absorbance in the visible region. CO production was evaluated by GC analysis of headspace gas samples and quantifiying the amount using a calibration curve.

Initial iterations of the photosystem resulted in miniscule amounts of CO produced that were almost below the detection of the GC. Though hardly a success, this did prove that the photosystem was capable of reducing CO_2 and efforts focused on improving the efficiency. It was identified that during the reaction, the DIRs precipitated out of solution after the purge of CO_2. The excess CO_2, while advantageous for CO production by CODH II, overwhelmed the phosphate buffer and lowered the pH of the solution. As the nanomaterials were only water soluble by the capping ligand of MPA, the drop in pH protonated the coordinated thiolate groups and precipitated the nanorods out of solution. To counter this, bicarbonate was added and the concentration of the buffers were increased 5-fold for pH stability while still maintaining a high concentration of CO_2 for the enzyme. Further optimization included varying the component concentrations and purge times to increase the amount of CO produced.

Before the final optimization, another method for CO detection was briefly explored - monitoring CO production via changes in pressure. Quantifying CO using GC is limited in the number of data points that can be collected during the assay and it requires sampling of the headspace which could cause oxygen contamination. Previous studies of photoenzymatic hydrogen production use a pressure sensor to detect the build up of H_2, giving real time quantification.[37] Theoretically, a similar setup could be used for CO_2 reduction given that CO is

less soluble in water than CO_2.[38] Furthermore, the CO_2 concentration could be stabilized with the addition of carbonic anhydrase as it would maintain an equilibrium between bicarbonate and aqueous CO_2 despite consumption by CODH II. Unfortunately, compared to GC quantification, the pressure sensor was unreliable. (Fig. 4) Over an hour, the pressure fluctuated while GC timepoints demonstrate a steady increase in CO production. Several factors could be attributing to the fluctuation of pressure observed. First, the pressure sensor detects the pressure of all gasses in the system including CO, CO_2, N_2, and trace amounts of H_2 (from the anoxic box atmosphere). With the stir bar agitating at the liquid-gas interface, it is likely that all of those gases are shifting in equilibrium for both phases causing the fluctations. The solution is allowed to equilibriate for 15 minutes, but controls show that even after an hour the pressure did not stabilize. With inconsistent results monitoring by pressure sensor was discarded for the more reliable quantification using GC time points.

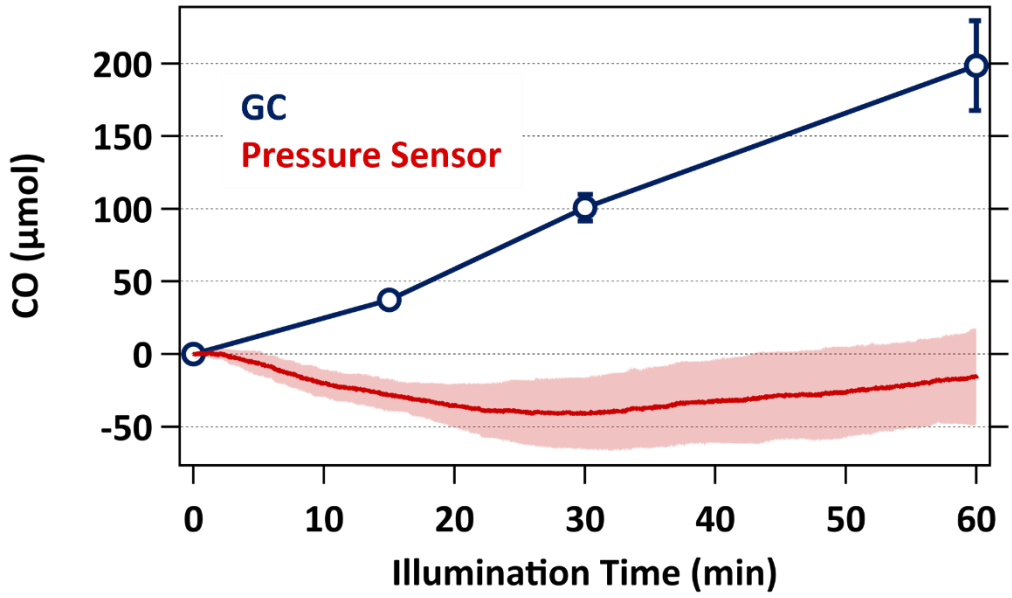

Figure 3.4 Comparison of GC vs pressure sensor for detection of CO. Standard deviation of the pressure sensor is shown in the lighter shade of red.

To validate the CO production observed by the photosystem, several control experiments were performed under identical conditions while removing one of the main components (photosensitizer, mediator, enzyme) (Fig. 5A). No CO was detected in any of these experiments, justifying the incorporation of each main component in the system. The capping ligand on the DIR is negatively charged and the solution-exposed residues on CODH are positively charged, promoting electrostatic coordination of CODH onto the DIR surface.[29] Direct reduction of the enzyme by the DIR is possible considering the conduction band edge of the CdS shell is lower than CO_2 reduction by CODH at pH 7 (< -700 mV and -520 mV, respectively).[39] Despite those factors, no CO is detected from the photosystem when the redox mediator is absent. It could be likely that the presence of buffer high salts (250 mM of $NaPO_4$ and $NaHCO_3$) in the photosystem caps the charges removing the electrostatic attraction. It is also possible that CODH II binds to the DIR in an orientation that is not suitable for electron transfer.

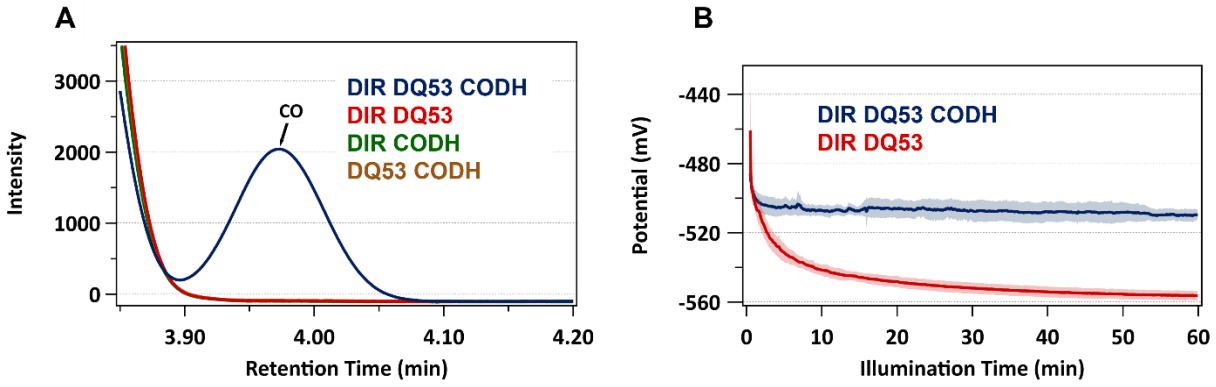

Figure 3.5 Photosystem controls and solution potential. A) GC traces of CO produced by full CODH-DIR photosystem and control experiments each lacking a component (DIR, DQ53, CODH). B) Solution potential of the photosystem generated by the mediator redox couple with or without enzyme, determined using the Nernst equation and mediator concentrations.

Illumination of the photosensitizer reduces the mediator and lowers the redox potential of the solution which can be calculated using the Nernst Equation and the concentration of reduced redox mediator (Fig. 5B). Continuous illumination of the photosystem in the presence of the enzyme that is actively consuming the reduced mediator produces a steady state solution potential of approximately -510 mV. Without the enzyme, the potential is at -550 mV, below the the redox potential of the reversible reduction of CO_2.

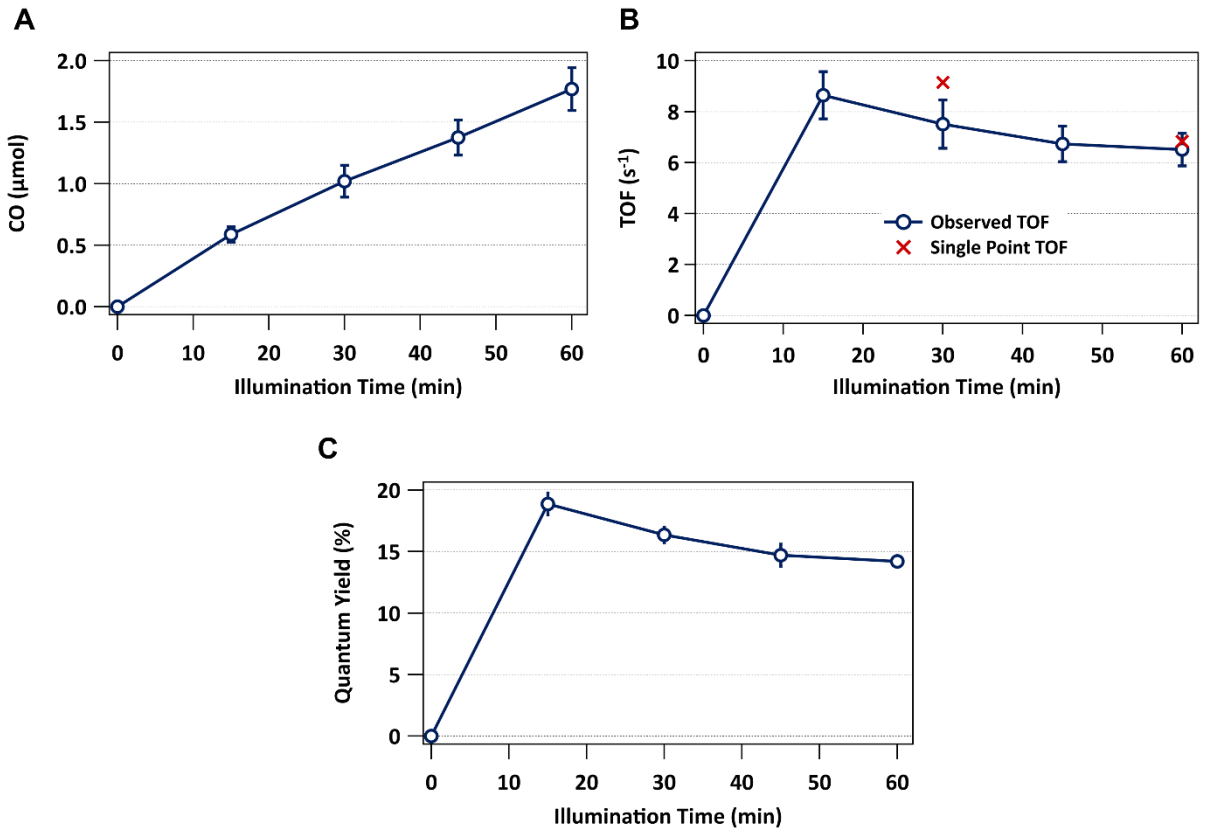

Figure 3.6 Catalytic performance of the photosystem. A) Amount of CO produced over time using the photosystem. B) Turnover frequencies over time of the photosystem. The blue Xs are single timepoints TOFs under identical conditions without previous sampling. D) The quantum yield of the photosystem using 445 nm light. In all cases, error bars represent standard deviation of 3 trials.

After 1 hour of illumination, 1.77 μmol of CO was produced (Fig. 6A) based on GC quantification. No H_2 or any CO_2 reduction products were detected by GC - consistent with the high selectivity towards CO production previously observed by CODH. At the initial time point of 15 minutes, the observed turnover frequency (TOF) reached a maximum at 8.6 s^{-1} then slowly decreased to 6.4 s^{-1}, indicating that the rate of CO production decreases over time (Fig 6B). It is unlikely that this decrease in TOF is due to consumption of substrates/reagents (CO_2 and the sacrificial electron donor MPA) as they are present in excess. Two explanations for this decrease are possible. First, CODH II is extremely sensitive to oxygen, becoming deactivated in its presence. Reactivation of the enzyme is possible under reducing conditions, albeit with significantly less activity.[40] The decrease in activity occurs after sampling, so it is likely that sampling inadvertently introduces oxygen into the photosystem and deactivates a significant portion of the enzyme. As a simple control to test this, trials with single timepoints were performed. At 30 minutes, the single point TOF, is significantly higher at 9.1 s^{-1} than the previous sampling TOF of 7.5 s^{-1} (Fig xx) and closely aligns with the 15 minute timepoint of 8.6 s^{-1}. In addition, previous attempts at sampling the photosystem multiple times were unattainable due to the inadverdant oxygen contamination. Thus, it is highly likely that oxygen has leaked into the system after sampling, lowering the observed activity of the photocatalytic system.

Another factor to consider is autoinhibition of the enzyme over time. Previous literature has shown that CO_2 reduction by CODH II is inhibited by μM quantities of CO. Thus, as more CO is produced, enzyme activity should decrease due to product inhibition. This is evident when comparing the single point TOF of 6.8 s^{-1} and previously sampled TOF of 6.51 s^{-1} at the 1 hour timepoint. No prior oxygen leakage occurred in the single point TOF experiment providing evidence that the enzyme is being autoinhibited by CO. To further verify, the concentration of

aqueous CO was calculated at 1 hour timepoints using Henry's Law to compare against the literature provided inhibition constant. The aqueous concentration of CO is ~30 μM, significantly higher than the reported K_I of 5.4 μM.[33]

Overall, a maximum quantum yield of ~19% was observed after 15 minutes of illumination and eventually plateaus to ~15% after an hour (Fig. 6C). Due to the limited number of timepoints, it is unclear if the actual maximum TOF/QY is at 15 minutes. Despite the decrease in QY, these results are an order of magnitude greater than previously described photoenzymatic systems and become comparable to molecular catalyst-based photosystems for CO_2 to CO conversion.[28, 41, 42]

3.2.2 - Infrared Absorption of CO Inhibited CODH

The strategy to identify the spectral features of CO bound to the active site of CODH II focused on allowing the previously described photosystem to run until inhibition then monitoring any absorbance changes in the IR region. The CODH II based photosystem was adapted into an IR cell and illuminated for at least an hour to ensure full inhibition. To prevent concentration-based aggregation, the photosensitizer was switched from CdSe/CdS DIR to CdSe quantum dots (QD) to utilize 532 nm light (for later transient adsorption studies) and due to the latter being easier to synthesize/use and more stable at higher concentration.

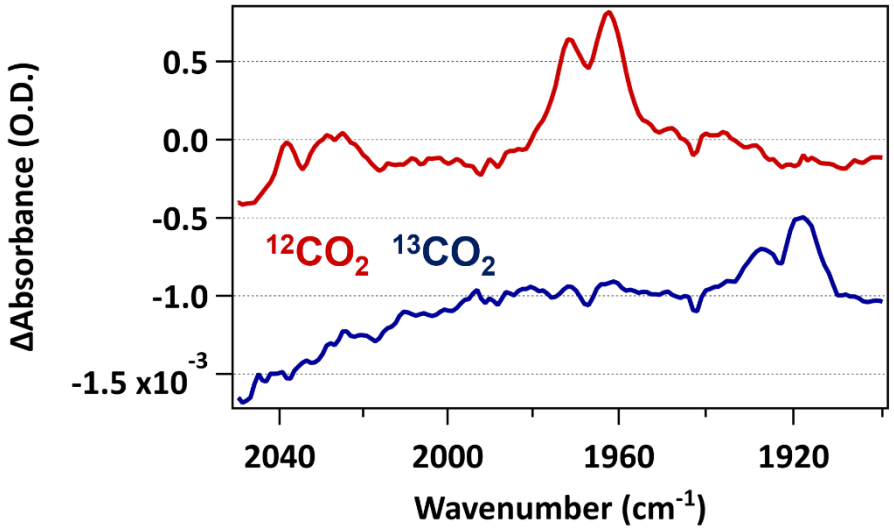

Figure 3.7 Difference spectra of CO inhibited CODH II after illumination. In red is using natural abundance CO_2 and sodium bicarbonate. In blue is using isotopically labeled bicarbonate. Spectra are after 1 hour of illumination with 532 nm laser

Before illumination, no infrared features were observed in the M-CO stretch region as expected and previously reported.[15] After 1 hour of irradiation, two peaks developed at frequencies of 1971 and 1962 cm^{-1} – nearly identical to two of the spectral features previously identified for the related CODH/ACS (Fig 7).[17] Unlike the prior study no peaks were observed at 2074 or 1901 cm^{-1}, suggesting those features may be specific to CODHs of CODH/ACS or the enzyme complex as a whole. Interestingly an absorbance feature was identified near 1938 cm^{-1} similar to the 2044 cm^{-1} peak which could be free CO in the gas channel after it has left the C-cluster. In addition to M-CO stretches, the previous CODH/ACS study also identified possible metal bound carboxylate peaks at 1741 and 1727 cm^{-1}.[17] No such peaks were observed in that region for CODH II.

To validate these absorbance features are Ni-CO stretches, ^{13}C labeled CO_2 (in the form of sodium carbonate in the buffer) was used to observe any isotopic shifts in the peaks. After 1 hour of illumination, two peaks were identified at the frequencies of 1927 and 1918 cm^{-1} at roughly 44

cm^{-1} downshifted from the ^{12}C labeled peaks (Fig. 7). As with the natural abundance peaks, the ^{13}C absorbance features are nearly identical to previous literature.[17] No other IR peaks were observed in the region, though this may be due to a lower concentration of $^{13}CO_2$ present since the samples were not purged with CO_2 like the ^{12}C sample.

Since an isotopic shift was observed, the 1971 and 1962 cm^{-1} are identified to be the Ni-CO stretches in the active site. Based on the proposed mechanism, it is unclear why two peaks are formed as only 1 CO molecule is formed in the active site.[3] Several possible explanations for the double peak are hypothesized. CODH is a homodimer with two distinct active sites and the two observed Ni-CO stretching frequencies could be due to a difference in orientation between the two C-clusters. Slight differences in the 3D geometry of the active site such as hydrogen bonding to the CO would change the frequency of the Ni-CO stretch. The binding of CO (and CN) in the active site is debated with two orientations observed in crystal structures: bent vs linear Ni-C-O arrangements (Fig. 2).[1, 10, 12, 13] The two frequencies observed could be these different orientations. A key difference between these orientations is the hydroxyl/water ligand coordinated at the pendant Fe1 which for the linear arrangements is not present.[10, 14] The Fe1 also adopts an alternative position closer to the Ni in the linear arrangement as well.[14] In CO_2, the hydroxyl/water is from the coordinated oxygen from CO_2 so it would be present. Cyanide in both orientations form two hydrogen bond contacts, but with the presence of the hydroxyl/water ligand after CO_2 reduction it's unclear what effect that may have on the orientations or frequencies. It is also possible differences in residue or metal positions could results in slightly different binding orientations. Another possibility is that one frequency is the CO bound to the active site in a catalytically relevant position, while the other is a secondary CO bound in a different orientation due to the relatively high local concentration of carbon monoxide. To explore these hypotheses,

time resolved infrared experiments were conducted at both frequencies to determine whether each one is catalytically relevant.

3.2.3 - Kinetics of Enzyme Reduction by the Reduced Mediator

Several steps were taken to maximize IR signal as CO inhibition studies resulted in the low absorbance change of ~1 mO.D. for 500 µM of CODH. First, the pathlength of the IR cell was increased from the standard 75 µm to 127 µm which based on Beer's law would increase the absorbance by 1.7x. Next, the concentrations of QDs and mediator were all increased (to higher values of 0.8 O.D. and 60 mM, respectively) to maximize the concentration of reduced mediator available, resulting in a maximum of ~1.6 mM of the radical species based on 808 nm absorbance changes. Considering the CODH-catalyzed CO_2 reduction requires two electrons, a maximum concentration of ~800 µM of enzyme could be fully turned over under these redox conditions.

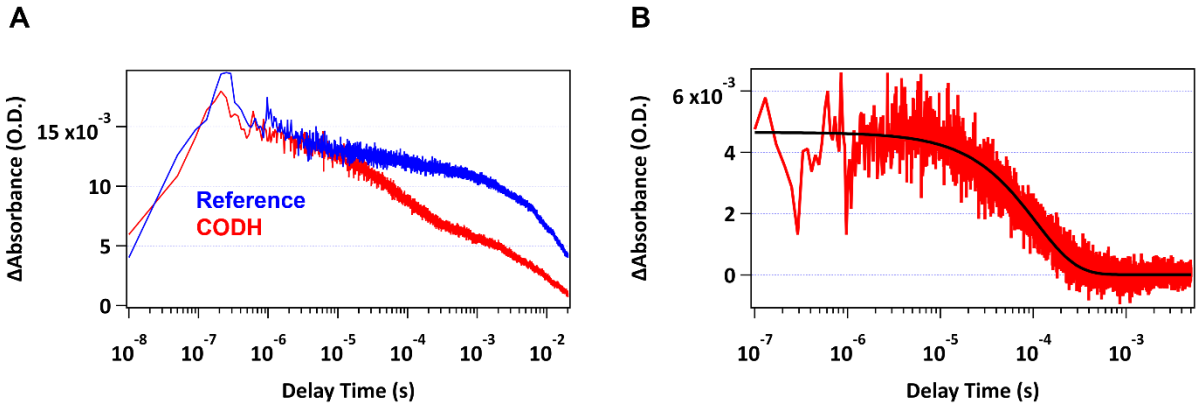

Figure 3.8 Transient visible absorbance spectra of the reduced mediator. A) Visible absorbance spectra from the reference side (blue) and sample/CODH side (red) of the IR cell. Delay time refers to the amount of time after initial laser flash. B) The enzyme consumption spectra from subtraction of the reference trace and the CODH trace. The black line is the single exponetial fit.

The redox mediator gives an absorbance in the visible region upon reduction.[43] By using an in-tandem visible probe to monitor the reduced mediator during transient absorbance-IR (TAIR) spectroscopy, one can observe the transfer of electrons to the mediator and then subsequently to the enzyme. In Fig 8A, the averaged visible absorbance traces for the CODH II and reference samples are compared. The reference sample, a control, is prepared identically to the CODH II sample except it contains deoxymyoglobin instead of CODH. Deoxymyoglobin does not interact with the redox mediator but is used to match the pump wavelength (532 nm) absorbance given by CODH thus matching the water background IR changes due to solution heating from laser pulse. Without a final electron acceptor in the Mb reference sample to consume the mediator radical, any absorbance changes limited to mediator reduction can be observed. The corrected visible spectra fit an exponential decay with two components in the Mb sample. The first component at ~2 μs is attributed to charge recombination, or the electron transfer from the radical species back to the hole on the photosensitizer.[24] The second component occurs at later timescales (ms) and is attributed to the disproportionation reaction between reduced mediator molecules resulting in the insoluble neutral species and has been a previously described phenomena in.[43]

Subtracting the Mb reference visible spectrum from the CODH visible spectrum removes these irrelevant background components and highlights a single exponential decay of enzyme reduction by the mediator. Lifetimes for this transfer range between 80 to 120 μs (Fig. 8B). Based on current literature of CODH, the mediator is likely reducing the B-cluster which then transfers electrons to the C-cluster active site and starts the catalytic cycle.[5, 6] Interestingly, the amount of radical consumed by CODH was consistent across experiments regardless of the overall concentration of mediator produced. Between ~200 μM to ~300 μM of $DQ53^{+\bullet}$ is consumed by CODH despite excesses of more than double this concentration produced. Thus only 100 to 150

μM of CODH II was reduced since complete enzyme turnover requires 2 electrons, even though the total concentration of enzyme was much greater at 800 μM. Several explanations for these observations are possible. First, it is likely that the actual concentration of fully functioning enzyme is slightly lower due to underloading of the metal clusters during purification/preparation, since a fully reconstituted CODH has proved difficult.[44] It is also possible that only the fraction of enzyme in electrostatically bound to the QDs are available for reduction, due to the competing disproportionation reaction of the mediator radical. The fluctuations in consumed mediator appear to correlate to the slight varying concentrations of QDs in each experiment but proving this hypothesis would require more QD concentration titration experiments.

3.2.4 – Transient Absorption for Identified Ni-CO Stretches

To determine if either of the Ni-CO stretches observed during CO inhibition studies are catalytically relevant to CODH, the transient infrared absorption signals of 1971 and 1962 cm^{-1} were monitored after a 10-nanosecond laser pulse induced potential jump.[22] Monitoring at the 1971 cm^{-1} frequency, a single exponential rise with a lifetime of 94 μs is observed (fig xx) and it subsequently decays back to the baseline with a lifetime of 7.2 ms. The first phase is most likely the Ni-CO stretch forming after cleavage of CO_2 in the active site.[3] The decay is likely the bound CO dissociating from the Ni as the enzyme turns over. The lifetime for the rise is identical to those observed for electron transfer to the enzyme, suggesting that the reduction of the B-cluster (assumed to be the site for initial electron transfer) is the rate limiting step.

At the lower frequency of 1962 cm^{-1}, an initial rise with a lifetime of 165 μs is followed by a decay in signal of 6.4 ms – both features fitting to a single exponential. This is also likely the formation of a Ni-CO in the active site and its dissociation, similar to the observations seen in 1971 cm^{-1}. In contrast with the higher frequency band, the initial phase appears to be nearly two fold slower and slightly delayed (>40 μs) after mediator consumption. It should be noted that since all traces are sourced from one sample and the higher frequency (1971 cm^{-1}) was probed before the lower frequency (1962 cm^{1}), there may be unforeseen differences or delays due to a portion of the sample already being reduced, endogenously produced CO, or other redox effects from low solution redox potentials. It is possible for CO to be present when the 1962 cm^{-1} frequency was probed which would slow the rate of CO_2 reduction. Repeat experiments yielded similar lifetimes to the initial TAIR results with the 1971 cm^{-1} appearing to be faster than 1962 cm^{-1}. Further experiments swapping the frequency order will be necessary to confirm any differences in rates of formation between 1962 cm^{-1} and 1971 cm^{-1}. In the observed decay phases, both frequencies have lifetimes in the millisecond range and thus suggests that the CO dissociates for each species at similar timescales.

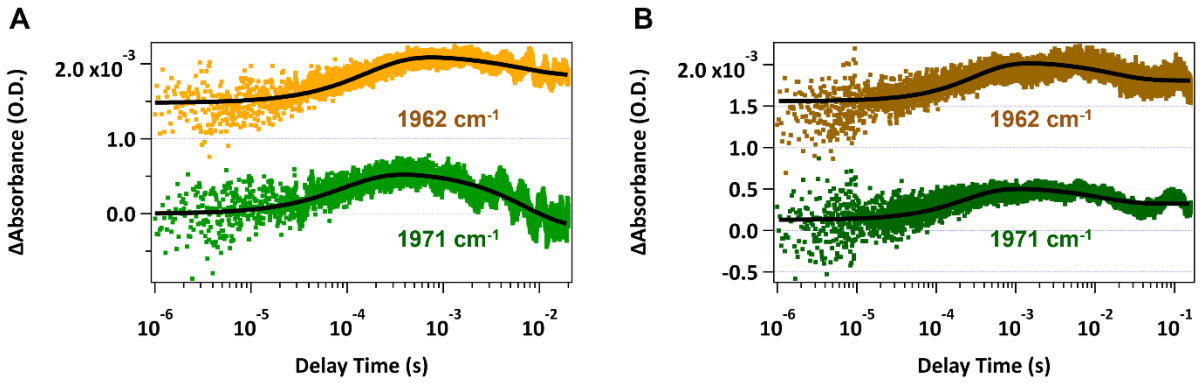

Figure 3.9 Transient absorption of the Ni-CO stretches of CODH II. A) Initial transient absorption experiment at the two frequencies (green for 1971 cm^{-1} and yellow for 1962 cm^{-1}). B) Repeat experiments on the sample for monitoring CO inhibition.

The sample was probed at both 1971 and 1962 cm^{-1} again immediately after the initial experiments concluded to observe the kinetics of CO inhibtion (Fig. 9A). In the prescence of CO, both frequencies exhibit slower kinetics (~2-fold) with a single exponential rise lifetimes of 206 and 320 μs observed for 1971 and 1962 cm^{-1} while the decay lifetimes are 14 and 18 ms, respectively. Only a slight decay of 0.2 mO.D. is observed, suggesting that the majority of CO is not dissociating from the Ni in the active site. It's possible CO trapped in the gas channel is preventing CO disassociation or the molecule is rebinding to active site after formation. Intriguingly, the 1971 cm^{-1} rise occurs faster than 1962 cm^{-1} providing more evidence that the former species forms more rapidly.

The transient IR data implies both frequencies are kinetically competent as they exhibit absorbance changes within the turnover timescales (~9 s^{-1} or ~100 ms) previously described for CO_2 reduction by CODH II. This refutes the possibility that the Ni-CO stretches are only observed due to inhibition. The kinetics of the frequencies are similar and refute the possibility that these are different Ni-CO states or orientations on the same active site. Instead, it suggests that the two frequencies are of CO formation and dissociation at two slightly different active sites. As mentioned before, CODHs contain two active sites (C-clusters) positioned at opposite ends of the complex and based on crystal structures appear to be identical though multiple positions exist.[1] The different frequencies may be the result of different active site geometries and could be the bent or linear observed in crystal structures. It is unclear from the FTIR and TAIR which frequency could be which state. The linear arrangement should form faster as the position is closer than the bent to the orientation of CO_2 in the active site.[2] If the 1971 cm^{-1} frequency is indeed faster, it could be the linear orientation. Transient experiments cannot give distinct conclusions on the

active site geometry and more extensive experiments using other spectroscopy techniques such as electron paramagnetic resonance are required to validate this hypothesis.

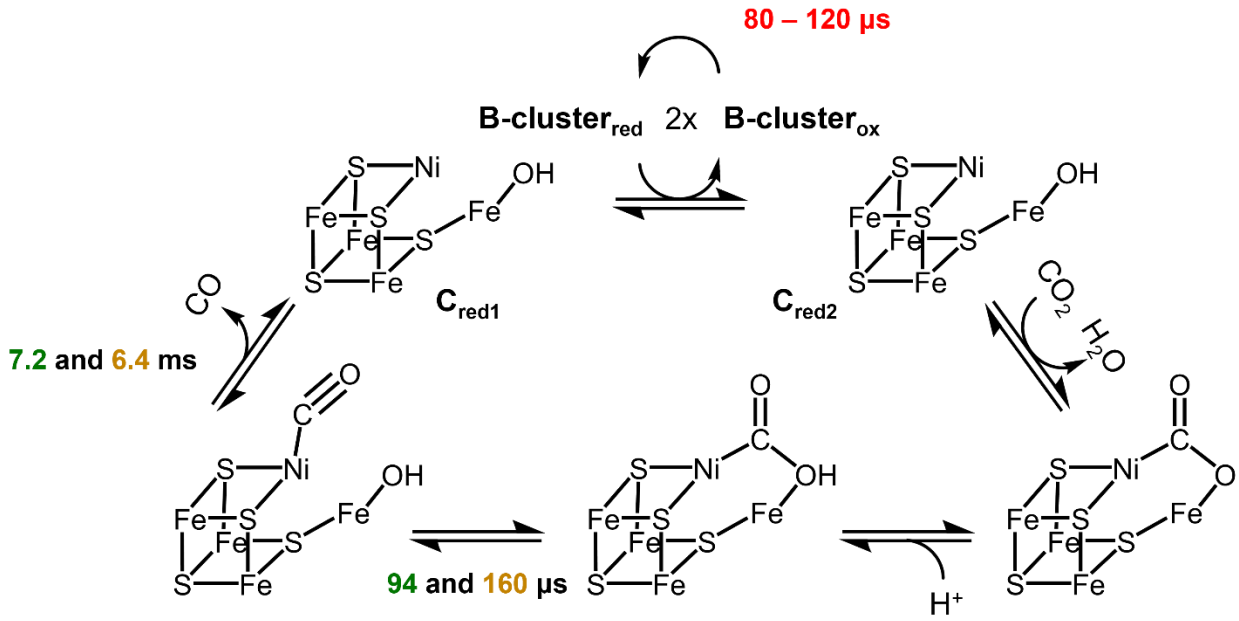

Figure 3.10 The proposed mechanism with kinetic data. The kinetic lifetimes from transient absorption experiments are colored based on the probe beam. Red is visible mediator reduction, green is the 1971 cm^{-1}, and yellow is the 1962 cm^{-1}.

The second result of the transient IR experiments is that CO formation occurs at the same timescale as enzyme reduction. In the proposed catalytic cycle (Fig. 10), two electrons are transferred to the solvent exposed B-cluster which flow to the C-cluster and convert the C_{red1} resting state to the C_{red2} state. CO_2 then binds with the carbon atom (C) to the Ni and one of the oxygen atoms (O) to Fe1 after the hydroxide ligand is protonated to form water and leaves.[2] The O bound to the Fe1 is protonated and the C-O bond is cleaved forming CO coordinated to the Ni. The kinetics observed suggest two possibilities: a) either CO_2 binds (and the hydroxide ligand dissociates) extremely fast after reduction to C_{red2} or b) CO_2 is already coordinated in C_{red1} or in the one electron intermediate, C_{int}. The general consensus is that CO_2 binding only occurs after

reduction of the C_{red1}.[8, 31, 45, 46] Since the reaction requires two electrons, it is possible that CO_2 binding and hydroxide ligand dissociation occur after the first electron transfer, then proton-dependent CO formation occurs after the second electron transfer. As the vibrational modes of a bound or coordinated CO_2 are not yet known, it's unclear based solely on the observed transient data which possiblity is occuring. Identifying these frequencies and observing the kinetics of CO_2 directly would answer this question. Regardless, CO_2 must be present in the active site before reduction as diffuse through the gas channel would require likely be on the millisecond timescale.[47]

3.3 – Conclusions

In this chapter, the first photosystem incorporating CODH II for CO_2 reduction is described. Inspired by previous photoenzymatic systems for hydrogen production, efficient photoreduction of CO_2 was achieved using nanocrystalline CdSe/CdS dot-in-rods, diquat-based DQ53, and CODH II as the photosensitizer, redox mediator, and biocatalyst respectively. In particular, the inclusion of the redox mediator proved to be essential for efficient CO_2 photoreduction as controls without DQ53 did not produce detectable levels of CO. After optimizing buffer conditions for maximum substrate concentration and photosensitizer performance, an initial QY of ~19% was observed for the photosystem despite issues with oxygen contamination and product inhibition. These results are more than an order of magnitude more efficient than other enzymatic photosystems and represent a new standard for efficient photoenzymatic CO_2 reduction.[28] Future work will focus on optimization of reaction conditions including other photosensitizers or redox mediators to improve efficiency, potentially to those of photoenzymatic hydrogen production. The successful application of semiconductor photosensitizers in combination with a redox mediator for CODH photoactivation demonstrates

that this setup could be used for other redox enzymes for photobiocatalysis or mechanistic investigations.[19, 20]

Troublesome for CO_2 photoreduction, the issue of product inhibition proved to be vital for identifying the elusive Ni-CO stretches of CODH II at 1971 and 1962 cm^{-1}. Surprisingly, not one but two IR absorbance features in the M-CO region were identified after inhibition of the enzyme in the photosystem. Isotopic labeling further validated both features as Ni-CO stretches. While similar IR bands (and 4 others) were previously identified in the CODH/ACS complex, these results confirm these specific features as Ni-CO modes of the C-cluster of [NiFe] CODH.[17] Two IR frequencies suggest different orientations of either the bound CO or the residues/C-cluster. Different active site positions are observed for CODH including two different proposed CO orientations which may be the frequencies observed.[10, 14] A difference of a hydrogen bond or other variations in the Ni-CO arrangement could cause the 9 cm^{-1} difference between the two features.[48] This could be investigated using deuterated samples would cause a shift in one of the IR frequencies if it is facilitating in hydrogen bonding.

Transient absorption experiments confirmed both frequencies are catalytically relevant to the mechanism and not solely characteristics of CO inhibition. The observed absorbance changes are the first direct kinetic data for CO formation and its subsequent dissociation from the C-cluster for [NiFe] CODH enzymes. Furthermore, the dynamics of both frequencies are nearly identical suggesting these are not different binding orientations of the same active site but are the formation and dissociation of CO at two slightly different active sites. Based on the kinetics of the redox mediator, it was concluded that initial reduction of the B-cluster is the rate limiting step for CO_2 reduction. The observed enzyme reduction and formation of CO occur at similar lifetimes suggesting that CO_2 is present in the active site and either binds quickly after electron transfer or

that it occurs in the C_{red1} or C_{int} states. It's possible that CO_2 binding occurs after the initial electron transfer as it requires the dissociation of the Fe1 hydroxide ligand. The observed CO formation then occurs as the C-cluster is reduced again and CO_2 is protonated.

The next step in unravelling the CODH mechanism will focus on the protonation step that results in CO formation. Kinetic isotope experiments using D_2O would validate the proposed step and may shift the frequencies as well. Future directions include exploring the gas tunnel CO frequencies potentially observed in the FTIR CO inhibition experiments. Resolving the kinetics of CO moving into the gas tunnel would provide further evidence that the dissociation of CO from the active site was observed and elucidate the mechanism of inhibition. In addition, to decipher CO_2 binding with this setup will require resolving the metal carboxylate frequencies. Altogether this could provide a more complete picture of the mechanism as CO_2 binding, CO formation and disassociation at the C-cluster, and diffusion of CO to the solvent could be kinetically observed. Lastly, transient and steady state experiments of active site variants of CODH II (specifically His93 and Lys563) could provide further mechanistic details for these enzymes.

To summarize, an efficient system to photoactivate CODH II was developed and used as the basis for time resolved spectroscopic investigations into the enzyme's mechanism. The identification of two catalytically relevant Ni-CO stretches is unusual and suggests the active site forms two different conformations.

3.4 - Materials and Methods

3.4.1 - Synthesis and Preparation of CdSe/CdS Dot-in-Rods (DIR)

Procedure was adapted from literature.[24]

CdSe Seed: In a 3-neck round bottom flask, 0.06 g of Cadium Oxide (CdO) (purchase from Alfa Aesar), 3 g of Trioctylphosphine oxide (TOPO) (purchased from TCI) and 0.28 g of

Octadecylphosphonic acid (ODPA) (purchased from TCI) were combined and heated to 150 ˚C for 2 hours while under vacuum. A Se precursor solution was also prepared by dissolving 0.058 g of Se into 0.5 mL of trioctylphosphine (TOP). After 2 hours, the flask was placed under an N_2 atmosphere and heated to 350 ˚C. After the solution became clear, 1.5 mL of TOP was injected into the flask. Once the temperature recovered to 340 ˚C, the Se precursor solution was injected, and the solution was allowed to react until color change. The flask was then removed from heat and cooled to room temperature. A small volume of hexanes was added to the mixture for it to remain liquid.

CdS Shell: A CdS shell was grown over the CdSe seed to create the CdSe/CdS dot-in-rod. In a 3-neck round bottom flask, 0.06 g of CdO, 3 g of TOPO, 0.08 g of hexylphosphonic acid (HPA) (purchased from Alfa Aesar) and 0.28 g of ODPA were combined and heated to 150 ˚C for 2 hours while under vacuum. The S and CdSe seed precursor solution was prepared by dissolving 0.12 g of S and 5-10 mg of precipitated seeds into 1.5 mL of TOP. After 2 hours, the flask was placed under an N_2 atmosphere and heated to 350 ˚C. After the solution became clear, 1.5 mL of TOP was injected into the flask. Once the temperature recovered to 340 ˚C, the S and CdSe seed precursor solution was injected. The solution was allowed to for 1 min or until color change. The flask was then removed from heat and cooled to room temperature. A small volume of hexanes was added to the mixture for it to remain liquid.

3.4.2 - Ligand Exchange of CdSe/CdS DIR

Procedure adapted from literature.[24]

Synthesized CdSe/CdS DIR were ligand exchanged with 3-mercaptapropionic acid in order to solubilize in an aqueous environment. Briefly, the DIR were purified by precipitation with methanol and centrifugation. This was repeated 2-5 times to remove excess TOPO. The purified

DIR were refluxed in the dark, for 2 hours, under N_2 in methanol with 10 mM 3-mercaptapropionic acid (MPA). The pH of the solution was adjusted to pH >10 using tetramethyl ammonium hydroxide. Afterwards the DIR were precipitated and centrifuged with 50 mM borate buffer containing 10 mM MPA and 10 mM triscarboxyethyl phosphide. DIR were stored in an air-free environment.

3.4.3 - Synthesis of the Mediator DQ53

Procedure was adapted from literature.[24]

In an air free 3-neck round bottom flask, 5 mL of 1,3 dibromopropane and 0.25 g of 5,5'-dimethyl-2,2'-bipyridine were combined. The flask was refluxed at 100-110 ˚C and reacted for 3-5 hours until the solution turned a pale cloudy-yellow. Afterwards the flask was cooled with an ice bath and the solid was collected on a frit. The pale-yellow precipitate was washed with cold hexanes. The product was crystallized from methanol.

3.4.4 - Enzyme Preparation and Purification

*Ch*CODH expression and purification was performed by Kareem Aboulhosn and Daniel Esckilsen at the University of Michigan. Purification is performed anaerobically and described previously.[44] Anywhere from 20-25 grams of cells are prepared for sonication in a 20mM Sodium phosphate, 0.4M Sodium chloride pH 7.5 buffer, and with added cell paste, homogenized into a slurry. 0.25 mg/ml lysozyme, 0.5mM PMSF, an aliquot of 50mg/ml DNAse are added to the sonicate, and 5mM BME is maintained throughout the purification. Cell slurry is sonicated at amplitude 80, 10 minutes total, 15 seconds on, 10 seconds off, then the cells are transferred to a Beckman Coulter ultracentrifuge tube. The tube is capped and heated for 10 minutes at 80-90 C in a water bath. The sonicate is ultracentrifuged for 1h at 30,000 rpm, then brought back into the glovebox, and supernatant is separated from the pellet. The supernatant is loaded onto a Bio-rad

column containing High Performance Nickel NTA resin, a His-tagged affinity purification system. The protein is eluted with a 100mM-500mM imidazole, linear gradient, at 1ml/min, over a total of 150ml. CODH II elutes pure from roughly 200-250mM imidazole. The fractions are characterized by a CO oxidation assay indicating enzyme activity, Rose Bengal assay to determine protein concentration, and SDS-PAGE showing purity.2 Protein is concentrated and buffer exchanged into 50mM Tris, 5% Glycerol pH 7.5 in an Amicon stirred cell. Final concentrated stocks are characterized once more for activity, concentration, and purity. Final activity of CODH II can be upwards of 500 U/mg at room temperature.

3.4.5 - GC Parameters and Calibration Curve for Detection of CO

An Agilent 7890A gas chromatograph (GC) was used to detect CO production. The method was developed from literature.[28] The reaction vessel was pierced with a gastight Hamilton syringe with 50 μL of headspace sampled. Immediately before injection, 25 μL of sample was ejected then the remaining 25 μL was quickly injected onto the GC equipped with a 1.5 mm diameter split/splitless liner, Restek ShinCarbon ST micropacked column, and a pulsed discharge detector using a high-purity He carrier gas. The oven temperature was held at 40 ˚C for 4 minutes and then heated from 40 to 100 ˚C at a rate of 10 min-1. Separation of H2, N2, CO and CO2 was achieved.

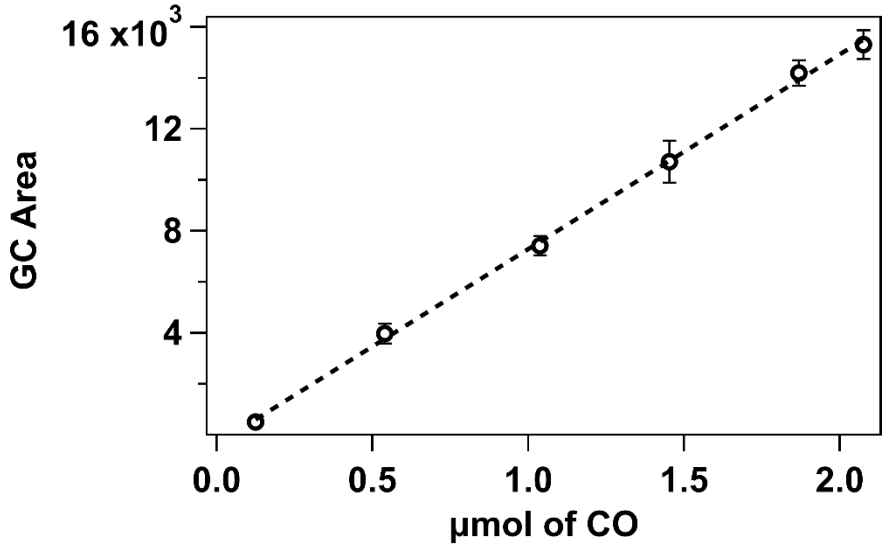

Figure 3.11 GC calibration curve for CO.

Known amounts of pure CO was injected into the headspace of a cuvette containing 1.4 mL of buffer at 1 atm, 20°C. With a magnetic stir bar spinning at the gas-liquid interface, the headspace of the cuvette was left to equilibrate for 20 minutes. Then, 50 µL of the headspace was sampled. Of the sampled volume, 25 µL was pushed out immediately before plunging the needle into the GC septum, and 25 µL was injected into the GC. Each point on the calibration curve were generated from triplicate data, and the errors bars are standard deviation of each triplicate. The moles of CO added were calculated using the density and molecular weight of CO, 1.14 g/L and 28.01 g/mol respectively. At 20 ˚C at 1 atm, 20 µL of CO corresponds to 0.813 µmoles. The slope of the calibration curve is 7630 unit peak area / nmols CO with $R^2 = 0.999$.

3.4.6 - Standard Photoreduction Assay Conditions

Photoreduction of CO2 assays were carried out as follows. A solution of 100 nM CODH II, 5 mM DQ53, and 0.25 O.D. DIRs in a buffer of 0.25 M NaPO4, 0.25 M NaHCO3, and 50 mM MPA was placed into a small volume quartz cuvette. Preparation of the reaction mixture occurred

in an anaerobic chamber to ensure anoxic conditions. The cuvette was sealed with a rubber septum and subsequently the headspace of the cuvette was purged with CO2. We assume the pressure of the system to be 1 atm considering the headspace was purged in an anaerobic chamber with a comparable atmosphere to the outside air. The cuvette was removed from the anaerobic chamber to monitor the reaction via an Ocean Optics spectrometer. The reaction was stirred using a magnetic stir bar and initiated by illumination with a 445 nm diode laser from Thorlabs. The reaction occurred at room temperature. At 15-minute intervals, 50 μL headspace was sampled with 25 μL injected onto the GC. Detailed method for GC detection of CO in the above section. Control experiments were conducted in an identical procedure, only omitting one of the following components: CODH II, DQ53, DIR. All assays were run in triplicate.

3.4.7 - Quantum Efficiency Calculations

Quantum yield of the DIRs was determined by measuring mediator reduction from photoexcitation using photosystem assay conditions. Briefly, a solution containing 0.25 O.D. DIRs, 5 mM DQ53 and a buffer of 0.25 M $NaPO_4$, 0.25 M $NaHCO_3$, 50 mM MPA at pH 7.5 were placed in a septum sealed cuvette. The headspace of the cuvette was purged with CO_2. The DIRs were photoexcited with a 445 nm laser diode at ~5 mW from Thorlabs that was gated by a mechanical shutter with a 10 s on and off cycle. The solution was agitated using a magnetic stir bar. Production of DQ53 radical was measured using an Ocean Optics QE65000 CCD spectrometer with a 35W Xe lamp.

Quantum yield of the nanorods was calculated using the following equation:[30]

$$Quantum\ Yield = \frac{moles\ of\ product}{moles\ of\ photons\ absorbed} \quad (1)$$

$$Quantum\ Yield = \frac{moles\ of\ product}{Laser\ Power\ (eV) * photons\left(\frac{1}{eV}\right) * \%\ of photons\ absorbed\ vs\ total * (1 - scatter) * \frac{1}{N_A}} \quad (2)$$

For the QE of prepared DIRs a yield of 61% was calculated using Equation (2) as follows

$$61.5\% = \frac{4.03*10^{-8}\ \text{moles of DQ53}^{+}}{0.0049\ W*10\ s*\frac{eV}{(1.602*10^{-19})W*s}*\left(\frac{photon\ (445\ nm)}{2.78\ eV}\right)*(1-10^{-0.25OD})*(1-0.14)*\frac{1}{N_A}}$$

3.4.8 - Sample Preparation for Infrared Experiments

All sample preparation occurred under an anaerobic atmosphere For IR experiments, CODH and nanomaterial were buffer exchanged a minimum of 6x from the respective storage solutions into the reaction buffer of 0.25 M NaPO4, 0.25 M NaHCO3, and 50 mM MPA using 10 kDa molecular weight cutoff filters (Millipore). Samples were concentrated to 15-20 μL and assembled in small volume vials. The headspace of these vials was purged with CO_2 (except for the isotopically labeled sample) to ensure enough substrate then injected into the IR cell using a gas tight syringe. The IR cell consisted of two copper plates housing 2 CaF_2 windows separated by a Teflon spacer. A butyl rubber seal was used to allow injection of the sample into the cell. Set screws layered with grease were also used to seal the ports of one of the CaF_2 windows maintaining the anaerobic environment. In the FTIR experiments, a reference side of the cell was composed of reaction buffer. The concentration of the enzyme was 500 μM and DQ53 was 30 mM. In the transient absorption experiments, the reference side included QDs, mediator and myoglobin to match the 532 nm absorbance of the sample side. The concentration of the enzyme was increased to 800 μM and DQ53 was 60 mM.

3.4.9 - Steady State CODH CO Inhibition FTIR Conditions

FTIR spectra were obtained using a Varian 660 FTIR spectrometer equipped with an additional MCT detector cooled through liquid nitrogen. The FTIR beam was directed outside of the spectrometer using gold-plated mirrors into a dry air purged box with the IR cell in the beam

path on top of a copper stage to allow lateral movement for collection of the sample and reference side. A resolution of 2 cm^{-1} with 1024 or 2048 FTIR scans averaged to reduce noise.

Illumination of CODH to induce the CO inhibited state used a Q-switched Nd:YLF laser (Crystalaser Inc.) set at 527 nm and aligned to ~500 μm spot. After illumination, FTIR spectra were immediately collected to observe absorbance changes. Difference spectra were obtained by subtracting the dark spectra from the proceeding illuminated spectra and were performed using Resolution Pro software for the FTIR.

3.4.10 - Time Resolved Infrared Spectroscopy of CODH

Time Resolved IR spectroscopy experiments were performed using the setup previously described.[23] The 532 nm pump beam was produced from the frequency doubled 1064 nm from a Surelite Nd:YAG (Continuum) operating at 10 Hz and the wavelength was selected using a harmonic separator. An 808 nm diode was used to visibly probe mediator reduction during the experiment. The visible probe was observed using a silicon photo-diode detector (Thor Labs Inc.). IR absorbance was monitored using a Quantum Cascade Laser (Daylight Solutions) tunable in the range of 1900-2000 cm^{-1}. A series of IR polarizers were used to optically align the beam and attenuate the intensity to an MCT detector. The photodiode was used during experiments to identify the position of both beams. Collection of the probe beams was initiated using the pump beam. All three beams were aligned to a 50 μm spot. The overlap of the beams was confirmed by maximizing the visible potential jump and the increased water IR absorbance due to heating of the sample from the pump beam (IR temperature jump) of the reference side. Each experiment is the average of 15-20 laser shots to account for power fluctuations of the pump beam. After each laser shot, the sample position was shifted to probe a new area as CODH II is inhibited by the presence of CO which is formed after photoreduction.

The resulting raw IR signal are difference spectra as it's calculated as $\Delta A = -\log(I_{light}/I_{dark})$. The reference IR signal was used to correct for the water IR temperature jump observed on both sides of the sample. The final IR spectra of CODH thus is the subtraction of the reference signal. Analysis of the transient data included global fitting using Igor Pro 8. The equation used was a derived version of the integrated first order rate law:

$$Abs = y_0 + Ae^{-x/\tau} \quad (3)$$

With *A* referring to the amplitude of the exponential decay/growth function. The variable τ is the lifetime of the function correlating to the time at which 37% or 1/e of the amplitude has decayed/grown. Lifetime is the inverse of the rate or *k*.

3.5 - References

1. Can, M.; Armstrong, F. A.; Ragsdale, S. W., Structure, function, and mechanism of the nickel metalloenzymes, CO dehydrogenase, and acetyl-CoA synthase. *Chem. Rev.* **2014,** *114* (8), 4149-4174.

2. Dobbek, H., Mechanism of Ni, Fe-Containing carbon monoxide dehydrogenases. *Metallocofactors that Activate Small Molecules* **2018**, 153-166.

3. Alfano, M.; Cavazza, C., The biologically mediated water–gas shift reaction: structure, function and biosynthesis of monofunctional [NiFe]-carbon monoxide dehydrogenases. *Sustainable Energy & Fuels* **2018,** *2* (8), 1653-1670.

4. Heo, J.; Staples, C. R.; Ludden, P. W., Redox-dependent CO2 reduction activity of CO dehydrogenase from Rhodospirillum rubrum. *Biochemistry* **2001,** *40* (25), 7604-7611.

5. Wittenborn, E. C.; Guendon, C.; Merrouch, M.; Benvenuti, M.; Fourmond, V.; Léger, C.; Drennan, C. L.; Dementin, S., The solvent-exposed Fe–S D-cluster contributes to oxygen-resistance in Desulfovibrio vulgaris Ni–Fe carbon monoxide dehydrogenase. *ACS catalysis* **2020,** *10* (13), 7328-7335.

6. Craft, J. L.; Ludden, P. W.; Brunold, T. C., Spectroscopic Studies of Nickel-Deficient Carbon Monoxide Dehydrogenase from Rhodospirillum rubrum: Nature of the Iron− Sulfur Clusters. *Biochemistry* **2002,** *41* (5), 1681-1688.

7. Dobbek, H.; Svetlitchnyi, V.; Gremer, L.; Huber, R.; Meyer, O., Crystal structure of a carbon monoxide dehydrogenase reveals a [Ni-4Fe-5S] cluster. *Science* **2001,** *293* (5533), 1281-1285.

8. Fesseler, J.; Jeoung, J. H.; Dobbek, H., How the [NiFe4S4] cluster of CO dehydrogenase activates CO2 and NCO−. *Angew. Chem. Int. Ed.* **2015,** *54* (29), 8560-8564.

9. Wang, V. C. C.; Can, M.; Pierce, E.; Ragsdale, S. W.; Armstrong, F. A., A unified electrocatalytic description of the action of inhibitors of nickel carbon monoxide dehydrogenase. *Journal of the American Chemical Society* **2013,** *135* (6), 2198-2206.

10. Gong, W.; Hao, B.; Wei, Z.; Ferguson Jr, D. J.; Tallant, T.; Krzycki, J. A.; Chan, M. K., Structure of the α2ε2 Ni-dependent CO dehydrogenase component of the Methanosarcina barkeri acetyl-CoA decarbonylase/synthase complex. *Proceedings of the National Academy of Sciences* **2008,** *105* (28), 9558-9563.

11. Hansen, H. A.; Varley, J. B.; Peterson, A. A.; Nørskov, J. K., Understanding trends in the electrocatalytic activity of metals and enzymes for CO2 reduction to CO. *The journal of physical chemistry letters* **2013,** *4* (3), 388-392.

12. Amara, P.; Mouesca, J.-M.; Volbeda, A.; Fontecilla-Camps, J. C., Carbon monoxide dehydrogenase reaction mechanism: a likely case of abnormal CO2 insertion to a Ni− H− bond. *Inorg. Chem.* **2011,** *50* (5), 1868-1878.

13. Kung, Y.; Doukov, T. I.; Seravalli, J.; Ragsdale, S. W.; Drennan, C. L., Crystallographic snapshots of cyanide-and water-bound C-clusters from bifunctional carbon monoxide dehydrogenase/acetyl-CoA synthase. *Biochemistry* **2009,** *48* (31), 7432-7440.

14. Jeoung, J.-H.; Dobbek, H., Structural basis of cyanide inhibition of Ni, Fe-containing carbon monoxide dehydrogenase. *Journal of the American Chemical Society* **2009,** *131* (29), 9922-9923.

15. Ciaccafava, A.; Tombolelli, D.; Domnik, L.; Fesseler, J.; Jeoung, J.-H.; Dobbek, H.; Mroginski, M. A.; Zebger, I.; Hildebrandt, P., When the inhibitor tells more than the substrate: the cyanide-bound state of a carbon monoxide dehydrogenase. *Chemical Science* **2016,** *7* (5), 3162-3171.

16. Ciaccafava, A.; Tombolelli, D.; Domnik, L.; Jeoung, J. H.; Dobbek, H.; Mroginski, M. A.; Zebger, I.; Hildebrandt, P., Carbon monoxide dehydrogenase reduces cyanate to cyanide. *Angew. Chem. Int. Ed.* **2017,** *56* (26), 7398-7401.

17. Chen, J.; Huang, S.; Seravalli, J.; Gutzman, H.; Swartz, D. J.; Ragsdale, S. W.; Bagley, K. A., Infrared studies of carbon monoxide binding to carbon monoxide dehydrogenase/acetyl-CoA synthase from Moorella thermoacetica. *Biochemistry* **2003,** *42* (50), 14822-14830.

18. George, S. J.; Seravalli, J.; Ragsdale, S. W., EPR and infrared spectroscopic evidence that a kinetically competent paramagnetic intermediate is formed when acetyl-coenzyme A synthase reacts with CO. *Journal of the American Chemical Society* **2005,** *127* (39), 13500-13501.

19. Greene, B. L., Progress and Opportunities in Photochemical Enzymology of Oxidoreductases. *ACS Catalysis* **2021,** *11* (23), 14635-14650.

20. Lee, S. H.; Choi, D. S.; Kuk, S. K.; Park, C. B., Photobiocatalysis: activating redox enzymes by direct or indirect transfer of photoinduced electrons. *Angew. Chem. Int. Ed.* **2018,** *57* (27), 7958-7985.

21. Schmermund, L.; Jurkaš, V.; Özgen, F. F.; Barone, G. D.; Büchsenschütz, H. C.; Winkler, C. K.; Schmidt, S.; Kourist, R.; Kroutil, W., Photo-biocatalysis: biotransformations in the presence of light. *ACS Catalysis* **2019,** *9* (5), 4115-4144.

22. Sanchez, M. L. K.; Konecny, S. E.; Narehood, S. M.; Reijerse, E. J.; Lubitz, W.; Birrell, J. A.; Dyer, R. B., The Laser-Induced Potential Jump: A Method for Rapid Electron Injection into Oxidoreductase Enzymes. *The Journal of Physical Chemistry B* **2020,** *124* (40), 8750-8760.

23. Greene, B. L.; Wu, C.-H.; McTernan, P. M.; Adams, M. W. W.; Dyer, R. B., Proton-coupled electron transfer dynamics in the catalytic mechanism of a [NiFe]-hydrogenase. *Journal of the American Chemical Society* **2015,** *137* (13), 4558-4566.

24. Sanchez, M. L. K.; Sommer, C.; Reijerse, E.; Birrell, J. A.; Lubitz, W.; Dyer, R. B., Investigating the kinetic competency of Cr HydA1 [FeFe] hydrogenase intermediate states via time-resolved infrared spectroscopy. *Journal of the American Chemical Society* **2019,** *141* (40), 16064-16070.

25. Greene, B. L.; Taguchi, A. T.; Stubbe, J.; Nocera, D. G., Conformationally dynamic radical transfer within ribonucleotide reductase. *Journal of the American Chemical Society* **2017,** *139* (46), 16657-16665.

26. Barber, J.; Tran, P. D., From natural to artificial photosynthesis. *Journal of The Royal Society Interface* **2013,** *10* (81), 20120984.

27. Wang, Y.; He, D.; Chen, H.; Wang, D., Catalysts in electro-, photo-and photoelectrocatalytic CO2 reduction reactions. *Journal of Photochemistry and Photobiology C: Photochemistry Reviews* **2019,** *40*, 117-149.

28. Zhang, L.; Can, M.; Ragsdale, S. W.; Armstrong, F. A., Fast and selective photoreduction of CO2 to CO catalyzed by a complex of carbon monoxide dehydrogenase, TiO2, and Ag nanoclusters. *ACS catalysis* **2018,** *8* (4), 2789-2795.

29. Woolerton, T. W.; Sheard, S.; Reisner, E.; Pierce, E.; Ragsdale, S. W.; Armstrong, F. A., Efficient and clean photoreduction of CO2 to CO by enzyme-modified TiO2 nanoparticles using visible light. *Journal of the American Chemical Society* **2010,** *132* (7), 2132-2133.

30. Chica, B.; Wu, C.-H.; Liu, Y.; Adams, M. W. W.; Lian, T.; Dyer, R. B., Balancing electron transfer rate and driving force for efficient photocatalytic hydrogen production in CdSe/CdS nanorod–[NiFe] hydrogenase assemblies. *Energy & Environmental Science* **2017,** *10* (10), 2245-2255.

31. Jeoung, J.-H.; Dobbek, H., n-Butyl isocyanide oxidation at the [NiFe4S4OH x] cluster of CO dehydrogenase. *JBIC Journal of Biological Inorganic Chemistry* **2012,** *17* (2), 167-173.

32. Svetlitchnyi, V.; Peschel, C.; Acker, G.; Meyer, O., Two membrane-associated NiFeS-carbon monoxide dehydrogenases from the anaerobic carbon-monoxide-utilizing eubacterium Carboxydothermus hydrogenoformans. *J. Bacteriol.* **2001,** *183* (17), 5134-5144.

33. Wang, V. C. C.; Ragsdale, S. W.; Armstrong, F. A., Investigations of two bidirectional carbon monoxide dehydrogenases from Carboxydothermus hydrogenoformans by protein film electrochemistry. *ChemBioChem* **2013,** *14* (14), 1845-1851.

34. Chica, B.; Ruzicka, J.; Kallas, H.; Mulder, D. W.; Brown, K. A.; Peters, J. W.; Seefeldt, L. C.; Dukovic, G.; King, P. W. J. J. o. t. A. C. S., Defining intermediates of nitrogenase MoFe protein during N2 reduction under photochemical electron delivery from CdS quantum dots. **2020,** *142* (33), 14324-14330.

35. Reiss, P.; Protiere, M.; Li, L., Core/shell semiconductor nanocrystals. *small* **2009,** *5* (2), 154-168.

36. Sanchez, M. L. K.; Wu, C.-H.; Adams, M. W. W.; Dyer, R. B., Optimizing electron transfer from CdSe QDs to hydrogenase for photocatalytic H 2 production. *Chem. Commun.* **2019,** *55* (39), 5579-5582.

37. Han, Z.; Qiu, F.; Eisenberg, R.; Holland, P. L.; Krauss, T. D., Robust photogeneration of H2 in water using semiconductor nanocrystals and a nickel catalyst. *Science* **2012,** *338* (6112), 1321-1324.

38. Sander, R., Compilation of Henry's law constants (version 4.0) for water as solvent. *Atmospheric Chemistry and Physics* **2015,** *15* (8), 4399-4981.

39. Hamby, H.; Li, B.; Shinopoulos, K. E.; Keller, H. R.; Elliott, S. J.; Dukovic, G., Light-driven carbon− carbon bond formation via CO2 reduction catalyzed by complexes of CdS nanorods and a 2-oxoacid oxidoreductase. *Proceedings of the National Academy of Sciences* **2020,** *117* (1), 135-140.

40. Merrouch, M.; Hadj-Saïd, J.; Domnik, L.; Dobbek, H.; Léger, C.; Dementin, S.; Fourmond, V., O2 Inhibition of Ni-Containing CO Dehydrogenase Is Partly Reversible. *Eur. J. Chem.* **2015,** *21* (52), 18934-18938.

41. Li, X.; Yu, J.; Jaroniec, M.; Chen, X., Cocatalysts for selective photoreduction of CO2 into solar fuels. *Chem. Rev.* **2019,** *119* (6), 3962-4179.

42. Wang, J.-W.; Jiang, L.; Huang, H.-H.; Han, Z.; Ouyang, G., Rapid electron transfer via dynamic coordinative interaction boosts quantum efficiency for photocatalytic CO2 reduction. *Nature communications* **2021,** *12* (1), 1-11.

43. Sanchez, M. L.; Wu, C.-H.; Adams, M. W.; Dyer, R. B. J. C. C., Optimizing electron transfer from CdSe QDs to hydrogenase for photocatalytic H 2 production. **2019,** *55* (39), 5579-5582.

44. Burton, R.; Can, M.; Esckilsen, D.; Wiley, S.; Ragsdale, S. W., Production and properties of enzymes that activate and produce carbon monoxide. In *Methods Enzymol.*, Elsevier: 2018; Vol. 613, pp 297-324.

45. Terranova, U., Residues surrounding the active centre of carbon monoxide dehydrogenase are key in converting CO2 to CO. *JBIC Journal of Biological Inorganic Chemistry* **2021,** *26* (5), 617-624.

46. Breglia, R.; Arrigoni, F.; Sensi, M.; Greco, C.; Fantucci, P.; De Gioia, L.; Bruschi, M., First-principles calculations on Ni, Fe-containing carbon monoxide dehydrogenases reveal key

stereoelectronic features for binding and release of CO2 to/from the C-cluster. *Inorg. Chem.* **2020,** *60* (1), 387-402.

47. Leroux, F.; Dementin, S.; Burlat, B.; Cournac, L.; Volbeda, A.; Champ, S.; Martin, L.; Guigliarelli, B.; Bertrand, P.; Fontecilla-Camps, J., Experimental approaches to kinetics of gas diffusion in hydrogenase. *Proceedings of the National Academy of Sciences* **2008,** *105* (32), 11188-11193.

48. Schneider, S. H.; Boxer, S. G., Vibrational stark effects of carbonyl probes applied to reinterpret IR and Raman data for enzyme inhibitors in terms of electric fields at the active site. *The Journal of Physical Chemistry B* **2016,** *120* (36), 9672-9684.

Chapter 4: Photoreduction of the Air Tolerant State in [FeFe] Hydrogenases

4.1 – Introduction

Sustainable hydrogen production is necessary to reduce CO_2 emissions and supply an alternative energy source.[1-3] [FeFe] hydrogenases are metalloenzymes able to efficiently catalyze the reversible reduction of protons into hydrogen using a unique cofactor termed H-cluster with a diiron reaction site.[4, 5] In the presence of oxygen, the H-cluster produces reactive oxygen species which specifically degrades the diiron core and gives the enzymes high oxygen sensitivity, limiting their effectiveness as catalysts.[6] Sensitivity to oxygen varies amongst known [FeFe] hydrogenases as several are able to form an air tolerant inactivated state to protect the H-cluster.[7-9]

Figure 4.1 The three proposed mechanisms of reactivation of the air tolerant state for [FeFe] hydrogenases.

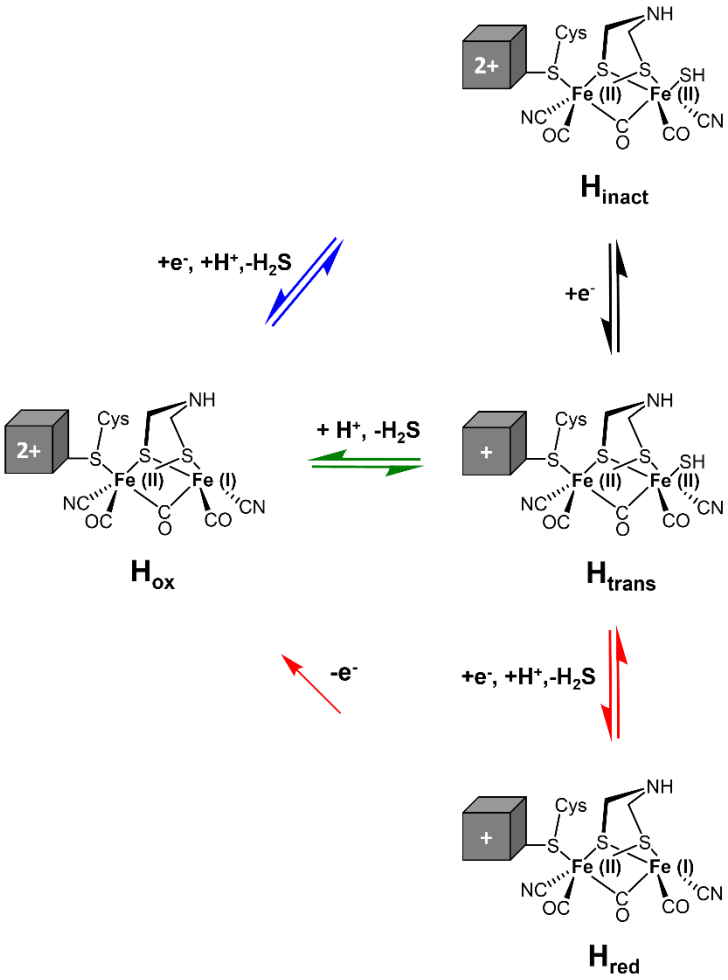

The mechanism is drawn in the reactivation direction. In green is the mechanism of Rodríguez-Macia et al. In red is Felbeck et al. In blue is the mechanism shown by CbA5H.

The inactivated state or H_{inact} was initially discovered during the aerobic purification of the hydrogenase from *Desulfovibrio desulfuricans* which reported air stability of at least a month.[10] Further spectroscopic investigations yielded that the state is overoxidized with the H-cluster possessing $[4Fe\text{-}4S]^{2+}$ and Fe(II)/Fe(II) oxidation states.[11] At the open coordination site of the distal Fe is a sulfide ligand which prevents both hydrogen formation and oxygen evolution.[8] Reactivation of the enzyme is proposed to occur via reduction of the [4Fe-4S] cluster which forms the intermediate H_{trans} state followed by a protonation event releasing the sulfide and forming the catalytic resting state of H_{ox} (Fig. 1).[12] Identification of these states are best resolved following the shift in IR bands of the carbon monoxide and cyanide stretches of the H-cluster. A competing mechanism, based on the [FeFe] hydrogenase (*Cr*HydA1) of *Chlamydomonas reinhardtii*, postulates reduction of H_{trans} in addition to protonation to form the one-electron reduced state of H_{red} (Fig. 1).[13] Auto-oxidation of H_{red} results in the H_{ox} state observed in previous experiments. It may be possible that the mechanism of reactivation is enzyme specific as CbA5H from *Clostridium beijerinckii* uses a unique neighboring cysteine to protect the H-cluster from oxidation damage.[9, 14] CbA5H is observed reversibly converting between H_{inact} and H_{ox} without noticeable formation of the H_{trans} state likely due to using a residue instead of sulfide (Fig. 1).[14] Deciphering the specific mechanism of the oxygen tolerant state is key for further utilization of [FeFe] hydrogenases as catalysts. Previous studies have used chemical reductants/oxidants to probe the mechanism, but photo-initiated enzyme reduction coupled with time-resolved spectroscopy allow for a more direct observation of the catalytic cycle.[12, 14-16] This method has been utilized before to investigate the kinetic competency of the redox states in proton reduction, thus it should be possible to also observe reactivation of the oxygen tolerant state through a similar approach.[17] Specifically the

reactivation of *Dd*HydAB is explored in this chapter, to verify the first proposed mechanism (Fig. 1 in green).

4.2 - Results and Discussion

4.2.1 - Light-Titrated Reduction of Inactivated *Dd*HydAB

To unravel the mechanism of H_{inact}, *Dd*HydAB was photoactivated and monitored using FTIR spectroscopy to observe the IR band shifts of the redox states. Photoactivation was achieved using CdSe nanorods and the redox mediator propyl-diquat, PDQ. Specifically, CdSe nanorods were selected as the photosensitizer for their low quantum efficiency to provide minimum driving force for reactivation in order to observe any intermediate states.[18] Initial FTIR spectra indicated the enzyme was solely in the H_{inact} state with distinct peaks at 1847 cm^{-1}, 1983 cm^{-1}, and 2007 cm^{-1} (Fig. 2) .[11] This initial spectrum was subtracted from each illuminated spectra to identify absorbance changes as the enzyme is photoreduced.

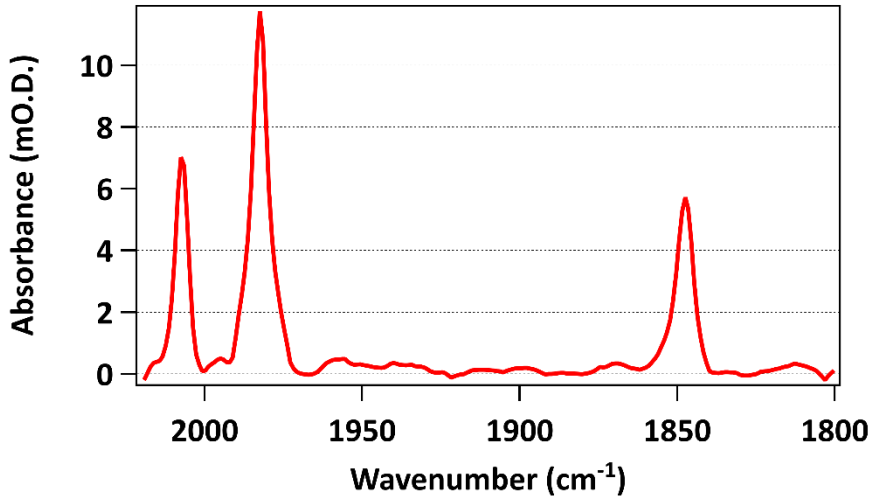

Figure 4.2 The dark spectra of *Dd*HydAB in the H_{inact} state.

Illumination of the sample resulted in bleaching of the initial peaks at 1847 cm^{-1}, 1983 cm^{-1}, and 2007 cm^{-1} as electrons are injected into the enzyme. An absorbance increase was observed at frequencies 1988 cm^{-1}, 1975 cm^{-1}, and 1835 cm^{-1} indicative of formation of H_{trans}. Maximum

absorbance for each peak was reached at ~3 minutes of illumination, followed by subsequent bleach of the frequencies which coincides with the growth of H_{ox} peaks at 1965 cm^{-1}, 1940 cm^{-1} and 1802 cm^{-1}. A small amount of $H_{red}H^+$ (the protonated form of H_{red}) at 1894 cm^{-1} is formed late in the experiment approximately after 5 minutes of illumination. Formation of H_{red} indicates the enzyme is beginning the catalytic cycle for proton reduction. No evidence of H_{red} was observed, though the protonation of the state likely occurs too fast at pH 7 for observation via FTIR spectroscopy. In the later light titrations, CO-inhibited $H_{ox}CO$ was also detected from the growth of frequency at 2017 cm^{-1} and shifting of the H_{trans} 1975 to 1972 cm^{-1}. This state results from decomposition of the H cluster which yields 3 CO molecules that can inhibit at the distal Fe of other holoenzymes, implying slight degradation of the sample which is expected over time.[19]

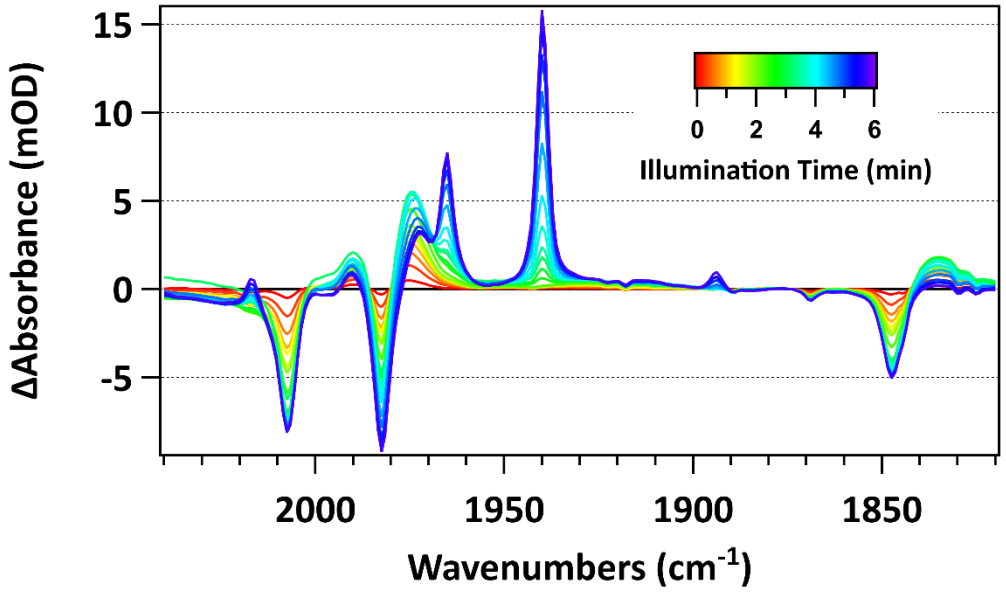

Figure 4.3 Photoreduction of the H_{inact} state of *Dd*HydAB. The spectra are colored based on illumination time.

Using the extinction coefficient for the IR bands, the concentration of each redox state can be monitored. The results reemphasize the direct formation of H_{trans} after reduction of H_{inact} as the former is immediately detected after initial illumination. This is expected as both mechanisms

propose the one-electron reduction as the first step. The next state observed, H_{ox}, increases while H_{trans} plateaus before eventually decreasing suggesting the transformation of H_{trans} to H_{ox}. At this point in the experiment, no H_{red} or $H_{red}H^+$ spectral peaks are observed. Auto-oxidation of H_{red} to H_{ox} is unlikely as the photosensitizer and redox mediator generate a reducing environment. No new peaks corresponding to intermediates were observed. For *Dd*HydAB, these results confirm the mechanism of H_{trans} to H_{ox}. Repeating the experiment with *Cr*HydA1 would elucidate if a similar mechanism is observed for a different hydrogenase or if reactivation is enzyme specific.

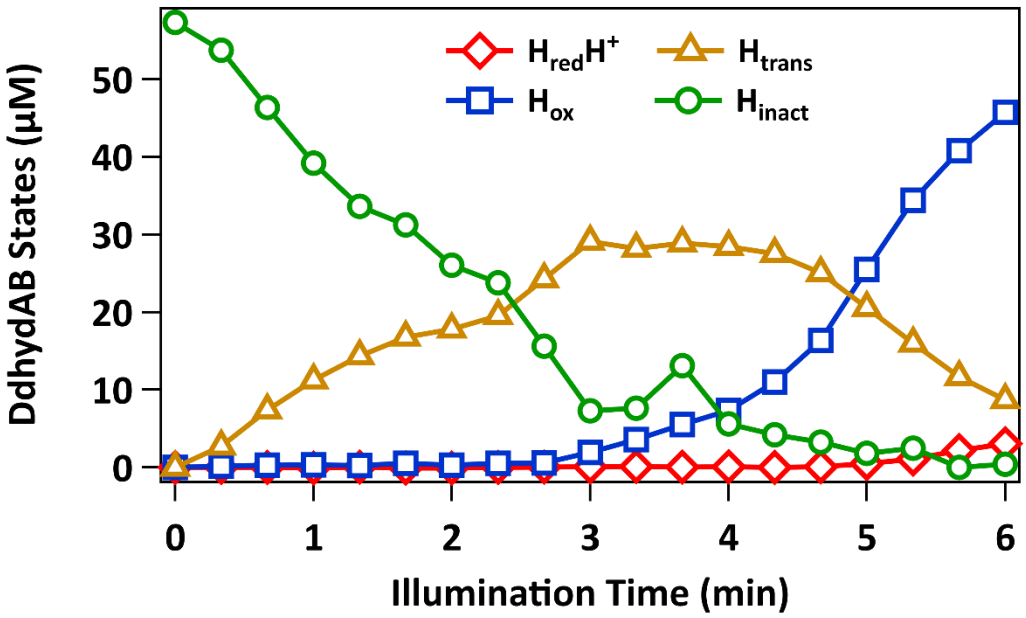

Figure 4.4 The population of states during illumination. Concentration was calculated using the extinction coefficients. Wavenumbers selected were 2007 cm^{-1} for H_{inact}, 1975 cm^{-1} for H_{trans}, 1940 cm^{-1} for H_{ox}, and 1894 cm^{-1} for $H_{red}H^+$.

The kinetics of H_{inact} activation are not known but based on these results appear to be quite slow. Illumination of the sample was in 20 second steps, but FTIR spectra collection took upwards of 15 minutes which would allow the system to potentially reach equilibrium after each light titration. While the initial reduction of H_{inact} to H_{trans} was controlled through limited exciton

generation, the transformation of H_{trans} to H_{ox} should not be electron dependent. Instead, its proposed to occur after protonation and disassociation of the sulfide ligand.[12] It's unclear which is the rate limiting step in the formation of H_{ox}, but at pH 7, it's likely protonation happens rather quickly. The IR cell is sealed, and the sample is prepared under an anaerobic atmosphere, but illumination occurs in air and the full experiment took >12 hours so it is possible oxygen may have leaked in over time. Oxygen is known to oxidize H_{trans} to H_{inact} and its presence in the sample may explain the slow conversion of H_{ox}.[12] Confirmation of this would be simple - repeat the experiment but stop illuminating after formation of H_{trans}. Oxidation back to H_{inact} would confirm the presence of oxygen. To fully resolve the kinetics of H_{inact} reactivation, transient absorption experiments would need to be performed. These experiments which could also identify potential redox intermediates in between the reactivation of H_{inact}.

4.3 - Conclusions

Reactivation of the oxygen tolerant state in [FeFe] hydrogenases is not completely understood with competing theories proposed.[12-14] In this Chapter, photoreduction of H_{inact} of *Dd*HydAB from *Desulfovibrio desulfuricans* was performed resulting in observed bleaches of frequencies corresponding to the state and formation of H_{trans} IR bands followed by H_{ox}. H_{red} was not observed and the protonated $H_{red}H^+$ was only detected late in the experiment after the majority of the enzyme was in the H_{ox} state. These results suggest reactivation proceeding from H_{inact} to H_{trans} to H_{ox} and providing direct evidence to confirm the mechanism proposed by Rodríguez-Macia et al.[12] The conversion of H_{trans} to H_{ox} occurred relatively slowly which could be due to the presence of an oxidant (oxygen) or the protonation and disassociation of the sulfide does not transpire quickly.

Future directions will focus on transient absorption experiments to observe the kinetics of reactivation and to identify any possible catalytic intermediates as well. The sulfide ligand should be IR active with a M-SH stretch, though the absorbance would low as these peaks are not as intense as CO vibration frequencies. A M-SH IR band has been observed in the [NiFe] hydrogenases and it should be possible for [FeFe] hydrogenases with enough sample.[20] Identification of this frequency would help resolve the mechanism, giving direct evidence for the disassociation of the ligand needed to form the resting state H_{ox}. Light induced reactivation of other enzymes such as *Cr*HydA1 and CbA5H would be necessary to determine a consensus mechanism concerning the oxygen tolerant state.

4.4 - Materials and Methods

4.4.1 - Synthesis and Preparation of CdSe Nanorods

Procedure was modified from literature.[17]

Together, 0.08 g of Cadium Oxide (CdO) (purchase from Alfa Aesar), 4.8 g of Trioctylphosphine oxide (TOPO) (purchased from TCI) and 0.78 g of hexylphosphonic acid (HPA) (purchased from Alfa Aesar) were combined in a 3-neck round bottom flask and heated for 2 hrs at 150 ˚C for 2 while under vacuum. Then the flask was placed under an N_2 atmosphere and heated to 250 ˚C until clear as the CdO dissolves. Immediately a solution of 0.2 g of Se dissolved in 3.64 mL of trioctlyphosphine was injected and allowed to react until the solution turned red. The flask was quickly removed and cooled using compressed air to quench the reaction. The nanorods were diluted with hexanes to keep the solution liquid at room temperature.

4.4.2 - Ligand Exchange of CdSe Nanorods

Procedure adapted from literature.[17]

Synthesized CdSe nanorods were purified and washed from excess TOPO by successive rounds of methanol precipitation and centrifugation. The purified CdSe nanorods were resuspended in pH >10 methanol with 10 mM 3-mercaptapropionic acid (MPA) then refluxed in the dark, for 2 hours, under N_2 at 70˚C. The pH of the solution was adjusted to pH >10 using tetramethyl ammonium hydroxide. Lastly the NRs were methanol precipitated and centrifuged and resuspended in the storage solution of 50 mM borate buffer containing 10 mM MPA and 10 mM triscarboxyethyl phosphide. NRs were filtered to remove the remaining TOPO/uncapped particles and stored in an air-free environment.

4.4.3 – Synthesis of PDQ

Procedure was adapted from literature.[17]

In an air free 3-neck round bottom flask, 5 mL of 1,3 dibromopropane and 0.25 g of 2,2'-bipyridine were combined. The flask was refluxed at 100-110 ˚C and reacted for 3-5 hours until the solution turned a pale cloudy-yellow. Afterwards the flask was cooled with an ice bath and the solid was collected on a frit. The pale-yellow precipitate was washed with cold hexanes. The product was crystallized from methanol.

4.4.4 – Enzyme Preparation

The [FeFe] hydrogenase *Dd*HydAB was expressed and purified by James Birrell at the Max Planck Institute for Chemical Energy Conversion and as described previously.[21]

4.4.5 - Sample Preparation for Infrared Experiments

For IR experiments, hydrogenase and nanomaterial were buffer exchanged a minimum of 6x from the respective storage solutions into the reaction buffer of 50 mM NaPO4, and 50 mM MPA using 10 kDa molecular weight cutoff filters (Millipore). Samples were concentrated to 15-

20 μL and assembled in small volume vials before injection into the IR cell using a gas tight syringe. The IR cell consisted of two copper plates housing 2 CaF_2 windows separated by a 75 μm Teflon spacer with a butyl rubber seal to allow injection of the sample into the cell. Set screws were also used to seal the ports of one of the CaF_2 windows to maintain the anaerobic environment. The reference side of the cell was composed of reaction buffer and the reference protein myoglobin.

4.4.6 - Steady State CODH CO Inhibition FTIR Conditions

FTIR spectra were obtained using a Varian 660 FTIR spectrometer equipped with an additional MCT detector cooled through liquid nitrogen. The FTIR beam was directed outside of the spectrometer using gold-plated mirrors into a dry air purged box with the IR cell in the beam path on top of a copper stage to allow lateral movement for collection of the sample and reference side. A resolution of 2 cm^{-1} with 4096 FTIR scans averaged to reduce noise.

Photoactivation of hydrogenase was achieved using a 5 mW, 532 nm laser diode. After each consecutive illumination, FTIR spectra were collected to observe absorbance changes. Difference spectra were obtained by subtracting the dark spectra from the proceeding illuminated spectra and were performed using Resolution Pro software for the FTIR then analyzed with Igor Pro 8.

4.5 - References

1. Osman, A. I.; Mehta, N.; Elgarahy, A. M.; Hefny, M.; Al-Hinai, A.; Al-Muhtaseb, A. a. H.; Rooney, D. W., Hydrogen production, storage, utilisation and environmental impacts: a review. *Environmental Chemistry Letters* **2021**, 1-36.

2. Turner, J. A., Sustainable hydrogen production. *Science* **2004,** *305* (5686), 972-974.

3. Yu, M.; Wang, K.; Vredenburg, H., Insights into low-carbon hydrogen production methods: Green, blue and aqua hydrogen. *Int. J. Hydrogen Energy* **2021,** *46* (41), 21261-21273.

4. Birrell, J. A.; Rodriguez-Macia, P.; Reijerse, E. J.; Martini, M. A.; Lubitz, W., The catalytic cycle of [FeFe] hydrogenase: A tale of two sites. *Coord. Chem. Rev.* **2021,** *449*, 214191.

5. Land, H.; Senger, M.; Berggren, G.; Stripp, S. T., Current state of [FeFe]-hydrogenase research: biodiversity and spectroscopic investigations. *ACS catalysis* **2020,** *10* (13), 7069-7086.

6. Swanson, K. D.; Ratzloff, M. W.; Mulder, D. W.; Artz, J. H.; Ghose, S.; Hoffman, A.; White, S.; Zadvornyy, O. A.; Broderick, J. B.; Bothner, B., [FeFe]-hydrogenase oxygen inactivation is initiated at the H cluster 2Fe subcluster. *Journal of the American Chemical Society* **2015,** *137* (5), 1809-1816.

7. Darensbourg, M. Y.; Weigand, W., Sulfoxygenation of active site models of [NiFe] and [FeFe] hydrogenases–a commentary on possible chemical models of hydrogenase enzyme oxygen sensitivity. *Eur. J. Inorg. Chem.* **2011,** *2011* (7), 994-1004.

8. Rodríguez-Maciá, P.; Galle, L. M.; Bjornsson, R.; Lorent, C.; Zebger, I.; Yoda, Y.; Cramer, S. P.; DeBeer, S.; Span, I.; Birrell, J. A., Caught in the Hinact: Crystal Structure and Spectroscopy Reveal a Sulfur Bound to the Active Site of an O2-stable State of [FeFe] Hydrogenase. *Angew. Chem. Int. Ed.* **2020,** *59* (38), 16786-16794.

9. Winkler, M.; Duan, J.; Rutz, A.; Felbek, C.; Scholtysek, L.; Lampret, O.; Jaenecke, J.; Apfel, U.-P.; Gilardi, G.; Valetti, F., A safety cap protects hydrogenase from oxygen attack. *Nature communications* **2021,** *12* (1), 1-10.

10. Glick, B. R.; Martin, W. G.; Martin, S. M., Purification and properties of the periplasmic hydrogenase from Desulfovibrio desulfuricans. *Can. J. Microbiol.* **1980,** *26* (10), 1214-1223.

11. Roseboom, W.; De Lacey, A. L.; Fernandez, V. M.; Hatchikian, E. C.; Albracht, S. P. J., The active site of the [FeFe]-hydrogenase from Desulfovibrio desulfuricans. II. Redox properties, light sensitivity and CO-ligand exchange as observed by infrared spectroscopy. *JBIC Journal of Biological Inorganic Chemistry* **2006,** *11* (1), 102-118.

12. Rodríguez-Maciá, P.; Reijerse, E. J.; van Gastel, M.; DeBeer, S.; Lubitz, W.; Rüdiger, O.; Birrell, J. A., Sulfide protects [FeFe] hydrogenases from O2. *Journal of the American Chemical Society* **2018,** *140* (30), 9346-9350.

13. Felbek, C.; Arrigoni, F.; de Sancho, D.; Jacq-Bailly, A.; Best, R. B.; Fourmond, V.; Bertini, L.; Léger, C., Mechanism of Hydrogen Sulfide-Dependent Inhibition of FeFe Hydrogenase. *ACS Catalysis* **2021,** *11* (24), 15162-15176.

14. Corrigan, P. S.; Tirsch, J. L.; Silakov, A., Investigation of the unusual ability of the [FeFe] Hydrogenase from Clostridium beijerinckii to Access an O2-Protected State. *Journal of the American Chemical Society* **2020,** *142* (28), 12409-12419.

15. Greene, B. L., Progress and Opportunities in Photochemical Enzymology of Oxidoreductases. *ACS Catalysis* **2021,** *11* (23), 14635-14650.

16. Sanchez, M. L. K.; Konecny, S. E.; Narehood, S. M.; Reijerse, E. J.; Lubitz, W.; Birrell, J. A.; Dyer, R. B., The Laser-Induced Potential Jump: A Method for Rapid Electron Injection into Oxidoreductase Enzymes. *The Journal of Physical Chemistry B* **2020,** *124* (40), 8750-8760.

17. Sanchez, M. L. K.; Sommer, C.; Reijerse, E.; Birrell, J. A.; Lubitz, W.; Dyer, R. B., Investigating the kinetic competency of Cr HydA1 [FeFe] hydrogenase intermediate states via time-resolved infrared spectroscopy. *Journal of the American Chemical Society* **2019,** *141* (40), 16064-16070.

18. Reiss, P.; Protiere, M.; Li, L., Core/shell semiconductor nanocrystals. *small* **2009,** *5* (2), 154-168.

19. Morra, S.; Duan, J.; Winkler, M.; Ash, P. A.; Happe, T.; Vincent, K. A., Electrochemical control of [FeFe]-hydrogenase single crystals reveals complex redox populations at the catalytic site. *Dalton Transactions* **2021,** *50* (36), 12655-12663.

20. Tai, H.; Nishikawa, K.; Higuchi, Y.; Mao, Z. w.; Hirota, S., Cysteine SH and glutamate COOH contributions to [NiFe] hydrogenase proton transfer revealed by highly sensitive FTIR spectroscopy. *Angew. Chem.* **2019,** *131* (38), 13419-13424.

21. Berggren, G.; Adamska, A.; Lambertz, C.; Simmons, T. R.; Esselborn, J.; Atta, M.; Gambarelli, S.; Mouesca, J. M.; Reijerse, E.; Lubitz, W., Biomimetic assembly and activation of [FeFe]-hydrogenases. *Nature* **2013,** *499* (7456), 66-69.

Chapter 5: Conclusions

5.1 – Conclusions

Redox enzymes catalyze many useful chemical transformations for a variety of biocatalytic purposes such as organic synthesis and alternative fuel generation.[1-3] The high specificity and efficiency of redox enzymes enables them to be exquisite catalysts, but they are designed for biological purposes and often require effort to develop these enzymes for industrial reactions.[4-6] This dissertation focuses on three groups of redox enzymes for biocatalytic reactions: Old Yellow Enzymes for asymmetric hydrogenation and desaturation, Carbon Monoxide Dehydrogenase for CO_2 reduction and Hydrogenase for hydrogen production.

A current limitation to biocatalysis is the lack of suitable enzymes for industrial reactions with many suffering from narrow substrate scopes.[7] Engineering enzymes using directed evolution is a powerful tool to overcome this limitation but is time and cost intensive.[8] In Chapter 2, an alternative approach is presented by exploring the genetic diversity of the Old Yellow Enzyme (OYE) family. Sequence similarity networks and other bioinformatic tools were utilized to systematically organize and explore the unknown sequence space of the OYE family. From this analysis, family-wide substrate profiling identified both specific OYE subgroup activity trends and novel potential biocatalysts unique catalytic activities. Widespread reverse, desaturase activity was also detected amongst the novel enzymes and brief investigations into the desaturase activity suggest redox potential of the enzyme does not play as crucial a role in this reaction as previously thought. Altogether through a combination of bioinformatics and synthetic biology techniques, the biocatalytic potential of the OYE family was assessed while also providing insight into the catalytic factors governing ene reductase and desaturase activity.

Understanding the mechanistic details of the catalytic cycle of redox enzymes is crucial for not only their application in biocatalysis, but also successful protein engineering of the enzymes

and the development of more sustainable catalysts.[1, 9] In Chapter 3, an efficient photosystem using Carbon Monoxide Dehydrogenase (CODH) II from *C. hydrogenoformans* was developed and utilized for spectroscopic investigations into the mechanism of CO_2 reduction. The photosystem displayed a 10-fold increase in quantum yield compared to previous systems.[10] The affinity for CO inhibition of the photosystem was exploited to identify two IR bands of CO bound to the active site of the enzyme. Subsequent transient absorption experiments revealed that both IR frequencies are catalytically relevant and are likely the dynamics of CO formation and disassociation in the active site. Furthermore, the kinetics of initial enzyme reduction and CO formation occur at nearly identical lifetimes suggesting that CO_2 binding occurs rapidly. To conclude, the development of the photosystem led to the identification of Ni-CO stretches of the active site and the first direct spectroscopic kinetic information for CODH catalyzed CO_2 reduction.

As enzymes are not evolved for industrial purposes, stability remains a key shortcoming with metalloenzymes in particular suffering from oxygen sensitivity.[11] In Chapter 4, the reactivation of the oxygen inactive state of [FeFe] hydrogenase was examined using infrared spectroscopy. Using light-titrations, the H_{inact} state of *Dd*HydAB from *Desulfovibrio desulfuricans* was reduced and the mechanism was monitored using FTIR. Observing the population changes via the IR peaks revealed the conversion of the H_{inact} state to the H_{trans} to the resting H_{ox} state, verifying the previously proposed mechanism.[12] Understanding the reactivation is key towards overcoming the obstacle of oxygen sensitivity in hydrogenase.

Overall using a wide range of techniques from bioinformatics to spectroscopy, this dissertation investigated redox enzymes for biocatalysis addressing distinct issues such as the discovery of novel OYE biocatalysts for asymmetric hydrogenation and desaturation, the

development and usage of light-driven spectroscopic tools for CODH catalyzed CO_2 reduction, and the exploration of the oxygen insensitive state of the [FeFe] hydrogenases.

5.2 – Future Outlook

The work in this dissertation serves as the basis for a variety of different future directions in utilizing redox enzymes for biocatalysis. The bioinformatic exploration of the OYE family presented numerous avenues for further investigations for biocatalysis and enzymology such as the prevalence of the single domain OYEs with iron sulfur cluster motifs. Uncovering the factors contributing to the observed unique activity of novel OYEs is another possible direction with an emphasis on the near ubiquitous desaturase activity observed in the family. Furthermore, the amount of sequence and functional information is ideal for machine learning algorithms which could identify the key factors responsible for the different substrate profiles observed.[13]

For CODH, the photosystem developed will lead to spectroscopic studies to verify other catalytic steps in the proposed cycle such as the protonation event that leads to CO formation and the movement of CO into the gas channels. Time resolved spectroscopic investigations of active site variants could identify possible roles for the residues. The revelation that Co bound to the active site displays two IR frequencies will result in further studies to identify the two binding orientations either through crystallography or spectroscopy.

Lastly, the observation of reactivation of the oxygen insensitive state of the [FeFe] hydrogenases will help to elucidate the mechanism of this state. Using time resolved spectroscopy, possible intermediates can be identified in addition to the kinetics of reactivation. Investigations using other hydrogenases such as those from *Chlamydomonas reinhardtii* and *Clostridium beijerinckii* could resolve if these enzymes follow a general or enzyme specific mechanism.[14, 15]

5.3 – References

1. Lee, S. H.; Choi, D. S.; Kuk, S. K.; Park, C. B., Photobiocatalysis: activating redox enzymes by direct or indirect transfer of photoinduced electrons. *Angew. Chem. Int. Ed.* **2018,** *57* (27), 7958-7985.

2. Léger, C.; Bertrand, P., Direct electrochemistry of redox enzymes as a tool for mechanistic studies. *Chem. Rev.* **2008,** *108* (7), 2379-2438.

3. Zhao, H.; van der Donk, W. A., Regeneration of cofactors for use in biocatalysis. *Curr. Opin. Biotechnol.* **2003,** *14* (6), 583-9.

4. Adams, J. P.; Brown, M. J. B.; Diaz-Rodriguez, A.; Lloyd, R. C.; Roiban, G. D., Biocatalysis: a pharma perspective. *Adv. Synth. Catal.* **2019,** *361* (11), 2421-2432.

5. Bell, E. L.; Finnigan, W.; France, S. P.; Green, A. P.; Hayes, M. A.; Hepworth, L. J.; Lovelock, S. L.; Niikura, H.; Osuna, S.; Romero, E., Biocatalysis. *Nature Reviews Methods Primers* **2021,** *1* (1), 1-21.

6. Bornscheuer, U. T.; Huisman, G. W.; Kazlauskas, R. J.; Lutz, S.; Moore, J. C.; Robins, K., Engineering the third wave of biocatalysis. *Nature* **2012,** *485* (7397), 185-194.

7. Pyser, J. B.; Chakrabarty, S.; Romero, E. O.; Narayan, A. R., State-of-the-art biocatalysis. *ACS Cent. Sci.* **2021,** *7* (7), 1105-1116.

8. Rodríguez Benítez, A.; Narayan, A. R., Frontiers in biocatalysis: profiling function across sequence space. ACS Publications: 2019.

9. Can, M.; Armstrong, F. A.; Ragsdale, S. W., Structure, function, and mechanism of the nickel metalloenzymes, CO dehydrogenase, and acetyl-CoA synthase. *Chem. Rev.* **2014,** *114* (8), 4149-4174.

10. Zhang, L.; Can, M.; Ragsdale, S. W.; Armstrong, F. A., Fast and selective photoreduction of CO2 to CO catalyzed by a complex of carbon monoxide dehydrogenase, TiO2, and Ag nanoclusters. *ACS catalysis* **2018,** *8* (4), 2789-2795.

11. Rodríguez-Maciá, P.; Galle, L. M.; Bjornsson, R.; Lorent, C.; Zebger, I.; Yoda, Y.; Cramer, S. P.; DeBeer, S.; Span, I.; Birrell, J. A., Caught in the Hinact: Crystal Structure and Spectroscopy Reveal a Sulfur Bound to the Active Site of an O2-stable State of [FeFe] Hydrogenase. *Angew. Chem. Int. Ed.* **2020,** *59* (38), 16786-16794.

12. Rodríguez-Maciá, P.; Reijerse, E. J.; van Gastel, M.; DeBeer, S.; Lubitz, W.; Rüdiger, O.; Birrell, J. A., Sulfide protects [FeFe] hydrogenases from O2. *Journal of the American Chemical Society* **2018,** *140* (30), 9346-9350.

13. Yang, K. K.; Wu, Z.; Arnold, F. H., Machine-learning-guided directed evolution for protein engineering. *Nature methods* **2019,** *16* (8), 687-694.

14. Felbek, C.; Arrigoni, F.; de Sancho, D.; Jacq-Bailly, A.; Best, R. B.; Fourmond, V.; Bertini, L.; Léger, C., Mechanism of Hydrogen Sulfide-Dependent Inhibition of FeFe Hydrogenase. *ACS Catalysis* **2021,** *11* (24), 15162-15176.

15. Corrigan, P. S.; Tirsch, J. L.; Silakov, A., Investigation of the unusual ability of the [FeFe] Hydrogenase from Clostridium beijerinckii to Access an O2-Protected State. *Journal of the American Chemical Society* **2020,** *142* (28), 12409-12419.